390
11-17-80

MASTER

Dr. 2013

DOE/NOAA/OTEC-28
Distribution Category UC-64

OTEC COLD WATER PIPE DESIGN FOR PROBLEMS CAUSED BY VORTEX-EXCITED OSCILLATIONS

By
Owen M. Griffin

March 14, 1980

Work Performed Under Contract No. EG-77-A-29-1078

Naval Research Laboratory
Marine Technology Division
Washington, D. C.

U.S. Department of Energy

Solar Energy

DISTRIBUTION OF THIS DOCUMENT IS UNLIMITED

DISCLAIMER

This report was prepared as an account of work sponsored by an agency of the United States Government. Neither the United States Government nor any agency Thereof, nor any of their employees, makes any warranty, express or implied, or assumes any legal liability or responsibility for the accuracy, completeness, or usefulness of any information, apparatus, product, or process disclosed, or represents that its use would not infringe privately owned rights. Reference herein to any specific commercial product, process, or service by trade name, trademark, manufacturer, or otherwise does not necessarily constitute or imply its endorsement, recommendation, or favoring by the United States Government or any agency thereof. The views and opinions of authors expressed herein do not necessarily state or reflect those of the United States Government or any agency thereof.

DISCLAIMER

Portions of this document may be illegible in electronic image products. Images are produced from the best available original document.

DISCLAIMER

"This book was prepared as an account of work sponsored by an agency of the United States Government. Neither the United States Government nor any agency thereof, nor any of their employees, makes any warranty, express or implied, or assumes any legal liability or responsibility for the accuracy, completeness, or usefulness of any information, apparatus, product, or process disclosed, or represents that its use would not infringe privately owned rights. Reference herein to any specific commercial product, process, or service by trade name, trademark, manufacturer, or otherwise, does not necessarily constitute or imply its endorsement, recommendation, or favoring by the United States Government or any agency thereof. The views and opinions of authors expressed herein do not necessarily state or reflect those of the United States Government or any agency thereof."

This report has been reproduced directly from the best available copy.

Available from the National Technical Information Service, U. S. Department of Commerce, Springfield, Virginia 22161.

Price: Paper Copy $10.00
Microfiche $3.50

ABSTRACT

Vortex-excited oscillations of marine structures result in reduced fatigue life, large hydrodynamic forces and induced stresses, and sometimes lead to structural damage and to destructive failures. The cold water pipe of an OTEC plant is nominally a bluff, flexible cylinder with a large aspect ratio (L/D = length/diameter), and is likely to be susceptible to resonant vortex-excited oscillations. The objective of this report is to survey recent results pertaining to the vortex-excited oscillations of structures in general and to consider the application of these findings to the design of the OTEC cold water pipe. Practical design calculations are given as examples throughout the various sections of the report.

This report is limited in scope to the problems of vortex shedding from bluff, flexible structures in steady currents and the resulting vortex-excited oscillations. The effects of flow non-uniformities, surface roughness of the cylinder, and inclination to the incident flow are considered in addition to the case of a smooth cylinder in a uniform stream. Emphasis is placed upon design procedures, hydrodynamic coefficients applicable in practice, and the specification of structural response parameters relevant to the OTEC cold water pipe. There are important problems associated with the shedding of vortices from cylinders in waves and from the combined action of waves and currents, but these complex fluid/structure interactions are not considered in this report.

DISTRIBUTION OF THIS DOCUMENT IS UNLIMITED

THIS PAGE

WAS INTENTIONALLY

LEFT BLANK

CONTENTS

Executive Summary v

Foreword and Acknowledgments ix

Magnitude Of The Problem x

1. Introduction 1

   1.1 Objectives and justification 1
   1.2 Scope of the investigation 2

2. Background 3

   2.1 Historical aspects 3
   2.2 Ocean engineering programs 5

3. Oscillations In Line With The Flow 6

   3.1 Resonant response characteristics 6
   3.2 Hydrodynamic loads 10
   3.3 Reynolds number and full-scale effects 10

4. Cross Flow Oscillations 12

   4.1 Resonant response characteristics 12
   4.2 Hydrodynamic loads 18
   4.3 Roughness and shear effects 24
   4.4 Yaw or inclination effects 29
   4.5 Coherence of the shedding due to lock-on 31

5. Prediction Methods And Design Procedures 35

   5.1 General design procedures 35
   5.2 Practical design data 39

6. Computer Codes For Predicting And Modelling Vortex-Excited Oscillations 46

   6.1 The VORTOS code 47
   6.2 The DESADE code 48
   6.3 The HULPIPE code 50
   6.4 Other related codes 50

7. Elimination/Reduction And Avoidance Of Vortex-Excited Oscillations 51

DISTRIBUTION OF THIS DOCUMENT IS UNLIMITED

8. OTEC Cold Water Pipe Applications 54

8.1 Typical CWP examples 54
8.2 Recommended vortex-excited force and response coefficients 61

9. Summary 67

9.1 Conclusions 67
9.2 Recommendations 68

10. References 69

11. Appendices 79

4.1 The Prediction Of Cross Flow-Induced Forces And Displacements 79
A.1 Nomenclature 91
A.2 List of Figures 94

EXECUTIVE SUMMARY

Vortex-excited oscillations of marine structures result in reduced fatigue life, large hydrodynamic forces and induced stresses, and sometimes lead to structural damage and to destructive failures. The cold water pipe of an ocean thermal energy conversion (OTEC) plant is nominally a bluff, flexible cylinder with a large aspect ratio (L/D = length/diameter), and is likely to be susceptible to resonant vortex-excited oscillations. The objective of this report is to survey recent results pertaining to the vortex-excited oscillations of structures in general and to consider the application of these findings to the design of the OTEC cold water pipe. Practical design calculations are given as examples throughout the various sections of the report.

This report is limited in scope to the problems of vortex shedding from bluff, flexible structures in steady currents and the resulting vortex-excited oscillations. The effects of flow non-uniformities, surface roughness of the cylinder, and inclination to the incident flow are considered in addition to the case of a smooth cylinder in a uniform stream. Emphasis is placed upon design procedures, hydrodynamic coefficients applicable in practice, and the specification of structural response parameters relevant to the OTEC cold water pipe. There are important problems associated with the shedding of vortices from cylinders in waves and from the combined action of waves and currents, but these complex fluid/structure interactions are not considered in this report.

Sections 3 and 4 of the report give detailed discussions of the present state-of-the-art concerning vortex-excited oscillations of cylindrical structures of nominally circular cross-sections. Structures with rectangular cross-sections or fixed separation points are not thought to be

relevant to the OTEC cold water pipe. Particular attention is given to the hydrodynamic loads and resonant response characteristics for oscillations both in line and cross flow. Examples of data taken from experiments with full-scale marine structures are given for the few cases that are available. For the problem of cross flow oscillations, additional discussion is given to roughness and shear (non-uniform flow), yaw or inclination effects, and to the coherence of the shedding that accompanies vortex-excited oscillations.

In *Section 5* a discussion is given of prediction methods and design procedures that are available and that have been employed in practice. The parameters that must be considered in an assessment of the severity of vortex-excited oscillations are described and step-by-step procedures are given for making such an assessment. *Figs. 5.1* and *5.2* give these procedures in a block diagram format. Practical design equations for the amplification of the steady drag forces and the dependence of cross flow displacement amplitude upon the mass and damping parameters of the pipe are given in *Section 5.2 and Table 5.1.*

Several computer codes that have been developed for predicting the dynamic response due to cylindrical structures of vortex shedding are described in *Section 6.* The VORTOS code is based on a finite-element solution for the dynamics of beams in the frequency domain. It was developed primarily for the analysis of cylindrical members of marine structures at subcritical Reynolds numbers. It has not been applied to problems in the OTEC range of Reynolds numbers, i.e. Re = 10^6 and greater. DESADE is a code that was developed to analyze structural marine cable arrays. The code is directly applicable only to the dynamics of marine cable systems but it contains a resonant vibration analysis routine and methodology that has been adopted widely both in the Navy and in the private sector. The HULPIPE code is a time-domain analysis that has been used extensively in marine studies. In this code the coupled

motions of the plant hull and the cold water pipe can be solved, but only constant hydrodynamic force coefficients are permitted. Several additional codes that were developed for marine riser applications are discussed briefly.

Devices for the suppression and elimination of vortex-excited oscillations are discussed in *Section 7.* Porous shrouds, helically-wound fins and fairings have been employed successfully in marine applications to reduce the resonant oscillations due to vortex shedding, but not at the large Reynolds numbers that are characteristic of OTEC applications. *Fig. 7.3* gives several quantitative examples of the results that have been obtained with various types of vortex suppression devices in ocean engineering applications.

Several OTEC-related example problems are discussed in *Section 8* of this report. The examples chosen give a step-by-step guide to the designer who wishes to make an assessment of a structure's susceptibility to vortex-excited oscillations. *The examples chosen are particularly relevant to the OTEC cold water pipe* (CWP). The first two examples consider the calculation of the critical relative flow velocities for the onset of crossflow oscillations, one case (*Example 8.1*) for which the natural periods of the CWP are known and one case (*Example 8.2*) for which the natural periods of the CWP are calculated from simple beam theory. Two additional examples are also presented in this section. *Examples 8.3 and 8.4* outline the procedure for calculating the peak cross flow displacement amplitude $\bar{Y}_{MAX}$ from a least-squares fit to the well known dependence between $\bar{Y}_{MAX}$ and the reduced structural damping k_s. Actual OTEC cold water pipe design and structural parameters are employed in these examples. Where possible, recommendations are made for appropriate force coefficients that can be employed as practical design aids.

Section 9 of the report contains a brief summary and several OTEC-related recommendations and future needs in terms of problems concerned with vortex-excited oscillations.

A list of figures and a list of the nomenclature employed in the present report are included as appendices.

FOREWORD AND ACKNOWLEDGMENTS

This report has been prepared by the Naval Research Laboratory as part of the OTEC cold water pipe technology development program at the Office of Ocean Engineering, National Oceanic and Atmospheric Administration. The cooperation and helpful comments and criticisms of Dr. Richard Scotti of OOE, NOAA during the preparation of this report are appreciated. A number of helpful comments and suggestions also have been made by Dr. Steven Ramberg of NRL. The author also wishes to thank Professor T. Sarpkaya of the Naval Postgraduate School, Dr. R. B. Dean of Atkins Research and Development, and Dr. Roger King of BHRA Fluid Engineering for providing detailed reports of their experiments. The report was composed and edited by staff members of the Computerized Technical Composition Office at NRL.

MAGNITUDE OF THE PROBLEM

Problems that are caused by vortex shedding and the vortex-excited oscillations of marine structures often have been ignored in the past, largely because reliable experimental data and design methods have not been available. However, as marine construction has moved into deeper water and into harsher operating environments such as the North Sea, the need to design slender, flexible structures and structural members against vortex shedding-related problems has increased in importance. The steady and unsteady vortex-excited hydrodynamic forces and their associated deflections and vibrations cause amplified stress levels and fatigue, and they often lead to structural damage and eventually to failure.

Many types of marine structures are susceptible to vortex-excited oscillations. These include the risers and conductor tubes that are employed in oil exploration and production, deep water pipelines, and members of jacketed structures. Deep water piling installation and driving operations also are hampered sometimes by problems arising from vortex shedding. Several case studies have been documented in the literature in recent years. Among these was the installation of an offshore oil terminal in the United Kingdom during the late 1960's. Significant vortex-excited motions were encountered during the installation of pilings in a tidal flow, and these oscillations caused severe construction difficulties. A wide ranging test program was conducted both at the field site (16,17)* and in the laboratory (18,22) in order to determine the causes of the vibrations and to devise means of preventing them.

Laboratory tests and design studies were conducted in the mid 1970's to develop a riser fairing that would allow a semisubmersible drilling vessel to operate off the coast of Brazil in

*Numbers in parentheses denote references listed at the end of this report.

152m (500 ft) of water and in strong surface currents up to 4.1 m/s (8 kt). These tests resulted in the development of an economic and practical fairing device to suppress any vortex-excited oscillations (72).

The recent underwater installation of 187m (610 ft) long foundation piles for the Shell Oil production platform in the Cognac field of the Gulf of Mexico was judged to present several potential problems due to vortex-excited oscillations (45). Currents of sufficient magnitude to cause resonant oscillations of the piles had been measured at the installation site which has a water depth of 350 m (1150 ft). The anticipated problems included the "stabbing" of oscillation piles into sleeves in the platform base section, and oscillations of the stabbed piles during the subsequent driving operation. A program of laboratory tests was conducted to determine the susceptibility of model piles to resonant vortex excitation and suppression devices were developed. Estimates of static and dynamic stress levels during Cognac pile driving operations showed that cross flow vortex-excited oscillations would *triple* the maximum stresses relative to the non-vibrating pile (45). Under certain circumstances a fatigue life of *four days* was predicted for the bare piles when their exposed length of 130m (425 ft) was resonantly excited by currents with magnitudes of 0.46 m/s (0.9 kt).

The cold water pipe of an OTEC plant is a long, slender marine structure of cylindrical cross-section that typically will extend to depths of 1000 m (3280 ft) in the ocean from the platform of the plant. It is precisely this type of marine structure that is most susceptible to resonant excitation by vortex shedding due to the relative motion between the pipe and the water. The cold water pipe is considered by some to be the greatest engineering problem facing OTEC, and the reliable design of the pipe to withstand environmental forces over a long (30 year) life time is a principal objective of the on-going OTEC development program. Reliable

procedures to design marine structures against vortex shedding-related problems are available, but none of these have been applied directly to the design of the cold water pipe. It is only through laboratory and at-sea tests similar to those summarized above and described in detail later in this report that reliable procedures for the design of the OTEC cold water pipe can be developed, calibrated and put into practice.

OTEC COLD WATER PIPE DESIGN FOR PROBLEMS CAUSED BY VORTEX-EXCITED OSCILLATIONS

1. INTRODUCTION

1.1 Objectives and justification. It is often found that unstreamlined, or bluff, structures display oscillatory instabilities when exposed to wind or current flow past them. One common mechanism for generating these resonant, flow-excited oscillations is the organized and periodic shedding of vortices as the flow separates in an alternating fashion from opposite sides of the body. The flow field exhibits a dominant periodicity and the body is acted upon by time-dependent pressure loads which result in steady and unsteady drag forces in line with the flow as well as unsteady lift or side forces in the cross flow direction. If the structure is flexible and lightly damped, then resonant oscillations can be excited normal or parallel to the incident flow direction. For the more common cross flow oscillations, the body and wake have the same frequency near one of the natural frequencies of the structure, and near the Strouhal frequency at which pairs of vortices would be shed if the structure were stationary. *This phenomenon is commonly termed "lock-on" or "wake capture."*

Vortex-excited oscillations of marine structures and cables result in reduced fatigue life, amplified hydrodynamic forces, and sometimes lead to structural damage and to destructive failures. Flow-excited oscillations very often are a critical factor in the design of risers and offshore platforms, since these complex structures usually have bluff cylindrical elements which are prone to vortex shedding in an incident current. The cold water pipe of an ocean thermal

Manuscript submitted November 18, 1979.

energy conversion (OTEC) plant is typically a bluff, flexible cylinder with a large aspect ratio (L/D = length/diameter), and it is likely to be susceptible to current-induced vortex excitation. Thus an understanding of the nature of the fluid/structure interaction and the resultant flow-induced hydrodynamic loads is an important consideration in the reliable design of the OTEC cold water pipe and its associated mooring and riser cable systems. The cold water pipe is often cited as the greatest engineering problem in OTEC development.

Several recent texts, design manuals and survey articles have considered in various contexts the problems associated with vortex-excited oscillations. These include design manuals on the dynamics of marine structures (1), books on the general field of flow-induced vibrations (2), and articles on vortex shedding problems relative to marine structures (3), and a lengthy review article on the general topic of vortex-induced oscillations (4). The latter article has a listing of *one hundred thirty-four* references.

The objective of this report is to survey recent results pertaining to the vortex-excited oscillations of bluff structures in steady currents and to consider their application to the design of the OTEC cold water pipe. The physical scales of the experiments to be discussed range from small-scale laboratory studies to full-scale measurements on actual marine structures. These results are considered in the context of design methods which have been developed for the dynamic analysis of offshore structures and cable systems.

1.2 Scope of the Investigation. This report is limited in scope to the problems of vortex shedding from bluff, flexible structures in steady currents and the resulting vortex-excited oscillations. The effects of flow non-uniformities, surface roughness of the cylinder, and inclination to the incident flow are considered in addition to the case of a smooth cylinder in a uniform stream. Emphasis is placed upon the development of design procedures, hydrodynamic

coefficients applicable in practice, and the definition of structural response parameters relevant to the OTEC cold water pipe. There are important problems associated with the shedding of vortices from cylinders in waves and from the combined action of waves and steady currents, but these even more complex fluid/structure interactions are not considered in this report. These topics are considered to some extent in a recently-published working guide to estimating the hydrodynamic loadings on offshore structures due to waves and currents (5).

2. BACKGROUND

2.1 Historical aspects. The promise of a renewable source of base-load electric power from ocean temperature gradients has led to U.S. government funding of research and development of the Ocean Thermal Energy Conversion (OTEC) process over the past several years. From a very modest beginning in 1972 the OTEC program has grown to a 1979 R&D funding level of about $40 million.

An analysis sponsored by the U.S. Congress in 1978 (6) identified the primary unresolved technical problems in the OTEC concept. These included:

- The heat exchangers (evaporators and condensers), including the working fluid, construction materials, biofouling and corrosion;
- The ocean platform and cold water pipe;
- Open cycle vs. closed cycle processes;
- Underwater electric power transmission lines;
- The constructability and long-term reliability of an entire plant.

A more recent appraisal of these problems is given in the reports of the various working groups from the Sixth OTEC Conference held in June 1979 (7). These reports indicate that significant progress has been made during the past several years to justify proceeding with the development of a 10/40 MW_e pilot plant by 1985.

In 1881 the French physicist d'Arsonval apparently made the first serious proposal to extract energy from thermal gradients. However, it was not until 1926 that the French engineers Claude and Boucherot actually began to build an open cycle power plant that would utilize flash-evaporated, low pressure steam as the working fluid. A small plant was constructed and operated in 1928 with a temperature difference of only 20°C (36°F). It produced $60KW_e$, and only 25 percent of this total power output was needed to run the plant's auxiliary machinery (8,9). The input water to the flash evaporator was obtained from the coolant lines of a steel mill in Ougree-Marihaye, Belgium and the water for the condenser was pumped from the Meuse River.

Claude's later and more famous attempt (9) in Cuba to generate power at a shore-based site used the same basic plant. However, only 22 KW_e of power were generated because the operating temperature difference was only $\Delta T = 13°C$ (24°F) instead of the expected value of 28°C (50°F). A large cold water pipe, 1.8m (6 ft) in diameter and capable of serving a larger plant, was constructed after two unsuccessful attempts, but the pumping power requirements were greater than the plant's limited output. However, the plant did operate for eleven days before the cold water pipe was destroyed during a storm.

Claude and Boucherot constructed a floating power plant on-board the 10,000 ton cargo ship Tunisie. The basic design of the floating plant was the same as for the Cuba-based plant,

but the power output was expected to be 800 KW_e. The plant's major features are sketched in Fig. 2.1 and, with the exception of the open cycle Claude process power modules, the basic features of the system are remarkably similar in overall layout to the most recent OTEC plant concepts. The power plant ran poorly and Claude scuttled his floating equipment at sea. However the ship-mounted plant is similar to many recent proposed OTEC plants, most notably OTEC-I (10) which is shown in Fig. 2.2.

2.2 Ocean engineering programs. As an essential part of its operation, an OTEC power plant withdraws large amounts of cool water from the deeper layers of the ocean through a long cold water pipe (CWP) suspended from the OTEC platform. For a plant generating 40 MW_e of electric power, the CWP can be as large as 9.2m (30 ft) in diameter and 1000m (3,280 ft) long. When deployed in the ocean environment the CWP will experience hydrodynamic forces, both directly as well as indirectly through forces transmitted by the motions of the platform. An understanding of and the means of designing for these forces are essential steps toward ensuring the successful operation of OTEC plants.

An ocean engineering technology development program has been initiated for the Department of Energy by the National Oceanic and Atmospheric Administration (NOAA), Office of Ocean Engineering (OOE). The purpose of this program is to develop reliable engineering design methodologies for the prediction of the hydroelastic response of the CWP, the coupled platform/CWP, and the platform station-keeping and seawater systems throughout their life cycles. The 9.2m (30 ft) diameter, 1000m (3,280 ft) long CWP prototype presently envisioned for a 40 MW_e plant will operate at cold water flow rates up to 3.44×10^4 gallons per second (or a flow velocity of 13×10^4 liters per second) and is to have an expected life of 30 years.

The critical aspects of the NOAA/DOE cold water pipe technology development plan fall into the following three areas:

- Characterization of engineering properties of candidate CWP materials, especially in regards to strength and long term cyclic fatigue.
- Determination of the response of a CWP during tow-to-site and deployment operations
- Determination of the response of the platform/CWP system to all environmental loads during both normal operations and storm survival.

An overview of the CWP design and development program is presented in a recent paper (11)

Preliminary design concepts for the CWP presently under study (12,13) are shown in Fig. 2.3 to 2.5 and comprise the following categories:

- Rigid-wall pipe with or without articulated joints
- Compliant pipe
- Bottom-mounted pipe.

Materials under consideration for CWP construction include steel, concrete, fiber reinforced plastic (FRP), thermoplastics and elastomers/fabrics.

Two preliminary designs for a 10/40 MW_e pilot plant have been completed recently, one for a grazing plant by the Applied Physics Laboratory/Johns Hopkins University (APU/JHU) (14) and another for a spar platform by Gibbs & Cox, Inc. (15).

3. OSCILLATIONS IN LINE WITH THE FLOW

3.1 Resonant response characteristics. In the context of vortex-induced oscillations one usually thinks of vibrations lateral to the incident flow since the shedding of vortices produces periodic

forces in the cross flow direction at a frequency near the Strouhal value for vortices of the same sign. The in line component of the periodic force, which occurs at twice the Strouhal frequency, is typically an order of magnitude less than the cross flow component and, in wind, rarely excites the structure due to the small density of air. With the increased utilization of lightly-damped bluff structures in water, the likelihood of in line oscillations has been increased because of the larger fluid density and because of the lower velocities at which the vibrations are initiated.

Investigations of the in line oscillations of bluff cylinders began as a result of the troublesome and damaging vortex-induced oscillations of pilings during the construction of an oil terminal in England during the late 1960's. A description of the problems encountered at the construction site has been given by Sainsbury and King (16) and a discussion of subsequent full-scale experiments to ascertain the causes of the vibrations has been reported by Wootton, Warner, Sainsbury and Cooper (17).

A cylindrical bluff body is excited into cross flow oscillations when the reduced velocity reaches a value of $V_r = V/f_n D \cong 3.5$ to 5. This critical velocity is the reciprocal of the Strouhal number ($St = f_s D/V = 0.20$ to 0.29) evaluated at the condition $f_s \cong f_n$, where f_n is a natural frequency of the body. In line oscillations might be expected to occur at $V_r = 2.5$ since the periodicity in the drag fluctuations occurs at $2f_s$, or twice the Strouhal frequency. However, the in line oscillations occur over a range $V_r = 1.5$ to 4.0 and in two distinct resonant instability regimes separated by $V_r = 2.5$. The response in each of the two regions depends strongly on the non-dimensional parameter

$$k_s = \frac{2m\delta}{\rho D^2} \tag{3.1}$$

often called the "reduced damping", which is the product of the logarithmic decrement δ of the structural damping and the ratio of the mass of the structure per unit length to the displaced fluid mass per unit length (see Section 4). Typical laboratory-scale measurements of the dependence of the in line displacement amplitude upon both V_r and k_s are plotted in Fig. 3.1. An analogous dependence upon k_s for the cross flow displacement amplitude of oscillation in both air and water is well known for a wide variety of bluff cylindrical structures. The in line oscillations reach displacements of only about 0.25D peak-to-peak even at very low damping, whereas cross flow amplitudes of oscillation are known to reach 2 to 3D when the damping is small (see Fig. 9). Typical calculations of in line displacement amplitudes from the results in Fig. 3.1 are given in Example 3.1. The first three successive instability regions for both in line and cross flow motions are shown schematically in Fig. 3.2. All available evidence suggests that in line oscillations do not occur for values of the reduced damping $k_s > 1.2$. Also, a limiting lower Reynolds number for the onset of vortex-excited, in line oscillations in water is about Re = 1200 to 1500 (3).

Example 3.1 Calculation of the peak in line displacement amplitude $\bar{x}_{MAX}$ and the magnitude of the corresponding relative flow velocity $V/_{\bar{x}_{MAX}}$ for a cantilevered cylinder in water; from reference 19.

PROBLEM STATEMENT:

A slender, flexible circular cylinder with a 1 inch outside diameter is cantilevered normal to flowing water and is submerged over 73 percent of its length (19). The data plotted in Fig. 3.1 were taken from experiments conducted with this particular cylinder.

RESULTS REQUIRED:

(a) The magnitude V of the flow velocity that is associated with the peak in line displacement amplitude shown in Fig. 3.1;

(b) The peak in line displacement amplitude $\bar{x}_{MAX}$ at the water surface.

Step One:

The required value of V will be computed from equation (5.2),

$$V/_{\bar{x}_{MAX}} = (f_n D)\ V_r.$$

It is necessary to know the appropriate values of the reduced velocity V_r, the cylinder diameter D and the cylinder's natural frequency f_n. These data are available in Fig. 3.1 and reference 19. The peak in line displacement amplitude $\bar{x}_{MAX}$ was measured (in one case) for a cylinder with reduced damping $k_s = 0.38$ as noted in the figure, so that:

Reduced velocity $V_r = 2.2$ (at $\bar{x}_{MAX}/D$),
Peak displacement amplitude $\bar{x}_{MAX}/D = 0.12$.

In addition, from reference 19:

Cylinder diameter $D = 1$ in,
Natural frequency $f_n \approx 10$ Hz (in water), for $k_s = 0.38$.

Step Two:

The magnitude V of the relative flow velocity at the peak displacement amplitude is

$$V = (f_n D)\, V_r.$$

$$\therefore\ V = 10 \times (1/12) \times 2.2 \text{ ft/sec} = \underline{1.8 \text{ ft/sec}}$$

$$V = \underline{1.08 \text{ knots}}.$$

Step Three:

The peak displacement amplitude $\bar{x}_{MAX}/D$ in Fig. 3.1 is

$$\bar{x}_{MAX}/D = 0.12.$$

$$\therefore\ \bar{x}_{MAX} = 0.12 \times (1/12) \text{ ft} = \underline{0.01 \text{ ft}}$$

Two distinct flow patterns have been observed for the two resonant regions of the in line response. For $V_r < 2.5$ the flow is characterized by the shedding of two vortices of opposing sign from opposite sides of the cylinder during one motion cycle, while for $V_r > 2.5$ a single vortex is shed during each motion cycle and a street of alternately rotating vortices is formed downstream of the cylinder. Two such flow regimes had been postulated by Wootton et al (9) in trying to explain the appearance of two in line instability regions during the full-scale field

experiments at Immingham. The amplitude and frequency regions over which the in line vibrations control the vortex shedding are plotted in Fig. 3.3, taken from Griffin and Ramberg (20).

3.2 Hydrodynamic loads. Measurements of the steady and unsteady hydrodynamic loads due to in line oscillations have been made primarily by King (3,19). The magnitudes of the fluctuating in line force coefficiencts are plotted in Figs. 3.4 and 3.5 for the two instability regions shown in Fig. 3.1. The drag coefficient C_d' increases linearly with the displacement amplitude in each of the two instability regions. Measurements of the force coefficients in Figures 3.4 and 3.5 were made in tests conducted with smooth flexible cylinders vibrating in the fundamental and second normal modes. The Reynolds numbers of the experiments, however, are quite small, typically in the range of Re $\approx 5(10^3)$.

The steady drag coefficient C_D was also measured by King (3,19). At the Reynolds numbers just noted, the drag coefficients were obtained for flexible cylinders vibrating in line with the steady current. Typical mean values of $C_D = 1.26$ were measured with the vibrating cylinder. The oscillatory motion was superimposed upon a steady or quasi-steady deflection of the flexible cylinder due to the vortex shedding. Measurements of the in line oscillations and the accompanying forces have been made by King and Johns (21) for the case of two flexible cylinders, one in the wake of the other at various downstream distances. These experiments were performed in the same Reynolds number range as had been employed for the single cylinder tests.

3.3 Reynolds number effects and full-scale experiments. King obtained excellent agreement between measurements on a 1/27-scale model and a full-scale marine pile 457mm (18 in) diameter which was characterized by a Reynolds number of $6(10^4)$. These experiments are compared in Fig. 3.6. Both cylinders had very nearly the same combination of mass and damping parameters, with k_s (model) = 0.30 and k_s (full-scale) = 0.32. Some typical calculations of

k_s for the model are given in Example 3.2. Hardwick and Wootton (22) also obtained good agreement between model experiments and the Immingham field test data. An example of their comparison is given in Fig. 3.7. The Reynolds number range of the model experiments was Re = $6(10^3)$ to $20(10^3)$ while the full-scale measurements were made at Re = $2(10^5)$ to $6(10^5)$. The slightly greater displacement amplitudes of the model are due to its lower structural damping. Hardwick and Wootton suggest that the higher reduced velocities of the model are due to a slight effect of Reynolds number.

Example 3.2 Calculation of the reduced damping parameter k_s for a 1/27-scale model of a cantilevered marine piling; from reference 18.

PROBLEM STATEMENT:

A slender, flexible circular cylinder with a 0.68 inch outside diameter is cantilevered normal to flowing water as in Example 3.1. The hollow cylinder is made of PVC and filled with a mixture of water and sand to achieve the correct specific gravity (18). This example cylinder is the 1/27-scale model employed to obtain the data plotted in Fig. 3.6.

RESULTS REQUIRED:

(a) The effective mass m_e of the cylinder; this is the sum of the structural mass, the mass of the fluid-solid mixture inside the cylinder, and the added mass of the strucuture;

(b) The reduced damping parameter k_s of the flexible, cantilevered cylinder.

Step One:

The effective mass m_e (per unit length) will be calculated from equation (5.1), which is

$$m_e = m_s \text{ (structure)} + m_w \text{ (mixture in pipe)} + m_a \text{ (added mass)}.$$

The required data are given in Fig. 3.6 and reference 18, and are:

Structure effective mass m_s = 0.11 lb_m/ft,
Enclosed mass of water/sand in the cylinder, m_w = 0.21 lb_m/ft,
Diameter D = 0.68 in,
Log Decrement δ * = 0.067,

* For this example the log decrement is based upon the damping as measured in still water (18). To precisely calculate the structural damping the hydrodynamic damping should be subtracted from the listed value, δ = 0.067.

Step Two:

Assume that the added mass term is given by $m_a = (\pi/4)\,\rho_w D^2 C_{am}$ where the water density (fresh) $\rho_w = 62.4\ \mathrm{lb}_m/\mathrm{ft}^3$ and the added mass coefficient $C_{am} = 1$.

The added mass m_a and the total effective mass m_e can now be calculated.

$$\therefore\ m_a = (\pi/4) \times 1 \times 62.4 \times \left(\frac{0.68}{12}\right)^2 \mathrm{lb}_m/\mathrm{ft} = \underline{0.16\ \mathrm{lb}_m/\mathrm{ft}}$$

and

$$m_e = m_s + m_w + m_a = 0.11 + 0.21 + 0.16 = \underline{0.48\ \mathrm{lb}_m/\mathrm{ft}}$$

Step Three:

The required value of the reduced damping parameter k_s is given by equation (3.1),

$$k_s = \frac{2m_e\delta}{\rho_w D^2}\ .$$

From the data listed above, and the value of m_e just calculated, k_s is calculated as

$$k_s = (2 \times 0.48 \times 0.067)/(62.4 \times (0.68/12)^2)$$
$$= \underline{0.32}.$$

It is important from an applications standpoint to note that the vortex-excited instability in line with the flow is initiated at a flow speed ($V/f_nD = 1.2$) that is about *one-fourth* of the flow speed ($V/f_nD = 3.5$ to 5) at which the cross flow instability is initiated.

4. CROSS FLOW OSCILLATIONS

4.1 Resonant response characteristics. Measurements of the frequencies, displacements and forces which result from cross flow oscillations have been obtained by many investigators from experiments both in air and in water. In this section, the most recent of these experiments are summarized. Typical measurements for three spring-mounted cylinders in water are presented in Fig. 4.1. The results obtained are generally the same in both air and water; as the incident flow speed V, or the reduced velocity V_r as in Fig. 4.1, is increased the displacement amplitude first builds up to a maximum, after which it begins to decrease as the upper limit of the lock-on range between the vortex and vibration frequencies is approached. For the example shown in

the figure the limits between which the vibration displacements are above their resonant threshold amplitude ($\bar{Y} = 0.05D$) are given by $V_r = 5.5$ and 7.5, with the peak displacement occuring at $V_r \sim 6$. Note that the frequency of the oscillation is very nearly constant at a value close to the system's natural frequency f_n. This constitutes the familiar lock-on behavior that is characteristic of vortex-excited oscillations. Dean, Milligan and Wootton (24), while studying experimentally the response of flexible model offshore structures in flowing water, obtained limits of V_r between 4 and 8, with the maximum crossflow response measured near $V_{r,MAX} = 6$. This overall pattern of behavior is typical of measurements in water and similar fluids at *all* Reynolds numbers where vortex shedding takes place.

The inverse of the reduced velocity V_r or the Strouhal number corresponding to the peak vortex-excited displacement is plotted as the solid line in Fig. 4.2, adapted from the results of Wootton (25). The Reynolds numbers are typical of the range in which a large OTEC cold water pipe might operate. For the results in the figure the shedding frequency f_s was locked onto the natural frequency f_n of the cylinder, and the dashed line in represents the value of St corresponding to the initiation of lock-on. The cross flow motions of several full-scale cylinders are plotted in Fig. 4.3, from the results of Sainsbury and King (16). The data were taken from visual observations at the Immingham site but they clearly show the large displacement amplitudes that can be expected in water for long, flexible cylinders. The Reynolds numbers for the experiments in Fig. 4.3 were somewhat larger than 10^6, which approaches the range of OTEC applications. Cross flow oscillations greater than $\bar{Y}/D=0.1$ were initiated at $V_r = 3.5$ to 4, which agrees with the results in Figure 4.2. These large-amplitude oscillations were found to occur even though the incident current varied in magnitude from 2.4 m/s to 0.6 m/s and in horizontal direction by as much as 40° over the immersed length of the cylinder (18 to 29m). As noted recently by Dean and Wootton (26), full-scale data on the cross flow response of

cylinders are quite limited because large-amplitude motions lead to failure within a few cycles of the oscillations.

When Reynolds and Froude number effects are minimal, the peak vortex-excited displacement amplitude in the cross flow direction can be expressed from dimensional analysis as being dependent on three quantities, viz.

$$Y_{MAX} = f\left[\frac{f_s}{f_n}, \zeta_s, \mu\right]. \tag{4.1}$$

Here f_s/f_n is the ratio of the Strouhal and structural frequencies $f_s = St\ V/D$ and f_n, respectively; and ζ_s is the *structural* damping ratio. The parameter μ is a mass ratio, defined by $\mu = \rho\ D^2/8\pi^2 St^2 m$, which also results from the normalization of the force coefficients in the governing equation of structural motion as shown by Griffin and Koopmann (27) and Sarpkaya (28), for example. When there is a dependence upon Reynolds number, say between a laboratory model and a full-scale prototype, the "size number" or the product of the Strouhal and Reynolds numbers should be modeled as closely as possible. This parameter is given by

$$St\ Re = \frac{f_n D^2}{\nu}. \tag{4.1a}$$

In the preceding section it was noted that the peak in line displacement amplitude is a function primarily of a response or reduced damping parameter of the form

$$k_s = \frac{2m\delta}{\rho D^2}. \tag{3.1}$$

This formulation of the reduced damping can be written in the analogous form

$$\zeta_s/\mu = 2\pi\ St^2 k_s \tag{4.2}$$

when the damping is small and $\zeta_s = \delta/2\pi$. The importance of the reduced damping follows directly from resonant force and energy balances on the vibrating structure, as shown by Griffin (23) and Sarpkaya (4,28), for example. Moreover, the relation between Y_{MAX} and k_s or ζ_s/μ

holds equally well for flexible cylindrical structures with normal mode shapes given by $\psi_i(z)$, for the ith mode. If the cross flow displacement (from equilibrium) of a flexible structure is written as (see Appendix 4.1)

$$y_i = Y \psi_i (z) \sin \omega t \tag{A20}$$

at each spanwise location z, then the peak displacement is scaled by the factor (23,29,30)

$$Y_{EFF,MAX} = Y I_i^{1/2} / |\psi_i(z)|_{MAX} = Y/\gamma_i \tag{4.3a}$$

where

$$I_i = \frac{\int_0^L \psi_i^4 (z)\, dz}{\int_0^L \psi_i^2 (z)\, dz} \tag{4.3b}$$

and

$$\gamma_i = \frac{|\psi_i(z)|_{MAX}}{I_i^{1/2}} \tag{4.3c}$$

which is derived from considerations based on several versions of the so-called "wake oscillator" formulation (29,30).

Example 4.1 Calculation of the effective cross flow displacement amplitude $Y_{EFF,MAX}$ and the corresponding reduced damping ζ_s/μ as plotted in Fig. 4.4. The example given here is typical of one series of steps in the procedure to be employed in calculating the current-excited cross flow displacement amplitude of an OTEC cold water pipe.

PROBLEM STATEMENT:

Consider the case of a flexible circular cylinder with clamped-clamped end conditions, vibrating in the fundamental ($i = 1$) mode. This type of model was employed in a series of experiments conducted in flowing water by Dean, Milligan and Wootton (24) to study the vortex-excited oscillations of cylinders.

RESULTS REQUIRED:

(a) The reduced damping parameter ζ_s/μ as given by the horizontal scale in Fig. 4.4;

(b) The effective cross flow displacement amplitude $Y_{EFF,MAX}$ as given by the vertical scale in Fig. 4.4.

Step One:

The required value of ζ_s/μ is calculated from equation (4.2),

$$\zeta_s/\mu = 2\pi St^2 k_s,$$

where k_s is the reduced damping parameter of the form given in Example 3.2 and St is the Strouhal number. The data needed are given by Dean, Milligan and Wootton, so that from reference 24:

Reduced damping $k_s = \dfrac{2m\delta}{\rho D^2} = 1.27$

Displacement amplitude $\bar{Y}_{MAX} = 0.94$ in
Diameter $D = 1$ in
Strouhal number $St = 0.2$

For a cylinder with length/diameter ratio $L/D = 240$.

Step Two:

The reduced damping ζ_s/μ is now calculated from the above equation.

$$\therefore \zeta_s/\mu = 2\pi \times (0.2)^2 \times 1.27 = \underline{0.32}$$

Step Three:

The required value of $Y_{EFF,MAX}$ is calculated from equations (4.3),

$$Y_{EFF,MAX} = Y/\gamma_i, \quad Y = Y_{MAX}/D \tag{4.3a}$$

and

$$\gamma_i = \frac{|\psi_i(z)|_{MAX}}{I_i^{1/2}}. \tag{4.3c}$$

Here Y is the ratio of the measured cross flow displacement amplitude $\bar{Y}$ and the diameter D. γ_i is a modal scaling factor given by equation (4.3c). Some required data not listed above now can be obtained from Table A1 where values of $I_i^{1/2}$ and the equations for $\psi_i(z)$ are listed.

From Table A1:

For the case of a flexible cylinder with clamped-clamped end conditions, in the first bending mode ($i = 1$), the data are:

Modal scaling factor $I_i^{1/2} = 1.360$,
Characteristic function $|\psi_1(z)|_{MAX} = 1.586$ (half way along the beam, at $\bar{z}/L = 0.5$).

$$\therefore \gamma_1 = 1.586/1.360 = \underline{1.17}$$

The scaled displacement amplitude $Y_{EFF,MAX}$ is now calculated.

$$\therefore Y = \bar{Y}/D = 0.94\text{in}/1\text{ in} = 0.94$$

$$Y_{EFF,MAX} = Y/\gamma_1 = 0.94/1.17 = \underline{0.8}$$

This point is plotted in Fig. 4.4 and is denoted by the symbol (◪).

Experimental data for Y_{EFF} as a function of ζ_s/μ are plotted in Fig. 4.4. These results encompass a wide range of single cylinders of various configurations and flexure conditions at Reynolds numbers from 300 to 10^6. The various types of structures represented by the data points are given in Table 4.1. As a typical example, King (19,31) measured the deflections of a flexible cantilever in the fundamental mode. Peak-to-peak displacements as great as 2 to 4 diameters were measured for length/diameter ratios up to 20 to 30. The latter are typical of the OTEC cold water pipe. All available experiments to date indicate that the limiting unsteady displacement for a flexible, circular cylindrical structure is about $2Y_{EFF} \approx 2$ to 3 at low values of reduced damping. Note that for low values of ζ_s/μ the vortex-excited response is dominated by fluid dynamic forces. For ζ_s/μ between 0.03 and 0.5 the reduced damping increases by a factor of *sixteen* while the peak displacement amplitude decreases only by a factor of *two.*

Table 4.1. Vortex-excited cross flow displacement amplitude response of cylindrical structures.

Legend for Data Points in Fig. 4.4	
Type of cross-section and mounting; medium	Symbol
Various investigators, from Griffin (23):	
Spring-mounted rigid cylinder; air	• ○ ⊣ ◐
Spring-mounted rigid cylinder; water	♦
Cantilevered flexible circular cylinder; air	Δ
Cantilevered flexible circular cylinder; water	× ▽ ⊕
Pivoted rigid circular rod; air	□ ▲
Pivoted rigid circular rod; water	●
From Dean, Milligan and Wootton (24):	
Spring-mounted rigid cylinder; water	◩
Flexible circular cylinder ($L/D = 72$); water	◪

These results have been obtained both in air and in water, even though the mass ratios of vibrating structures in the two media differ by two orders of magnitude. For typical structures vibrating in water the mass ratio $\frac{2m}{\rho D^2}$ varies from slightly greater than 2 to about 10; in air the

mass ratios corresponding to Fig. 4.4 typically vary from $\frac{2m}{\rho D^2} = 30$ to 1000. The maximum unsteady displacement to which a given system can be excited is a function of the reduced damping, the product of the mass ratio and the structural log decrement or damping ratio. Sarpkaya (32) has demonstrated that an analogous dependence between $Y_{EFF,MAX}$ and k_S or ζ_s/μ is obtained for flexible structures vibrating in planar oscillatory flows which approximate the ocean wave environment under certain conditions.

4.2 Hydrodynamic loads. When a cylindrical body resonantly vibrates due to vortex shedding, the periodic motion is accompanied by increased coherence of the vortex shedding longthwise along the body and an amplification of the unsteady fluid forces. Though a number of measurements of the forces have been made, only recently has attention been given to understanding the mechanisms by which this fluid-structural interaction force is generated (4,33,34) and how results may be scaled with confidence to large Reynolds numbers (35). Further insights into the behavior of the steady and unsteady fluid loadings due to vortex shedding are important to the designer of offshore structures and cable systems from a purely practical standpoint, and from a basic standpoint it is important to further understand the complex nonlinear interactions between a vibrating bluff body and its wake.

The fluid forces which act on a resonantly vibrating, cylindrical structure due to vortex shedding have been characterized recently (23,27,36) and the various components of the total hydrodynamic force are:

- The exciting force component, by which energy is transferred to the structure;
- The reaction, or damping force, which is exactly out-of-phase with the structure's velocity;

- The "added mass" force, which is exactly out-of-phase with the structure's acceleration; and

- The flow-induced inertial force.

The various components can be deduced from the total hydrodynamic force as measured, say, by Sarpkaya (4,28) or the various components can be measured individually as shown by Griffin and Koopmann (27). This point is discussed at greater length in Appendix 4.1.

Some practical and useful comparisons can be made between the fluid forces measured when a cylinder is forced to vibrate and the fluid forces measured when the cylinder is resonantly excited by vortex shedding. The forced cylinder measurements discussed here were made in water by Sarpkaya (4,28) and Mercier (37) and the self-excited cylinder measurements were made in air and in water by Griffin and Koopmann, King and others listed in Table 4.3 (see reference 23).

Typical measurements reported by Sarpkaya appear in Figs. 4.5 through 4.8. The measured values for the inertia coefficient C_{mh} are shown in Figs. 4.5 and 4.7 as a function of the reduced velocity V_r, for displacements from equilibrium of $Y = \overline{Y}/D$ 0.5 and 0.75. Of particular note is the marked variation in C_{mh} in the vicinity of $V_r = 5$. This effect corresponds to the large phase shift in the fluid force relative to the vibratory displacement when the characteristic frequency of the flow is locked onto the vibration frequency. The fluid force on the cylinder is dominated by inertia contributions at the cylinder frequency at low reduced velocities. Measurements by Bearman and Currie (33) of the phase between the pressure at 90 degrees from the front stagnation point and the cylinder's displacement confirm this large inertia effect at low V_r.

The drag or resistance force C_{dh} is plotted in Figs. 4.6 and 4.8 as a function of V_r at the same displacements, $Y = 0.50$ and 0.75. This component of the total fluid dynamic force is negative and becomes dominant near $V_r = 5$. In effect, C_{dh} is the *negative of the lift coefficient as it is usually characterized*, so that the negative value of C_{dh} near $V_r = 5$ suggests a net transfer of energy to the cylinder in that region. These forced-cylinder results are comparable to the vortex-excited forces which act upon resonantly vibrating cylinders when the reduced damping is sufficiently small as in the left-hand portion of Fig. 4.4.

Example 4.2 Calculation of the excitation force coefficient C_{LE} (see equation (A10a)) from measurements of the hydrodynamic force coefficients during *lock-on*. The force represented by C_{LE} transfers energy to the structure during vortex-excited oscillations.

PROBLEM STATEMENT:

The excitation force, which is in phase with the velocity $\dot{y}$ of a vibrating structure, is the component of the total fluid dynamic force system that transfers energy to the structure (see Appendix 4.1.2). The excitation force coefficient C_{LE} (Equation (A10a)) can be calculated from measured force coefficients such as those represented by the data plotted in Figs. 4.6 and 4.8.

RESULTS REQUIRED:

(a) The phase angle ϵ between the force coefficient C_{dh} (see Fig. 4.8) and the excitation force coefficient C_{LE};

(b) The excitation force coefficient C_{LE} for typical conditions of *lock-on*.

Step One:

The required value of the phase angle ϵ is given by equation (A15) of Appendix 4.1,

$$\epsilon = \arctan\left(\frac{C_{mh}\ W + C_{dh}}{C_{mh} - W\ C_{dh}}\right).$$

The data for the calculation are obtained from Table 4.4. Choose the case $\bar{Y}/D = 0.75$ and $V_r = \dfrac{V}{f_n D} = 5$, so that for these conditions:

Inertia coefficient $C_{mh} = 1.0$ to 2.6,
"Drag" coefficient $C_{dh} = -0.6$,
Angle function* $W = 0.05$.

* Here W is a parameter based upon the structural parameters of a vibrating system, see equation (A23c) in Appendix 4.1.

Step Two:

The phase angle ϵ is calculated with the above equation, and is

$$\epsilon = \text{arc tan}\left(\frac{1.0 \times 0.05 + (-0.6)}{1.0 - 0.05 \times (-0.6)}\right) \text{ to arc tan}\left(\frac{1.6 \times 0.05 + (-0.6)}{2.6 - 0.05 \times (-0.6)}\right).$$

$$\therefore \epsilon = \underline{-28.1° \text{ to } -10.2°}.$$

Step Three:

The excitation force coefficient C_{LE} for the chosen conditions is given by equation (A10a) of Appendix 4.1,

$$C_{LE} = -C_{dh} \cos \epsilon.$$

$$\therefore C_{LE} = -(-0.6) \cos(-28.1°) \text{ to } -(-0.6) \cos(-10.1°)$$

$$C_{LE} = \underline{0.53 \text{ to } 0.59}$$

These points are plotted in Fig. 4.9 and are denoted by the symbol (0).

It should be noted that C_{mh} and C_{dh} are Fourier-averaged coefficients and contain only the components of the total fluid force at the vibration frequency f. Considerable power is contained in the fluid force spectrum at other frequencies (i.e. $2f$, the Strouhal frequency f_s) for reduced velocities outside of the regime of locking-on between the vortex and vibration frequencies.

The excitation component of the lift force is defined as*

$$C_{LE} = C_L \sin \phi = -C_{dh} \cos \epsilon \quad \text{(A10a)}$$

and is important from the standpoint of energy transfer to the vibrating structure. The measurements in Figs. 4.5 through 4.8 are now compared to previous measurements by other investigators. The maximum value of the force coefficient $-C_{dh}$ in Fig. 4.6 occurs at $V_r = 5$, and similar results were obtained at the displacements $Y = 0.13$, 0.25, and 0.75. The several values of $-C_{dh}$ and C_{mh} so obtained are listed in Table 4.2 together with the related values of the force

* For a definition of the notation employed in this discussion see the List of Symbols and Appendix 4.1.

Table 4.2. Hydrodynamic Forces on Circular Cylinders; from Sarpkaya (28).

Displacement, $Y = Y/D$	Inertia Coefficient,++ C_{mh}	Drag Coefficient, C_{dh}	Reduced Velocity, $V_r = 5$. Phase Angle, $\beta' = \arctan [C_{dh}/C_{mh}]$	Fluid Force Components, Equation A10+ Excitation, $-C_{dh}\cos\epsilon$	Damping, $-C_{mh}\sin\epsilon$	Inertia, $C_{dh}\sin\epsilon$
0.13	0.4	-0.2	-26.6°	0.18	0.18	0.089
0.25	0.4	-0.35	-41.2°	0.26	0.26	0.23
0.50	1.0 to 2.2	-0.9	-42° to -22.3°	0.67 to 0.83	0.67 to 0.83	0.67 to 0.83
0.75	1.0 to 2.2	-0.6	-28.8° to -11.9°	0.48 to 0.54	0.48 to 0.54	0.26 to 0.11

+ $\epsilon = \beta' + \gamma$ and $\gamma = \arctan W$, where $W = \dfrac{2\alpha\zeta_s}{1-\alpha^2}$, $\alpha = \dfrac{\omega}{\omega_n}$. In addition $W = 0.05$ is assumed (See Appendix 4.1).

++ The inertia coefficient is evaluated here in coordinates appropriate to a cylinder vibrating in a quiescent fluid or, equivalently, a fluid in uniform, steady motion.

components derived from them. For all of these cases of forced vibration the condition for self-excitation

$$C_{mh} - W C_{dh} > 0$$

is satisfied, thus assuring the possibility of the equivalent vortex-excited oscillation. The results for C_{LE} are plotted against the effective displacement in Fig. 4.9 together with a host of similar findings. The conditions under which the experiments were performed are described in Table 4.3.

The excitation component of the total hydrodynamic force, as just mentioned, is important because it is this component of the fluid force system that transfers energy to the structure and drives the vibration. A number of measurements of C_{LE} by various means are plotted in Fig. 4.9, and Table 4.3 describes the various conditions under which the experimental results were obtained. Several important characteristics of the unsteady lift and pressure forces that accompany vortex-excited oscillations are clear from the results. First there is a *maximum* of the exciting force coefficient at a peak-to-peak displacement between 0.6 and 1 diameters for all the cases shown in the figure. Second, the maximum of the force coefficient is approximately $C_{LE} =$ 0.5 to 0.6 for all but one case, the sole exception being the result at $C_{LE} =$ 0.75. C_{LE}

Table 4.3. The Excitation Force Coefficients on Vibrating Bluff Cylinders; Description of the Data in Figure 4.9

Symbol	Type of cylinder	Medium	Cylinder material	Investigator(s)
▲ ■	Flexible cantilever	Water	PVC PVC Aluminum Stainless steel	King (1977)
●	Pivoted rigid cylinder	Water & Air	Brass	Vickery and Watkins (1964)
+	Spring-mounted rigid cylinder	Air	Aluminum tubing	Griffin and Koopmann (1977)
□	Rigid cylinder, forced oscillations	Water	Stainless steel	Mercier (1973)
○	Rigid cylinder, forced oscillations	Water	Aluminum tubing	Sarpkaya (1978)
Δ	Flexible cantilever	Air	Aluminum	Hartlen, Baines and Currie (1968)

then decreases toward zero in all cases and results in a limiting effective displacement of 2 to 3 diameters (peak-to-peak). This limit is clearly shown by the displacement amplitudes measured at low reduced damping in Fig. 4.4.

The decomposition of the fluid dynamic forces described here is based upon the supposition that both flow-induced lift (excitation) and reaction (damping) forces act on a resonantly vibrating tube or cylinder. The "wake-oscillator" models developed by Blevins (3) and others are also based upon the hypothesis of a fluid damping or reaction force that is exactly out-of-phase with the cylinder's velocity. It is possible to deduce the reaction effect of the fluid from the measured force coefficients by means of the equations developed in Appendix 4.1,

$$C_{RE} = C_R \sin\phi_1 = -C_{mh} \sin\epsilon, \tag{A10c}$$

as a further step in comparing the two approaches described there. Some typical results are plotted in Fig. 4.10 and they support the fluid force decomposition described in Appendix 4.1. All of the measurements show the same general pattern of behavior even though some were made with freely vibrating cylinders in a wind tunnel and some were made with cylinders that were forced to vibrate in water.

The remaining force components, the added mass and the fluid inertia, can be obtained from the equations given in Appendix 4.1 when the force coefficients and the structural parameters of a cylindrical structure and its mountings (i.e., damping, natural frequency) are known. A detailed and related discussion of the forces and displacements that result from lock-on is given by Sarpkaya (4).

Not only are the unsteady forces amplified as shown in the preceding figures but the steady drag loads also are increased substantially as a result of vortex-excited oscillations. Sarpkaya (28) has measured steady drag coefficients as high as $C_D = 3.1$ for a cylinder vibrating in water at a displacement of $2Y_{MAX} = 1.7$. This represents an increase of nearly a factor of *three* from the drag on a stationary cylinder, i.e. $C_{DO} = 1.1$ in his case. Griffin, Skop and Koopmann (38) found that the drag coefficient was increased by as much as a factor of 1.8 from the stationary cylinder case ($C_{DO} = 0.9$) for their experiments plotted in Figs. 4.4 and 4.9. The steady drag amplification on circular cross-section cylinders due to vortex-excited oscillations is plotted in Fig. 4.11. The solid line on the figure is a least-squares fit to the data points (see Section 5.2).

4.3 Roughness and shear effects. Other factors also influence the hydrodynamic forces that result from vortex-excited oscillations, and among these are surface roughness and non-uniform velocities (shear). Sarpkaya (39) has measured the hydrodynamic forces on sand-roughened, forced

vibrating cylinders and has compared his measurements to comparable experiments with a smooth cylinder. Some typical results for the *total* hydrodynamic force coefficient $C_{T,MAX}$ are plotted in Fig. 4.12. Substantial increases are apparent in the total hydrodynamic force coefficient for the rough cylinder, though additional study is necessary to determine which components of the total force are amplified by the roughness. Nakamura (40) has measured the steady drag forces and Strouhal frequencies on rough circular cylinders at supercritical Reynolds numbers, and *has observed strong regular vortex shedding at* Re $\approx 4(10^6)$ *and above.* In this Reynolds number range the vortex-excited cross flow displacement amplitude of a rough cylinder *increased substantially* from the corresponding smooth cylinder experiment. This finding would tend to confirm Sarpkaya's measurements of amplified hydrodynamic forces due to surface roughness in addition to the force amplification due to lock-on. A comprehensive study of the effects of surface roughness on the steady drag was made by Miller (41) for the case of a stationary cylinder, and a recent OTEC program report considers this problem in some detail (42).

The effects of velocity gradients (shear) are difficult to quantify on the basis of available evidence, especially for structures which are vibrating. However, the sparse information that is available suggests that a full-scale cylindrical structure will vibrate at large displacement amplitudes even in the presence of non-uniform flow effects if the reduced damping is sufficiently small and the critical reduced velocity is exceeded (see Fig. 4.3). Some detailed experiments reported by Kwok and Melbourne (43) just recently give strong evidence that a flexible bluff structure with a circular cross-section will vibrate resonantly at large displacement amplitudes when a turbulent boundary layer type of shear flow is incident upon the cylinder. Kwok and Melbourne measured maximum tip displacements comparable to those in Fig. 4.4 for reduced dampings in the range $k_s = 2$ to 12 ($\zeta_s/\mu \sim 0.5$ to 3).

Stansby (44) investigated the phenomenon of lock-on for the cross flow vibrations of circular cylinders in a linear shear flow and has compared the results to comparable experiments in uniform flow. From these experiments Stansby developed empirical equations to predict the bounds for lock-on in a shear flow, based upon the assumption of universal similarity in the wakes of bluff bodies (34,35). However, these results are limited to cylinders with small length/diameter ratios (L/D = 8 to 16), relatively low Reynolds number (Re = 3000 to 10,000) and small displacement amplitudes ($\bar{Y}/D < 0.2$). Extrapolation of these results to OTEC applications should be approached with caution.

A recent paper by Fischer, Jones and King (45) describes some problems that were anticipated during the installation of foundation piles for the Shell Oil production platform in the Cognac field of the Gulf of Mexico. The problems stemmed largely from the predicted vortex-excited oscillations of the piles while they were being lowered from a derrick barge into sleeves in the platform base and while the inserted piles were being hammered into the sea bed. Maximum tip displacement amplitudes (cross flow) of 3.2 to 3.8 m (10.5 to 12.5 ft) from equilibrium were predicted for currents as low as 0.6 m/s (0.31 kt) at the platform site. These large-scale motions were expected to created difficulties while "stabbing" the piles into the sleeves, and they could also increase the risk of buckling and fatigue failures during the pile driving operations.

Experiments were conducted with model piles in three laboratories (45), for both the pile lowering and the pile driving operations. Uniform and non-uniform (shear) flows were modelled in the experiments. The shear parameter that characterizes a non-uniform flow is defined as

$$\bar{\beta} = \frac{D}{V_{REF}} \frac{\Delta V}{\Delta \bar{z}}, \tag{4.4}$$

where V is the magnitude of the incident flow velocity and $\bar{z}$ (in this case) in the depth of the water. The reference value V_{REF} is usually taken as the veolocity magnitude at half the distance along the structure, alhough the maximum value from a velocity profile is sometimes used. For the small-scale experiments reported by Fischer et al (45) the shear parameter was $\bar{\beta} = 0.01$ while at the actual Cognac site $\bar{\beta} = 0.01$ at depths between 100 m (330 ft) and 250 m (820 ft). Typical OTEC sites (Brazil offshore, Punta Tuna) are characterized by $\bar{\beta} = 0.01$ to 0.02 for a 9.2 m (30 ft) diameter cold water pipe.

The results from some typical model-scale experiments are plotted in Fig. 4.13. The tests were conducted with a 1:168 scale model of the large marine piles of diameter $D = 2.1$ m (6.9 ft). Both the full-scale and the model piles had specific gravities of 1.5. It is clear form the results in Fig. 4.13 that a shear flow with $\bar{\beta} = 0.01$ to 0.015 had virtually no effect on the vortex-excited displacement amplitudes in the cross flow direction. The data plotted in the figure correspond to a free-cantilever flexible beam with no tip mass at the free end. This configuration matched closely the "stabbed" pile before an underwater hammer was attached for driving it into the sea bed. The structural damping of the PVC model in Fig. 4.13 was $\zeta_s = 0.063$ and for a similar stainless steel model the damping was $\zeta_s \approx 0.015$; the two flexible cylinders experienced tip displacement amplitudes of $2\bar{Y} = 3D$ and 4D, respectively. These damping and displacement amplitude values would locate data points well toward the left-hand portion of Fig. 4.4 where hydrodynamic effects are dominant.

It was concluded from a study of the static and dynamic stress levels within the Cognac piles during driving that the large cross flow displacement amplitudes (of the level shown in Fig. 4.13) would triple the stresses from a corresponding stationary 130 m (426 ft) long pile (45). The apparent steady drag coefficient on the oscillating pile was $C_D = 2.12$; this is an

amplification of 230 percent from the drag coefficient $C_{DO} = 0.93$ when the pile was restrained. A fatigue life of four days was predicted for a stabbed pile (without a hammer attached) when it was exposed to a current of magnitude 0.46 m/sec (0.9 kt). Additional details and assumptions pertaining to the study are discussed in reference 45.

A flag-type or flexible tail fairing type of wake interference device was developed to suppress the cross flow oscillations. Such a device was tested successfully on the model piles, but the particular configuration was chosen because of the nearly unidirectional currents at the Cognac site (45). Few actual problems were encountered during the field installation, but in the case of one pile typical peak-to-peak displacement amplitudes of 3 m (9.8 ft) were measured. The cause of these cross flow oscillations was attributed to alternate vortex shedding.

A program of experiments recently was conducted to assess the effects of shear on vortex shedding from smooth and rough cylinders at large Reynolds numbers. The results were intended to be applicable specifically to the OTEC cold water pipe and have been reported by Rooney and Peltzer (46). The experiments were conducted with a cylinder of aspect ratio L/D = 16 at Reynolds numbers in the range of 1.5 (10^5) to 3 (10^5) in order to assess the minimum shear (as denoted by the shear parameter $\bar{\beta}$ given above) at which the characteristic lengthwise cellular vortex shedding pattern was initiated. An incipient cellular pattern of vortex shedding was observed at the weakest shear gradient, $\bar{\beta} = 0.007$, and persisted in stronger form over the test range to shear levels given by $\bar{\beta} = 0.04$. Most of the test runs, however, were carried out at values of the shear parameter, $\bar{\beta} = 0.007$ to 0.02, which are representative of OTEC site conditions. The results obtained by Rooney and Peltzer (46) provide a reasonably wide OTEC-applicable data base of circumferential mean pressure and vortex shedding frequencies for smooth and rough circular cylinders at subcritical, critical and supercritical Reynolds numbers.

The available evidence through 1978 relevant to shear flow effects on bluff bodies has been gathered in related OTEC cold water pipe report (42). More recent findings are given in the proceedings of the Fifth International Conference on Wind Engineering (see references 35 and 43) and in several of the references just cited.

4.4 Yaw or inclination effects. Yawed cylindrical structures are those which are inclined forward or backward in the plane of the incident flow. Many practical ocean engineering structures are inclined rather than normal to the incident flow; these include raked marine piles (see Fig. 4.3) and braced frame members of jacket structures. Two recent studies (47,48) have considered the effects of yaw upon the wakes of stationary and vibrating flexible cylinders. King (47) has studied the effects of yaw angle upon the criteria for the onset of vortex-excited oscillations and upon the steady drag forces acting on the structure. His study also includes a complete survey of previous studies on the subject through 1975. More recently Ramberg (48) has completed a detailed study of the combined effects of inclination and finite length (end conditions) on the vortex wakes of stationary and vibrating cylinders. Included in this study were the effects of yaw angle on the boundaries of the lock-on range for vibrating cylinders, and on the drag and pressure forces on stationary cylinders. The experiments of King and Ramberg covered the Reynolds number range from Re = 500 to $2(10^4)$.

Several conclusions were drawn from these investigations. Among the most important of King's findings was that yawing the structure *provides no protection against vortex-excited oscillations*, and sustained oscillations both in line and cross flow were recorded for yaw angles up to $\theta = 45°$ both into and away from the incident flow. The cylinder response was virtually the same whether the cylinder was inclined into or away from the flow, and a typical example (for inclination into the flow) is given in Fig. 4.14. There the reduced velocity V_r is based upon the normal component of the incident flow, $V \cos \beta$, where β is the angle between V and a plane

that is normal to the axis of the structure.* The lower peak displacement amplitudes again correspond to larger values of the reduced damping k_s. The yawed flexible cylinder results are plotted in Fig. 4.4 and are indistinguishable from the displacement amplitudes measured at normal incidence. The critical reduced velocities for the onset of in line and cross flow oscillations were once again found to be $V_r = 1.2$ and $V_r = 3.5$ to 5, with the appropriate velocity term being $V \cos \beta$.

King also made a detailed study of yaw angle effects on the drag coefficient of a stationary cylinder. This aspect of the investigation demonstrated that if the normal component of velocity, $V \cos \beta$, was employed as the velocity scale then a consistent value of drag coefficient C_D was obtained, and that C_D was equal to the equivalent value for a cylinder at normal incidence. Ramberg's findings suggest that the drag estimated in this way may be low and somewhat dependent on the experimental arrangement (48).

Ramberg undertook a detailed investigation of the flow around yawed cylinders with the primary objective being an examination of the Independence Principle and how it may be used correctly. This principle, as noted above, states that the proper velocity scale for characterizing the flow about and forces on bluff bodies is the component of the incident flow that is normal to the body. One conclusion of Ramberg's investigation was that the Independence Principle was not generally valid for stationary, yawed cylinders. It was found that the variation of the shedding frequency of the vortices deviated substantially from the Independence Principle for yaw angles greater than $\beta = 25°$ to 30°, and that the vortex shedding from stationary cylinders was strongly influenced by the end conditions.

A special case (one of only two) where the Independence Principle was found to apply

* The use of the normal component of velocity is called the "Independence Principle" and this is discussed in further detail later in this section.

was for the condition of lock-on between the vortex and the vibration frequencies. A typical example is shown in Fig. 4.15. The bounds for lock-on during cross flow oscillations are plotted for yaw angles up to 50° from normal incidence. The yawed cylinder results are in excellent agreement with comparable experiments performed with a cylinder positioned normal to the incident flow. The Reynolds number is low, but the general principle is demonstrated. The region inside the dashed lines and data points corresponds to the lock-on regime. The findings from Ramberg's investigation imply that the various methodologies for predicting vortex-excited oscillations at normal incidence can be applied with reasonable confidence to a cylinder at an angle of inclination to the flow. King's findings further suggest that such an extension of the results obtained at normal incidence is valid for flexible cylindrical structures in flowing water.

4.5 *Vortex coherence due to lock-on.* An important consequence of lock-on between the vortex and vibration frequencies is the greatly increased coherence or correlation of the vortex shedding along the length of the structure. Above a threshold cross flow displacement amplitude (typically $\overline{Y}/D = 0.05$ to 0.1) the shedding is in phase and the wake is nearly two-dimensional even at large Reynolds numbers. Koopmann (49) and Toebes (50) in experiments at low and high Reynolds numbers, respectively, were among the first to investigate the increased coherence of the shedding that accompanies lock-on. Koopmann's experiments were limited to Reynolds numbers below 300 but his flow-visualization photographs clearly showed that the vortex shedding was in phase along the vibrating cylinder when the cross flow displacement amplitude was above $2\overline{Y}/D = 0.1$. Toebes' experiments were conducted at much larger Reynolds numbers (Re $\sim$ 68,000), but detailed wake and pressure correlation measurements showed clearly that lock-on was accompanied by increased coherence of the shedding along the cylinder. The magnitude of the cross correlation function was reduced to values below unity only by the

effects of turbulent fluctuations in the wake, and the sign of the cross correlation measured along the cylinder indicated that the shedding was in phase for distances up to seven and one-half diameters when the displacement amplitude was above $2\bar{Y}/D = 0.16$. The results of these studies were limited by the relatively small length/diameter ratios, L/D = 7.5 to 12, that were possible. Novak and Tanaka (55) and Howell and Novak (56) also have investigated the effects of turbulence in the incident stream on the correlation effects that accompany lock-on. Smooth flow experiments were conducted by them to provide a baseline for comparison with the effects of various kinds of turbulence introduced into the incident flow. Blevins and Burton (57) have developed an empirical model for predicting the vortex-excited resonance, and this model takes account of the variation in correlation length at small displacement amplitudes.

Detailed investigations of the spanwise coherence that accompanies lock-on were made recently by Ramberg and Griffin (51,52). These experiments were conducted to investigate the wakes of vibrating cables as part of a overall program to develop a semi-empirical "wake-oscillator" model for predicting the cross flow response of structures (53,54). The spanwise correlation coefficient ρ_{AB} measured between two hot-wire probes in the wake of a vibrating cable is plotted in Fig. 4.16. There the normalized cross correlation function (correlation coefficient) for two periodic signals, measured at the spatial displacement Δz, is given by

$$\rho_{AB}(\Delta z) = \frac{\frac{1}{T}\int_0^T u_A(z,t)\,u_B(z+\Delta z,t)\,dt}{\sqrt{\frac{1}{T}\int_0^T u_A^2(z,t)\,dt}\;\sqrt{\frac{1}{T}\int_0^T u_B^2(z+\Delta z,t)\,dt}}$$

where u_A and u_B are the fluctuating velocity signals at probes A and B in the near wake of the cable (54). The correlation coefficient ρ_{AB} can also be defined in terms of the pressure fluctuations measured at two taps at varying displacements along a cylinder (56). Both probes were positioned above the cable so as to measure vortices of like sign and one probe was moved in a

direction parallel to the cable, which was vibrated at different displacement amplitudes. The results shown in the figure correspond to vibration frequencies equal to 90 percent of the Strouhal frequency f_s. There are three distinguishing characteristics of the correlation in vortex shedding along the cable (53). The shedding is in phase along the cable's half-wavelength as shown by the constant *sign* of the correlation coefficient ρ_{AB}. If the moveable probe was traversed past the node of the cable, a change in sign of ρ_{AB} was observed. The *degree* of the correlation was determined by the maximum value of ρ_{AB} (relative to unity) along the cable and the *extent* of the correlation was defined as the length along the cable that ρ_{AB} was equal to its maximum constant value. Typically it was observed that the $\rho_{AB,MAX} \approx 0.90$ to 0.96 for the frequencies that correspond to vortex-excited oscillations, $f \leq f_s$ as shown in Table 4.4. The vortex shedding was fully correlated in *degree* and *extent* over most of the half-wavelength of the cable (L = 12 to 14 D) where the displacement amplitude was greater than a threshold of $\bar{Y}$ = 0.05 to 0.1D.

Table 4.4. The degree of correlation (denoted by the maximum value of the correlation coefficient P_{AB}) in the wake of a vibrating cable; from reference 53.

Reynolds number = 1300		
Frequency ratio, f/f_s	Displacement amplitude, $2\bar{Y}/D$	Degree of correlation, $\rho_{AB,MAX}$
0.9	0.1	0.89
	0.2	0.94
	0.3	0.96
	0.4	0.96
	0.5	0.92
	0.6	0.92
1.0	0.1	0.88
	0.2	0.96
	0.3	0.96
	0.4	0.97
	0.5	0.97
	0.6	0.96

A further study of the coherence of the vortex shedding in the wake of a flexible cable was conducted by Ramberg and Griffin (54). It was found from spectral analysis of the vortex shedding that the component of the fluctuating pressure or velocity at the cable frequency was 15 to 20 times the component at the Strouhal frequency. The spanwise correlation coefficient ρ_{AB} attained values comparable to those shown in Table 4, as shown in Fig. 4.17. Note that magnitude of the spectral component C_n in Fig. 4.17 follows the distribution in displacement amplitude along the cable; this and other similar observations suggest that predictive models for vortex-excited oscillations can be correctly based upon local conditions, i.e. lift and drag forces, so long as the vortex and vibration frequencies are *locked-on.* As a practical matter it is reasonable to assume that at large displacement amplitudes the vortex shedding is coherent in *degree and extent* between nodal points on a vibrating flexible structure. As a nodal region is traversed lengthwise there is a 180 degree phase shift; the vortex shedding is again coherent in degree and extent but is shifted in phase from neighboring sections of the structure. The steady and unsteady hydrodynamic forces (drag, excitation, damping, etc.) vary with local displacement amplitude and are not constant over the length of the structure.

Similar findings were obtained by Novak and Tanaka (55) and Howell and Novak (56) for experiments conducted with cylinders vibrating in smooth flow. Results similar to those in Fig. 4.16 were obtained (55) when the cross correlation ρ_{AB} was measured between the signals from pressure taps at various spacings along a circular cylinder. When the complications of various types of turbulence and boundary layer profiles were added to the case of a low-turbulence uniform flow, Howell and Novak found that the displacement response of the cylinder was largely independent of the flow characteristics *if the structural damping was sufficiently small to cause lock-on.*

As the damping ratio ζ_s was increased, the displacement response of the flexibly-mounted cylinders became susceptible to the characteristics of the incident flow to the cylinder. The correlation coefficient at the pressures measured between two taps on the cylinder is plotted in Fig. 4.18. The cylinder employed during the experiments was a pivoted rigid rod of aspect ratio L/D = 10 in a deep boundary layer, but the results are very similar to those plotted in Figs. 4.16. In addition to the correlation profiles, Howell and Novak measured the cross flow displacement amplitudes as a function of structural damping (ζ_s = 0.01 to 0.11) and obtained results in various types of boundary layer (shear flow) environments. The measured amplitudes compare very well with those plotted in Fig. 4.4, and full lock-on was observed for the cylinder with ζ_s = 0.01 and $Y_{EFF,MAX} \approx 0.5$. These findings further suggest that flexible cylindrical structures with small reduced damping ζ_s/μ will be susceptible to resonant vortex-excited oscillations even if the incident flow is non-uniform (as discussed in Section 4.3).

A number of computer codes, prediction models and design procedures have been developed on the basis of the results just discussed. It has been found that local displacement amplitudes and forces can be predicted for flexible structures from empirical data that are measured in experiments conducted with rigid cylinders, so long as the condition of lock-on is met and that the frequency ratios f/f_s (or reduced velocities V_r) and displacement amplitudes are comparable in the two cases.

5. PREDICTION METHODS AND DESIGN PROCEDURES

5.1 General design procedures. Design procedures and prediction methods for the vortex-excited oscillations of structures have been developed only during the past several years. Previously a reliable experimental data base and accurate characterization of the phenomenon were unavailable, and it is only since marine construction has moved into deeper water and more harsh

operating environments that the need for sophisticated design procedures has arisen. The need to design slender, flexible structures against problems due to vortex shedding in the atmospheric environment also has spurred renewed efforts to develop new wind engineering design procedures. It should be emphasized, however, that reliable data are available only at subcritical Reynolds numbers.

The design procedures that are generally available have been reported by Blevins (2), Hallam, Heaf and Wootton (1), King (3), Skop, and Griffin and Ramberg (58,59). The following discussion will be structured similarly to that of Hallam et al. and King, whose primary applications thus far have been to the design of marine structures. The methods developed by Skop, Griffin and Ramberg have been applied primarily to the analysis of marine cable systems, though many of their basic findings have been incorporated by others. Blevins (2) discusses design problems due to flow-induced vibrations in general, including heat exchangers, overhead transmission lines and marine structures.

A general flowchart which lays out a calculation procedure for assessing the response of a structure due to vortex shedding is given in Fig. 5.1. Both single members and arrays of members are considered in the general procedure, but emphasis is placed here on the case of a single flexible cylinder. The reader should consult references 1 and 3 for further discussions of arrays of structural members. A second flowchart that describes the steps necessary to compute the amplified drag forces and steady deflections is given in Fig. 5.2.

All of the methods developed thus far are in common agreement and point out that the following parameters determine whether large-amplitude, vortex-excited oscillations will occur:

- The *logarithmic decrement* of *structural* damping, δ
- The reduced velocity, V/f_nD

- The mass ratio, $m_e/\rho D^2$.

Here m_e is the *effective mass* of the structure (see Appendix 4.1 and Example 3.2) which is defined as

$$m_e = \frac{\int_0^L m(x)\, y^2(x)\, dx}{\int_0^h y^2(x)\, dx} \tag{5.1}$$

where $m(x)$ is the cylinder mass per unit length including internal water and the added mass, joints, sections of different material, etc.,

$y(x)$ is the modal shape of the structure along its length,

L is the overall length of the structure, measured from its termination,

h is the water depth.

It should be noted here that these methods were developed originally for structural members that pierced the water surface, hence the length L might be greater than the depth h. The effective mass m_e would then define an equivalent structure whose vibrational kinetic energy was equal to that of the real structure. In the context of the OTEC cold water pipe, both limits of integration will be equal to L, the length of the pipe, since $h > L$ in all presently conceivable OTEC applications.

As described in the previous sections the mass parameter and the structural damping can be combined as

$$k_s = \frac{2m_e\delta}{\rho D^2} \quad \text{or} \quad \frac{\zeta_s}{\mu} = 2\pi St^2 k_s ,$$

which are called the reduced damping. As noted by Hallam, Heaf and Wootton (1), the reduced damping k_s is the ratio of the actual damping *force* (per unit length) and $\rho f_n D^2$, which

may be considered as an inertial force (per unit length). The results in the preceding sections also suggest criteria for determining the critical incident flow velocities for the onset of vortex-excited motions. They are:

$$V_{crit} = (f_n D)\, V_{r,crit} \tag{5.2}$$

where $V_{r,crit} = 1.2$ for in line oscillations and $V_{r,crit} = 3.5$ for cross flow oscillations at Reynolds numbers greater than about $5(10^5)$, in the range of OTEC applications, c.f. Fig. 4.2. For Reynolds numbers below 10^5, $V_{r,crit} = 5$.

An increase in the reduced damping will result in smaller amplitudes of oscillation and at large enough values of ζ_s/μ or k_s the vibratory motion becomes negligible. Reference to Fig. 4.4 suggests that oscillations are effectively suppressed at $\zeta_s/\mu > 4$ (or $k_s > 16$), but cylindrical structures in water fall well toward the left-hand portion of the figure. The measurements of in line oscillations by King (18) have shown that vortex-excited motions in that direction are effectively negligible for $k_s > 1.2$. The results obtained by Dean, Milligan and Wootton (24) and others shown on Fig. 4.4 indicate that the reduced damping can increase from $\zeta_s/\mu = 0.03$ to 0.5 (a factor of *sixteen*) and the peak-to-peak displacement amplitude is decreased only from 2 to 3 diameters to 1 diameter (a nominal factor of only *two or three*). At the small mass ratios and structural damping ratios that are typical of light, flexible structures in water the hydrodynamic forces predominate and it is difficult to reduce or suppress the oscillations by means of mass and damping control.

Step-by-step procedures for determining the deflections that result from vortex-excited oscillations have been developed by Skop, Griffin and Ramberg (58,59), by King (3), by Hallam, Heaf and Wootton (1) and by Mes (60). The steps to be taken are explained in detail in these references and generally should follow the sequence:

- Compute/measure vibration properties of the structure (natural frequencies or periods, normal modes, modal scaling factors, etc.)

- Compute Strouhal frequencies and test for critical velocities, V_{crit} (in line and cross flow), based upon the incident flow environment.

- Test for reduced damping, k_s, based upon the structural damping and mass characteristics of the structure or pipe.

If the structure is susceptible to vortex-excited oscillations, then

- Determine vortex-excited unsteady displacement amplitudes and corresponding steady-state deflections based upon steady drag augmentation according to the methods of reference (59), if applicable; see Fig. 5.2.

- Determine new stress distributions based upon the new steady-state deflection and the superimposed forced mode shape caused by the unsteady forces, displacements and accelerations due to vortex shedding.

- Assess the severity of the augmented stress levels relative to fatigue life, critical stresses, etc.

These general procedures are discussed in a later section of this report in relation to some simple OTEC cold water pipe design problems.

5.2 Practical design data. Several dynamic models of varying levels of sophistication have been developed to predict the displacements due to vortex-excited oscillation. One class of models, the so-called nonlinear "wake-oscillator" type have been discussed in detail elsewhere (2,4,26,29). In terms of OTEC applications, a discussion of the wake-oscillator formulation is

given by Hove, Shih and Albano (42). None of the wake-oscillator formulations proposed thus far has been developed to the stage where they represent a practical design procedure, but based upon a detailed study Dean and Wootton (26) have suggested that the wake-oscillator model of Skop and Griffin (see reference 53) is perhaps the most promising for future development.

Several empirical predictions of the dependence between the peak cross flow displacement amplitude and the reduced damping have been developed over the past five years. The three most widely used are listed in Table 5.1. The prediction curve developed by Griffin, Skop and Ramberg (58) is a least-squares fit to those data points in Fig. 4.4 that were available in 1976 (about two-thirds of the points now appearing in the figure). The Iwan and Blevins curve was developed during a study of one wake-oscillator formulation (2) and Sarpkaya's result is based upon a modeling study (4) similar to the one described in Appendix 4.1. The dimensionless mode shape factor γ is given by

$$\gamma_i = |\psi_i(z)|_{MAX}/I_i^{1/2}. \tag{5.3}$$

Representative maximum values of γ_i for different end conditions and mode shapes can be calculated from the results in Table A1. A sample calculation using one of the equations in Table 5.1 is given as Example 5.1.

All of the equations in Table 5.1 correctly model the self-limiting displacement amplitude that is shown at small values of reduced damping in Fig. 4.4. It is also important to note that all of these models are based upon the *structural damping ratio*, typically the still air value, for whatever mode of the structure is excited (see Appendix 4.1). The models in Table 5.1 tend to overpredict the cross flow displacement amplitude at $\bar{Y}/D < 0.05$ to 0.1 where the vortex shedding is not fully correlated over the length of the cylinder, but these small-amplitude cross flow oscillations are of more concern in gas flows rather than in water.

Table 5.1. Predictions of Cross Flow Displacement Amplitude Due to Resonant Vortex-Excited Oscillations as a Function of the Reduced Damping

Investigator	Predicted Displacement Amplitude
Griffin, Skop and Ramberg (58)	$\bar{Y}/D = \dfrac{1.29\gamma}{[1 + 0.43(2\pi St^2 k_s)]^{3.35}}$
Blevins (2)	$\bar{Y}/D = \dfrac{0.07\gamma}{(1.9 + k_s)St^2}\left[0.3 + \dfrac{0.72}{(1.9 + k_s)St}\right]^{1/2}$
Sarpkaya (4)	$\bar{Y}/D = \dfrac{0.32\gamma}{[0.06 + (2\pi St^2 k_s)^2]^{1/2}}$

Legend: $\bar{Y}$ = displacement amplitude (equation (A16)); D = cylinder diameter; m = mass or equivalent mass (equation (5.1)) per unit length; St = Strouhal number; k_s = reduced damping (equation 3.1)); γ = dimensionless mode shape factor (equation (5.3)), $\gamma = 1$ for a spring-mounted rigid cylinder, $\gamma = 1.3$ for the first mode of a cantilever, and $\gamma = 1.16$ for a sinusoidal mode shape (cable).

Example 5.1 Calculation of the vortex-excited cross flow displacement amplitude from a least-squares fit to the data in Fig. 4.4; see equation (5.6) and Table 5.1. This is an example of one series of steps in the procedure to be employed in a preliminary assessment of an OTEC cold water pipe's susceptibility to vortex-excited oscillations.

PROBLEM STATEMENT:

The peak cross flow displacement amplitude $\bar{Y}/D$ due to lock-on can be calculated for a variety of circular cylindrical beams when the mass and damping characteristics of the structure are known. An estimate of the expected $\bar{Y}/D$ is a necessary step in making an assessment of an OTEC cold water pipe's susceptibility to excitation by vortex shedding.

RESULTS REQUIRED:

(a) The reduced damping parameters k_s and ζ_s/μ for a flexible beam;

(b) The mode shape factor γ_i (equation (4.3c)) for a flexible beam;

(c) The maximum (or peak) cross flow displacement amplitude $\bar{Y}/D$.

Step One:

Consider the case of a clamped-clamped beam in the first bending mode ($i = 1$). The data required to estimate the reduced damping have been given in Example 4.1. They are:

Modal scaling factor $I_1^{1/2} = 1.360$

Normal mode $|\psi_1(z)|_{MAX} = 1.586$

Reduced damping $k_s = 1.27$ or $\zeta_s/\mu = 2\pi St^2 k_s = 0.32$

Step Two:

The mode shape factor γ_i for a clamped-clamped beam is given by equation (4.3c),

$$\gamma_i = \frac{|\psi_i(z)|_{MAX}}{I_i^{1/2}}.$$

For $i = 1$ the data listed above yield the required value of γ_i (as in Example 4.1).

$$\therefore \gamma_1 = 1.586/1.360 = \underline{1.17}$$

Step Three:

The cross flow displacement amplitude $\bar{Y}/D$ can be estimated from the least-squares fit, equation (5.6), to a portion of the data in Fig. 4.4. (Only data points available through 1976 were employed to develop this equation. Other points have been added to the curve since then.) Equation (5.6) gives the required relation between $\bar{Y}/D$ and ζ_s/μ,

$$\bar{Y}/D = \frac{1.29\,\gamma_i}{[1 + 0.43\,(\zeta_s/\mu)]^{3.35}}.$$

$$\therefore \bar{Y}/D = (1.29 \times 1.17)/(1 + 0.43 \times 0.32)^{3.35} = \underline{0.98}$$

This calculated value of $\bar{Y}/D = 0.98$ compares very well with the measured value $\bar{Y}/D = 0.94$ at the same reduced damping k_s (see Example 4.1). The recent measurements of Dean, Milligan and Wootton (24) *were not* employed in computing the least-squares fit, equation (5.6).

The drag coefficient C_D for a structure vibrating due to vortex shedding is increased as shown in Fig. 4.11. The ratio of C_D and C_{DO} (the corresponding drag coefficient for a cylinder that is restrained from oscillating) is a function of the displacement amplitude and frequency as given by the response parameter (59)

$$w_r = (1 + 2\bar{Y}/D)(V_r\,St)^{-1}. \tag{5.4}$$

Here again $2\bar{Y}$ is the double amplitude of the displacement, V_r is the reduced velocity and St is the Strouhal number. The ratio of the drag coefficients is given by

$$C_D/C_{DO} = 1\,, \quad w_r < 1 \tag{5.5a}$$

$$C_D/C_{DO} = 1 + 1.16(w_r - 1)^{0.65}, \quad w_r \geqslant 1 \tag{5.5b}$$

which is a least-squares fit to the data in Fig. 4.11. The equation

$$\bar{Y}_{MAX}/D = \frac{1.29\gamma_i}{[1 + 0.43(2\pi\,St^2\,k_s)]^{3.35}} \tag{5.6}$$

can be combined with equations (5.4) and (5.5) to compute the unsteady displacements, the drag amplification and the amplified static deflection that is due to the vortex excited oscillations. The local displacement amplitude along a flexible cylindrical structure (in the *ith* normal mode) is given by

$$\bar{y}(z) = \bar{Y}_i(z)\sin(2\pi ft) \tag{A20}$$

where

$$\bar{Y}_i(z) = Y_{EFF,MAX}\, D\, \psi_i(z)/I_i^{1/2}. \tag{A16a}$$

These equations are employed as outlined in Fig. 5.2 to iteratively compute the static deflection of a structure due vortex-excited drag amplification (the drag coefficient C_{DO} for the stationary cylinder is assumed to be known). Recommended values of C_{DO} for smooth and rough stationary cylinders are given by Hove, Shih and Albano (42) in a related OTEC report.

Example 5.2 Calculation of the steady drag amplification C_D/C_{DO} due to cross flow oscillations of a cylindrical beam. This is the procedure to be employed in calculating the drag amplification that accompanies vortex-excited oscillations.

PROBLEM STATEMENT:

When a cylindrical structure vibrates in an incident flow due to vortex shedding, the steady drag force is increased. For a cylinder of circular cross-section, the amplification in the drag due to cross flow lock-on is well documented as shown by the results in Fig. 4.11. A step-by-step procedure for calculating the drag is given in Fig. 5.2.

RESULTS REQUIRED:

(a) The maximum drag amplification C_D/C_{DO} for a flexible beam (C_{DO} is the drag on the cylinder when it is restrained from oscillating).

Step One:

The data required for calculating C_D/C_{DO} are given in Example 4.1. When the case of a clamped-clamped beam in the first bending ($i = 1$) mode is considered, the data are:

Displacement amplitude $\bar{Y}_{MAX}/D = 0.94$,
Reduced velocity $V_r/\bar{Y}_{MAX} = 5$,
Strouhal number $St = 0.2$.

Step Two:

The drag amplification C_D/C_{DO} is given by equation (5.5b), a least-squares fit to the data in Fig. 4.11,

$$C_D/C_{DO} = 1 + 1.16(w_r - 1)^{0.65}.$$

The parameter w_r, the horizontal axis in Fig. 4.11, is given by

$$w_r = (1 + 2\bar{Y}/D)\ (V_r St)^{-1}.$$

The required value of w_r is calculated from the data listed above. This specific case refers to the peak displacement amplitude of a flexible, clamped-clamped circular cylinder in flowing water, so that

$$w_r = (1 + 2 \times 0.94)\ (5.0 \times 0.2)^{-1} = \underline{2.88}.$$

The amplification of the local drag coefficient is then

$$C_D/C_{DO} = 1 + 1.16 \times (2.88 - 1)^{0.65} = \underline{2.75}.$$

For this location on the cylinder the drag due to vortex-excited oscillations is increased by 275% from the corresponding case when the cylinder is restrained. The *average* drag amplification over the entire length of the cylinder is calculated with the step-by-step method given in Fig. 5.2.

Blevins and Burton (57) have developed an empirical model for predicting the vortex-excited cross flow displacement amplitudes. Instead of being deterministic, however, the model is based upon random vibration theory in order to incorporate the effects of varying correlation length on the resonant response of the structure and the flow-induced forces. The details of the model are given by Blevins (2), and will not be repeated here since the variable correlation length effects are more applicable at cross flow displacements less that $\bar{Y}/D = 0.2$ and reduced dampings greater than $\zeta_s/\mu = 2$. This is somewhat beyond the range in Fig. 4.4 that is most applicable to marine structures.

In order to specify the excitation component of the lift forces, Blevins and Burton fitted a quadratic curve to the data of Vickery and Watkins (1964) and Hartlen, Baines and Currie (1968) that are plotted in Fig. 4.9. The curve is given by

$$C_{LE}(z) = a + b|\psi_i(z)|\ Y_{MAX} + C|\psi_i(z)|^2\ Y_{MAX}^2 \tag{5.7a}$$

with $a = 0.35$, $b = 0.60$ and $c = -0.93$, and C_{LE} is evaluated from the equation

$$C_{LE} = \frac{\int_0^L C_{LE}(z)\, \psi_i(z)\, dz}{\int_0^L \psi_i(z)\, dz} \tag{5.7b}$$

which is discussed in Appendix 4.1. Blevins (2) has carried out the necessary integrations for a rigid cylinder ($\psi(z) = 1$), a pivoted rod ($\psi(z) = z/L$) and a sine (taut cable) mode ($\psi_i(z) = \sin(i\pi z/L)$). The results are listed in Table 5.2 for the case where the correlation length l_c is much larger than the length L of the cylinder. An additional case has been included as part of the present study: a pinned-free cylinder (the first three modes). This example is given in Section 8 and is somewhat representative of a simple OTEC cold water pipe configuration. The calculation of additional cases is straightforward.

The coefficients for a cubic fit to the data in Fig. 4.9 have been computed and are based upon a fit to all of the data points shown there. This cubic equation is given by

$$C_{LE} = a_1 + b_1\, Y_{EFF,MAX} + c_1\, Y^2_{EFF,MAX} + d_1\, Y^3_{EFF,MAX} \tag{5.8}$$

These new coefficients are listed as a_1, b_1, c_1 and d_1 in Table 5.3. This fitted curve to the data is valid between $Y_{EFF,MAX} = 0$ and $Y_{EFF,MAX} = 1.25$ ($2Y_{EFF,MAX} = 2.5$). The results in the table can be employed as inputs to a finite-element, elastic beam analysis of the resonant, vortex-excited response of a number of flexibly configured cylinders. However, it should be noted that the coefficient C_{LE} represents only the excitation force on the structure. For vibrations in water it is necessary to have an accurate and precise representation of the coefficients of the added mass, hydrodynamic damping and hydrodynamic inertia forces. These coefficients are not as well characterized as is C_{LE}, but they can be computed from the total force measurements of Sarpkaya (28), for example, as shown in Table 4.2 and Appendix 4.1.

Table 5.2 Excitation Force Coefficient C_{LE} for Three Cylindrical Structures; from reference 2.

Structure	Mode Shape $\psi_i(z)$	C_{LE} $(l_c > L)^+$
Rigid cylinder	1	$a + b(\bar{Y}/D) + c(\bar{Y}/D)^2$
Pivoted rod	$\bar{z}/L$	$a + \frac{2}{3} b(\bar{Y}/D) + \frac{c}{2}(\bar{Y}/D)^2$
Sine (taut cable) mode, $i = 1$	$\sin(\pi\bar{z}/L)$	$a + \frac{\pi}{4} b(\bar{Y}/D) + \frac{2}{3} c(\bar{Y}/D)^2$

[1] C_{LE} is the average value calculated from equations (5.7) and (5.8). $\bar{Y}/D$ is the peak displacement amplitude for a given mode. $a = 0.35$, $b = 0.60$, $c = -0.93$

Table 5.3 Excitation Force Coefficient C_{LE}; data from Fig. 4.9

Force coefficient: $C_{LE} = a_1 + b_1 Y_{EFF,MAX} + c_1 Y^2_{EFF,MAX} + d_1 Y^3_{EFF,MAX}$
where $a_1 = 0.12$, $b_1 = 2.12$, $c_1 = -3.57$, $d_1 = 1.45$
and the standard deviation of the curve $\sigma = 0.1$.

Effective displacement: $Y_{EFF,MAX} = \dfrac{(\bar{Y}_{MAX}/D)}{\gamma_i}$, $\gamma_i = \dfrac{|\psi_i(z)|_{MAX}}{I_i^{1/2}}$

In terms of $\bar{Y}_{MAX}/D$,

$$C_{LE}|_{\bar{Y}_{MAX}} = a_1 + (b_1/\gamma_i)(\bar{Y}_{MAX}/D) + (c_1/\gamma_i^2)(\bar{Y}_{MAX}/D)^2 + (d_1/\gamma_i^3)(\bar{Y}_{MAX}/D)^3 \text{*}$$

where the factor γ_i is evaluated for a given set of end fixities, i.e. free-pinned, pinned-pinned, clamped-clamped, etc. Here $\bar{Y}_{MAX}/D$ is the *peak* displacement along the beam.

6. COMPUTER CODES FOR PREDICTING AND MODELLING VORTEX-EXCITED OSCILLATIONS

There are a limited number of operational computer codes for calculating the the response of bluff structures to vortex shedding. Those which are most applicable to the OTEC cold water pipe and associated mooring cables are described in this section.

*Note that this form of the equation is slightly different than than introduced by Blevins (2) as given in equation (5.7a)

6.1 The VORTOS Code. VORTOS is a computer code developed by Atkins Research and Development in the United Kingdom. The essential features of the code are described in a recently published report (61). This program predicts the dynamic response of a flexible cylinder to vortex-excited oscillations in steady flow. The vibration amplitude and frequency response in a steady flow may be calculated for flexible cylindrical members of a variety of marine structures. The calculation is based upon experimental measurements of the cross flow response and the excitation forces using spring-mounted rigid cylinders and flexible cylinders (24).

The program is based upon the well-founded assumption that the lift force at each position along the length of a cylinder in steady flow is a sinusoidal function of time and is dependent upon the local incident flow velocity and displacement amplitude (19, 23, 24, 33). The cylinder is represented by simple finite elements (at this stage up to eleven in number) and the appropriate mass and stiffness matrices. The vortex shedding frequency is determined from the reduced velocity V_r for each element and is assumed to lock-on close to the natural frequency f_n of the structure at the critical velocities described in Sections 3, 4 and 5 of this report. More specifically, lock-on is assumed to occur if the Strouhal frequency is between $0.8f_n$ and $1.6f_n$ (61). The resonant, vortex-excited lift forces as a function of displacement amplitude for each vibrating element are derived from experimental data. An iterative procedure is employed to calculate the steady-state deflected shape of the cylindrical member and the maximum bending stresses are determined from the curvature. A typical comparison between the VORTOS prediction and experimental measurements taken with a long, flexible circular beam are plotted in Fig. 6.1. The important features of the code are described in more detail in reference 61, which also includes a worked example problem with output and a listing of the input data required to exercise the code.

Several factors that influence the utility of the code for OTEC applications should be mentioned. Shear effects are not taken into account explicitly since the developers of the code do not feel that the effects of velocity shear on vortex shedding have been quantified for flexible cylinders (62). The experimental data upon which the code is based were obtained at subcritical Reynolds numbers so that any extrapolation to high Reynolds numbers would have to be approached with caution. Also, no correction is made of the static deflection due to amplification of the steady drag on the structure as a result of the vortex-excited oscillations.

6.2. The DESADE code. The DESADE code was developed at NRL for computing the current-induced static deflections of structural cable arrays (63). As dimensioned the code can handle arbitrarily configured arrays of up to twenty-two cables. The cable can be electromechanical, wire rope or synthetic, and any number of discrete elements can be incorporated in the array. An option for parametric studies is included in the program together with an option for incorporating arbitrary current distributions over the array. A capability for taking account of the amplified deflections of the array due to vortex-excited strumming oscillations recently has been added to the DESADE code (59). The capabilities of the method of imaginary reactions (64), upon which DESADE is based, also have been extended recently to guyed tower configurations (65) and the strumming subroutines have been upgraded still further (66). The required input to the program is listed in detail in reference 63.

The strumming correction has been employed successfully in some recent marine applications. SEACON II (67) was an ocean-based cable array that was used to validate several array motion models. The SEACON structure was implanted by the Civil Engineering Laboratory (CEL) and consists essentially of three riser cables and a horizontal delta array as shown schematically in Fig. 6.2. The cables comprising the delta had uniform currents incident over

their respective lengths and were found to be subject to cable strumming. These strumming vibrations lead to increases in the effect steady drag coefficients and in the lift amplification over the cables as discussed earlier in this report. Since the drag coefficient is a basic parameter in all array motion computations, an accurate knowledge of its value is required in order to validate the various models for the analysis of cable structures. The drag amplification correction procedures used in the code are discussed in Section 5.

The steady drag coefficient was frequently 150 to 230% greater than the value of the nominal stationary-cable drag coefficient C_{DO} due to strumming of the SEACON II array. These large increases in the drag loads would be expected to have a significant effect on the magnitude of the predicted array motions. In Fig. 6.3 the measured motions of a point near the intersection of two cables on the horizontal delta of the SEACON II array are compared to the predicted motions during a semi-diurnal tidal cycle. The predicted motions were obtained using the computer code DESADE. The magnitude and direction (predominantly from the southeast) of the current during the cycle can be inferred from the movement of the measurement point from its zero current location designated by "X". The northern direction is shown on the plot as a reference.

The measured motion of the point is shown in Fig. 6.3 by the solid line, and the predicted motion using a constant stationary-cable drag coefficient $C_D = C_{DO} = 1.55$ (measured in water [21]) is given by the dashed line with circles (---O---). Finally, the predicted motion using $C_D = (C_D/C_{DO})C_{DO}$, with C_D/C_{DO} calculated from equation (5) and $C_{DO} = 1.55$, is shown by the dashed line (-----). Excellent agreement was obtained between the predicted and measured motions when the strumming-amplified steady drag coefficients were employed. It was also apparent, for the larger current magnitudes, that the displacement amplitudes predicted using

the nominal stationary-cable drag coefficient ($C_D = C_{DO} = 1.55$) were considerably smaller than the measured displacements.

6.3. The HULPIPE code. The HULPIPE code was developed by TRW and has been used extensively in marine studies (68). In terms of OTEC applications, the HULPIPE code solves the partial differential equations of the cold water pipe motion coupled with the ordinary differential equations of the plant hull motion. All computations are done in the time domain, and for the CWP both in space and in time. The hydrodynamic forces taken into account are the drag and inertia forces due to wave action, current-induced drag and lift forces, Coriolis forces due to the incident flow, and steady lift or side forces due to non-circular pipe cross-sections.

The code is subject to "small-deflection" theory limitations, i.e. to angular deflections less than 10°. Also, the hydrodynamic force inputs to HULPIPE are limited to constant values of the drag coefficient, the added mass and/or inertia coefficients and the vortex force coefficient. And an example of the program's application to an OTEC cold water pipe is given in Fig. 5.4.

6.4 Other related codes. The importance of including dynamic effects in the analysis of marine risers has been well established. A recent paper by Young, Fowler, Fisher and Luke (69) discusses a number of riser codes which have been developed in recent years and describes a computer program for predicting the dynamic response of marine risers to lateral forcing by waves (regular and random) and currents (vortex shedding). The program described by Young et al. is a frequency domain analysis that contains a "variable-increment" finite difference formulation that requires no linearization of the Morison equation in defining the hydrodynamic forces. Loading conditions on the riser include harmonic cross flow forcing to simulate vortex shedding, though few details were given of how the effects of vortex shedding actually were

taken into account. The analysis is based upon the differential equation for a tubular "beam-column" and is limited to small deflection theory, as was the HULPIPE code described in the preceding section. Either force or displacement boundary conditions at each end allow for ball joints, a freely suspended riser etc. Several other recent and noteworthy riser analyses are discussed also by Young, Fowler, Fisher and Luke. These include the finite-difference, time domain model of Sexton and Agbezuge (70) and the finite-element, time domain MARRS computer code of Gardner and Kotch (71).

7. ELIMINATION/REDUCTION AND AVOIDANCE OF VORTEX-EXCITED OSCILLATIONS

Vortex-excited oscillations sometimes can be reduced or suppressed by the installation of external devices that modify the flow field about the structure. Helical fins, porous shrouds and streamlined fairings have been used with some success (72,73), but in general it is preferable to design the structure itself to avoid the vortex-excited oscillations whenever possible.

There are three primary methods of preventing the in line and cross flow oscillations, as described in detail by Hallam, Heaf and Wootton (1), Dean and Wootton (26), and King, Prosser and Verley (73). These are:

(a) Control of the structural design so as not to exceed the critical values of reduced velocity $V_r = V/f_n D$;

(b) Structural design for sufficiently large mass and damping;

(c) Modification of the flow field around the cylinder either by altering the flow or the structural shape.

The first two methods were described in the preceding sections and will be further discussed later with regard to OTEC cold water pipe applications. The remainder of this section will focus primarily on the use of various types of spoilers to reduce the oscillations.

There are generally three methods which have been employed with success to reduce vortex-excited oscillations of flexible structures (except for cables, which will be discussed briefly later). These are strakes, or helically-wound fins, porous shrouds which fit over the cylindrical structure, and straight fins in various configurations. The three are shown in Fig. 7.1, from Hallam, Heaf and Wootton (3).

Strakes. Helical strakes have been widely employed in reducing the wind-excited oscillations of large chimneys. Strakes, however, cause difficulties in installation and handling and tend to increase the steady drag coefficient. A straked cylinder has a drag coefficient of $C_d = 1.3$. Hallam, Heaf and Wootton (3) discuss the optimum strake configuration; this is three helically-wound fins of about 10 percent of the cylinder diameter, with a pitch of 5. Semi-rigid strake windings have been developed specifically for offshore applications (74); an increase of 10 percent over the steady drag on the bare cylinder value is estimated.

Shrouds. Perforated shrouds have been employed successfully to eliminate the in line motion due to vortex shedding (17,73). The shroud is effective for all approach flow directions. An optimum shroud geometry should have a diameter 20 percent greater than the cylinder and an open area ratio of 36 percent, and should extend over 20 percent of the wetted length of the cylinder (73). Information that is available suggests that marine growth does not reduce the shroud's effectiveness.

Fins and fairings. Radial fins that extend along the length of the cylinder have been tested successfully to suppress vortex-excited oscillations (73) in line with the flow. The fins typically are

10 percent of the diameter of the cylinder and are fitted over about 20 percent of the cylinder's length at 45° from the front stagnation point. Such a device is effective only for small variations in the angle of the approach flow. These radial fins also induce a steady side, or lift, force. A streamline fairing that is fitted to the cylinder prevents the formation of strong vortices and has been employed successfully in deep water (72). However the fairing must be free to rotate in order to accommodate changes in the direction of the approach flow. Otherwise large bending moments will be induced. Grant and Patterson (72) describe in detail the design, testing and installation of a rotatable fairing for a 24 inch diameter drilling riser that was to operate in 500 feet of water with surface currents of 8 knots. The fairing section as installed is shown in Fig. 7.2. The fairing extended about 2 diameters downstream into the wake of the riser. Flag-type tail fairings were developed for use in the pile installation operations at the Cognac platform site (45).

An example of the reduction in displacement amplitude that can be achieved with radial fins and shrouds is shown in Fig. 7.3 from reference 73. The in line displacement amplitude of a raked (yawed) pile was reduced substantially by the installation of shrouds and radial fins. It should be kept in mind, however, that the Reynolds number of the flow was relatively small, near $Re = 10^4$. It is also important to remember that most effective solutions to the problem of suppressing vortex-excited oscillations are ad hoc in nature and it is often risky to apply a successful result for one installation to other situations. It is generally more effective to design the structure against problems due to vortex shedding and to attempt to modify the flow is the least satisfactory alternative.

For completeness, the suppression of vortex-excited strumming vibrations of flexible cables should be mentioned. This problem generally has been dealt with effectively, though with the usual penalties of increased drag, etc. Lengthy and authoritative discussions of strumming problems and their solution are given in recent reports by Hafen and Meggitt (75), Kline,

Nelligan and Diggs (76), and Vandiver and Pham (77). Again, solutions to the strumming suppression problem for marine cables are ad hoc in nature because the precise operating mechanisms of the various devices are not well known.

8. OTEC COLD WATER PIPE APPLICATIONS

8.1 Typical CWP examples. Two primary non-dimensional groups of relevant parameters must be considered in assessing the potential severity of vortex-excited oscillations. These are:

- the REDUCED VELOCITY, $V_r = \dfrac{V}{f_n D}$;
- and the REDUCED DAMPING, $k_s = \dfrac{2m\delta}{\rho D^2}$ or $\zeta_s/\mu = 2\pi St^2 k_s$.

The latter is a combination of the mass ratio $m/\rho D^2$ and the structural damping ratio ζ_s or the log decrement δ. *Both the reduced velocity and the reduced damping must be considered in a complete assessment.*

It is useful to consider as an application of the methods described in the preceding sections the vortex shedding characteristics of a representative OTEC cold water pipe design. For this first example one TRW fiberglass design is chosen for convenience. The design parameters of the pipe are given in reference 12 and are summarized in Table 8.1. The natural periods of the first four bending modes of the fiberglass pipe are listed in the table, and from these the in line and cross flow critical velocities can be calculated in a straightforward manner. A typical OTEC operating condition employed in recent studies is the offshore Puerto Rico and Brazil regions "grazing" mode which yields an incident flow of up to one knot (0.51 m/s) over the pipe length neglecting relative currents. This amounts to something of a "worst case" in terms of vortex shedding since the incident flow is uniform over the length of the pipe. From the velocities listed in Table 8.1 it is clear that for these conditions the 9.2m (30 ft) diameter pipe

would be in the critical velocity range for in line oscillations in the first two modes and for cross flow oscillations in the fundamental mode (see Example 8.1).

Table 8.1 The effects of vortex shedding on an OTEC cold water pipe; pipe parameters from reference 12.
Cylindrical fiberglass pipe, 50 mm (2 in.) wall thickness.
Diameter D = 9.2m (30 ft) Length L = 762m (2500 ft) L/D = 83

Mode of bending oscillation	Natural period, $T_{nat}(sec)$	Critical velocity, $V_{crit}(m/s(kt))$	
		In line	Cross flow
$i=1$	121	0.092 (0.18)	0.26 (0.50)
2	43.2	0.25 (0.48)	0.74 (1.43)
3	21.4	0.51 (1.0)	1.49 (2.89)
4	12.6	0.85 (1.65)	2.54 (4.92)

$$V_{crit} = V_{r,crit}(D/T_{nat}) \begin{cases} V_{r,crit} = 1.2 \text{ (In line)} \\ V_{r,crit} = 3.5 \text{(Cross flow)} \end{cases}$$

Note: Dashed underline denotes that critical velocities are exceeded by the incident flow in the range 0 to 1 knot (0 to 0.5 m/s).

Example 8.1 Calculation of the critical incident flow velocities of an OTEC cold water pipe when the cwp's natural periods are known.

PROBLEM STATEMENT:

The magnitudes V_{crit} of the critical incident flow velocities are those which correspond to the onset of in line and cross flow oscillations due to vortex shedding. In this example the procedures for calculating V_{crit} are given for the particular case when the natural periods of the cold water pipe are specified. A typical fiberglass pipe of the configuration discussed in detail by TRW (12) is considered here as the example.

RESULTS REQUIRED:

(a) The magnitude V_{crit} of the critical incident velocity for the onset of in line oscillations due to vortex shedding;

(b) The magnitude V_{crit} of the critical incident velocity for the onset of cross flow oscillations due to vortex shedding.

Step One:

Consider the case of a typical TRW fiberglass cold water pipe (12). The first four natural periods of the pipe were calculated and are listed in reference 12 and Table 8.1. The data required are:

Nominal length $L = 2500$ ft,
Fundamental period $T_{nat} = 121$ sec ($i = 1$),
Nominal diameter $D = 30$ ft.

For the onset of vortex-excited oscillation, the magnitudes of the critical velocities are given by equation (5.2),

$$V_{crit} = V_{r,crit}(D/T_{nat}),$$

where

$$V_{r,crit} = \begin{cases} 1.2 \text{ In line} \\ 3.5 \text{ Cross flow ; for Reynolds numbers greater than } 5(10^5). \end{cases}$$

Here $V_{r,crit}$ is the reduced velocity $V_r = V/f_nD$. The critical values of V_r are shown in Figs. 2.6 and 4.3 respectively for in line and cross flow oscillations. The Reynolds number of a 30 ft diameter cold water pipe is $3.4(10^6)$ in a one knot flow.

Step Two:

The magnitude of the *in line* critical velocity is

$$V_{crit} = 1.2 \times 30/121 \text{ ft/sec} = \underline{0.30 \text{ ft/sec}}$$
$$= \underline{0.18 \text{ knots}}$$

for the first bending ($i = 1$) mode.

Step Three:

The magnitude of the *cross flow* critical velocity is

$$V_{crit} = 3.5 \times 20/121 \text{ ft/sec} = \underline{0.87 \text{ ft/sec}}$$
$$= \underline{0.52 \text{ knots}}$$

for the first bending ($i = 1$) mode.

Both critical velocities for the fundamental mode are exceeded when the upper limit of the relative flow is *one knot*. Note: Additional results relevant to this example are listed in Table 8.1.

Only *nominal* values of the pipe diameter D and the length L were chosen to demonstrate the procedures for calculating V_{crit}. In the case of an incident flow with shear V_{crit} is the maximum value in the nonuniform velocity profile.

The critical, or onset, velocity is given by the entry $V_{crit} = 0.26$ m/s (0.5 kt) in Table 8.1. If the peak displacement amplitude occurs at a reduced velocity in the range $V_r = 6$ to 7.5, then the actual velocity range over which the maximum cross flow displacements are excited will be $V = 0.45$ to 0.57 m/s (0.88 to 1.1 knots). A grazing mode of operation near one knot is clearly

in the range of a first mode cross flow resonance if the reduced damping $\frac{2m\delta}{\rho D^2}$ of the pipe is sufficiently small $\left(\frac{2m\delta}{\rho D^2} < 10 \div 16\right)$. In addition both the first and second bending modes of the flexible pipe will be susceptible to in line oscillations when the damping is small $\left(\frac{2m\delta}{\rho D^2} < 1.2\right)$

Example 8.2 Calculation of the effective mass ratio $m_e/\rho D^2$ for a *hypothetical* thin-walled, water-filled cylindrical steel OTEC cold water pipe that is oscillating in sea water.

PROBLEM STATEMENT:

The effective mass m_e of a cylindrical structure in water (or any fluid) consists of the mass of the structure itself, the mass of any fluid or other material contained within the structure, and the added mass due to unsteady motion through the surrounding fluid. In this example a sample calculation of the effective mass of a steel cold water pipe is presented. Representative values of the pipe dimensions and properties are taken from recent OTEC cold water pipe system study (13).

RESULTS REQUIRED:

(a) The added mass m_a of a *hypothetical* cold water pipe due to its oscillatory motion;

(b) The effective mass ratio $m_e/\rho D^2$ of a *hypothetical* cold water pipe.

Step One:

The data required to calculate the equivalent mass m_e (per unit length) are given in reference 13:

Nominal diameter $D = 30$ ft
Pipe mass $m_s = 3500$ lb_m/ft
Sea water density $\rho = 64$ lb_m/ft^3.

The added mass of the pipe (per unit length) due to its oscillatory motion is

$$m_a = (\pi/4)\, \rho_w\, D^2\, C_{am},$$

where C_{am} is the added mass coefficient. If a value of $C_{am} = 1$ is assumed, then

$$m_a = (\pi/4) \times 64 \times (30)^2 \times 1 = \underline{45200\ lb_m/ft}.$$

Step Two:

The total effective mass m_e is given by the equation

$$m_e = m_s + m_w(\text{water in pipe}) + m_a\ (\text{added mass})$$

or

$$m_e = m_s + (\pi/4)\,\rho_w D^2 + (\pi/4)\,\rho_w D^2 C_{am}.$$

$$\therefore\ m_e = 3500\ \mathrm{lb_m/ft} + (\pi/4) \times 64 \times (30)^2\ \mathrm{lb_m/ft} + 45200\ \mathrm{lb_m/ft}$$
$$= \underline{93900\ \mathrm{lb_m/ft}}$$

The mass ratio $m_e/\rho D^2$ is given by the equation

$$\frac{m_e}{\rho_w D^2} = \frac{93900\ \mathrm{lb_m/ft}}{64 \times (30)^2\ \mathrm{lb_m/ft}} = \underline{1.63}.$$

This value ($m_e/\rho D^2 = 1.63$) is typical of thin-walled, water-filled cylindrical beams; see references 1 and 24. The mass of the pipe in water is dominated by hydrodynamic effects since only 4% of the total mass per unit length is due to the steel shell.

Note:

It is not the purpose of this brief example to specify the detail design of a prototype OTEC cold water pipe. *Nominal* dimensions such as the diameter D and length L are employed to demonstrate the step-by-step calculations that should be followed. Design complexities such as ribs, longitudinal stiffeners etc. are not considered in this preliminary assessment, but these factors would be important considerations in a complete detail design study.

An additional example now is considered in more detail. A steel cold water pipe has been proposed as a prime CWP baseline design candidate (12, 13, 78, 79), and the structural properties of steel are better known relative to offshore applications than are those of fiber-reinforced plastic, polyethylene and elastomers. The first three natural bending periods of a flexible steel pipe are listed in Table 8.3 (also see Example 8.2). For simplicity it is assumed that the pipe is a pinned-free flexible beam, so that the natural frequencies are given by (80,81)

$$f_n = \frac{(\lambda_l)^2}{2\pi}\sqrt{\frac{EI}{m_e L^4}}\,. \tag{8.1}$$

Here again m_e, the equivalent mass, is the sum of the (uniform) pipe mass, the mass of the water inside the pipe and the added mass of the water. The characteristic function and the coefficients for a pinned-free flexible beam are listed in Table 8.3.

If the incident flow environment is again considered to be that of the "grazing" mode near one knot, then Table 8.2 shows that the pipe again is susceptible to in line oscillations in the

Table 8.2 The effects of vortex shedding on an OTEC cold water pipe; cylindrical steel pipe parameters from references 13, 78 and 79.

Pipe parameters:

Nominal diameter D = 9.2m (30 ft) Length L = 1000m (3280 ft) L/D = 109

Mode of bending oscillation	Natural period, $T_{NAT}^{+}(sec)$	Critical velocity, $V_{crit}(m/s\,(kt))$	
		In line	Cross flow
$i=1$	121	0.092 (0.18)	0.26 (0.50)
		-----	-----
2	37.3	0.30 (0.58)	0.86 (1.67)

3	17.9	0.62 (1.20)	1.80 (3.49)

+It is assumed that the pipe is a pinned-free flexible beam; see equation (8.1).

$$V_{crit} = V_{r,crit}(D/T_{NAT}) \begin{cases} V_{r,crit} = 1.2 \text{ (In line)} \\ V_{r,crit} = 3.5 \text{(Cross flow)} \end{cases}$$

Note: Dashed underline denotes that critical velocities are exceeded by the relative currents in the range 0 to 1 knot (0 to 0.5 m/s).

Table 8.3 Characteristic functions for the natural modes of a flexible, free-pinned beam (80).

$$\bar{Y}_i(z,t) = \bar{Y}_{MAX}\,\psi_i(z)e^{j\omega_i t}$$

Characteristic function

$$i\text{th mode; } \psi_i(z) = \cosh\lambda_i(\bar{z}/L) + \cos\lambda_i(\bar{z}/L) - \alpha_i[\sinh\lambda_i(\bar{z}/L) + \sin\lambda_i(\bar{z}/L)]$$

$\bar{z} = 0$ free
$\bar{z} = L$ pinned

Natural frequencies and periods

$$i\text{th mode: } f_i = \frac{(\lambda_i)^2}{2\pi}\sqrt{\frac{EI}{mL^4}}, \quad T_i = \frac{1}{f_i}$$

i	λ_i	α_i	$I_i^{1/2}$	$\lvert\psi_i(z)\rvert_{MAX}$	γ_i
1	3.927	1.007	1.310	2	1.527
2	7.068	1	1.267	2	1.578
3	10.210	1	1.254	2	1.594

first two bending modes and to cross flow oscillations in the first bending mode. As in the case of the fiberglass pipe of the previous example, the maximum cross flow oscillations would be likely to occur in the range of relative velocities very close to the nominal grazing condition ($V = 0.45$ to 0.57 m/s or $V = 0.88$ to 1.1 knots).

The reduced damping k_s or ζ_s/μ of the structure also must be estimated in order to fully assess the potential severity of the vortex-excited oscillations. A thin-walled, water filled steel cylinder with a large slenderness ratio ($L/D = 80$ to 100) will typically have an equivalent mass ratio of about $m_e/\rho D^2 = 1.5$ to 3 (see Example 8.2). Typical values of the *structural* damping log decrement for such a configuration are in the range $\delta = 0.1$ to 0.2 (1). These values of m_e and δ combine to yield a range of estimated reduced damping of $k_s = 0.33$ to 0.66. This results in *estimated cross flow peak displacement amplitudes* between $\bar{Y}_{MAX}/D = 1.33$ to 1.60 as given by equation (5.6), a least-squares fit to the data in Fig. 4.4. The steady drag coefficient will be amplified by the oscillations by as much as $C_D/D_{D0} = 2.8$, according to equation (5.5b). These values of k_s also suggest that the pipe will be susceptible to in line oscillations, which can be analyzed by step-by-step methods similar to those given in the examples. The step-by-step calculations which lead to these estimated displacement amplitudes are given in Example 8.4 and the results are summarized in Table 8.4.

Table 8.4 Vortex-excited bending oscillations of a *hypothetical* thin-walled, water-filled steel OTEC cold water pipe.

Pipe parameters:

Nominal diameter $D = 9.2$ m (30 ft) Nominal length $L = 1000$ m (3280 ft)
Natural period $T_{nat} = 121$ sec (first bending mode) Effective mass ratio $m_e/\rho D^2 = 1.63$

Reduced damping, k_s	Displacement amplitude, $\bar{Y}_{MAX}/D$	$\bar{Y}_{MAX}(m\,(ft))$	Relative flow velocity at $\bar{Y}_{MAX}$ $V(m/s\,(kt))$
0.33	1.60	14.6 (48)	0.46 to 1.1 (0.88 to 1.1)
0.66	1.33	12.2 (40)	0.46 to 0.57 (0.88 to 1.1)

Note: It is assumed that the pipe acts as a free-pinned flexible beam. In the first bending mode the peak displacement amplitude occurs at the free end of the pipe.

These estimated displacement amplitudes are large enough to be potentially catastrophic and destructive, based on available offshore experience with flexible cylinders in steady currents (16,17,45,82). This example, though it represents only a simplified analysis, strongly suggest that the OTEC cold water pipe design process should include a careful and detailed study of the effects of vortex shedding. A detailed analysis might include a finite-element modelling of the slender beam configuration of the OTEC cold water pipe. Drag amplification and unsteady force amplification due to lock-on should be included in the analysis by means of an iterative process in order to determine the static deflection and forced mode shape of the pipe.

8.2 Recommended vortex-excited force and response coefficients. Experimental data for steady and unsteady force coefficients and vortex-excited displacements are available for application at subcritical Reynolds numbers ($Re < 2(10^5)$). This range of Reynolds numbers corresponds to model-scale and small test-scale OTEC cold water pipes. Relatively few data are available for applications in the higher Reynolds number ranges ($Re > 2\ (10^6)$), and prudent extrapolation of the results available at subcritical Reynolds numbers is the only near-term alternative. It is well established that strong periodic vortex shedding takes place from smooth and rough circular cylinders at Reynolds numbers in the range of full-scale OTEC cold water pipe applications (17, 35, 40, 41).

In terms of in line oscillations, both force coefficients and displacement responses are well documented at both the model scale and full scale. These results are summarized in Section 3 of this report; examples 3.1 and 3.2 give step-by-step applications of the results. However, in line oscillations due to vortex shedding reach displacement amplitudes of only about one-tenth of the more destructive cross flow oscillations in water. For this reason a primary concern should be cold water pipe design for oscillations in the cross flow direction, since it is generally

accepted in offshore design that unsteady deflections of the order of three diameters are catastrophic for most structural members (16,17,45,60,82).

Experimental data and design procedures derived from them are quite extensive for the case of cross flow oscillations. The most recent of these results that are directly relevant to the OTEC cold water pipe, at least for models and small test-scale CWP's, are summarized in Section 4 of this report; Examples 4.1 and 4.2 give applications of the basic data for cross flow deflections and forces. Specific OTEC-related problems are discussed in Examples 5.1 and 5.2, and Examples 8.1 to 8.4. Section 5 of this report is concerned with step-by-step design procedures; these are summarized in Figs. 5.1 and 5.2 for the two cases of unsteady deflections and static deflections, respectively. In terms of appropriate coefficients for use in the CWP design process, the following recommendations are made:

Example 8.3 Calculation of the critical fundamental mode velocities and the natural period of a steel cold water pipe (modelled as a free-pinned flexible beam).

PROBLEM STATEMENT:

A preliminary estimate of the magnitude V_{crit} of the incident flow velocities at which vortex-excited oscillations are initiated can be obtained for an OTEC cold water pipe by modelling the pipe as a free-pinned flexible beam. This configuration is a reasonable representation of a vertical cold water pipe attached by a universal joint to a floating OTEC plant. For this example the plant is assumed to be motionless and in a uniform current or, conversely, "grazing" at a uniform velocity through still water. The cold water pipe is assumed to be a uniform flexible beam of steel construction. The mass of the cold water pipe and its cross-section rigidity are taken from a recent OTEC cwp systems study (13).

RESULTS REQUIRED:

(a) The first bending mode natural frequency f_n and period T_n of a *hypothetical* OTEC cold water pipe;

(b) The magnitude V_{crit} of the critical velocity for the onset of vortex-excited in line oscillations;

(c) The magnitude V_{crit} of the critical velocity for the onset of vortex-excited cross flow oscillations.

Step One:

The data required for the calculations are taken from reference 13, Table 8.3, and Example 8.2.

Cross-section rigidity $EI = 3.82(10^{12})$ $lb_f ft^2$,
Nominal diameter $D = 30$ ft,
Pipe structural mass $m_s = 3500 lb_m/ft$,
Nominal length $L = 3280$ ft,
Flexible beam parameter $\lambda_i = 3.927$ $(i = 1)$.

To calculate the natural frequency f_n of the cold water pipe, the standard formula for a free-pinned flexible beam is employed. As given in Table 8.3, this is

$$f_n = \frac{(\lambda_i)^2}{2\pi} \sqrt{\frac{EI}{m_e L^4}}.$$

All quantities required are given above except for the effective mass m_e, which was calculated in Example 8.2.

Step Two:

From Example 8.2, $m_e = \underline{93900\ lb_m/ft}$.

Step Three:

The natural frequency f_n for the first bending mode $(i = 1)$ is given by

$$f_n = \frac{(3.927)^2}{2\pi} \sqrt{\frac{3.82 \times 10^{12} \times g_c}{93900 \times (3280)^4}}\ Hz\ .$$

Here, for dimensional consistency, $g_c = 32.2\ \dfrac{lb_m ft}{lb_f\, sec^2}$.

$$\therefore f_n = 8.26 \times 10^{-3}\ Hz$$

$$T_n = \frac{1}{f_n} = \underline{121\ sec}$$

Step Four:

For the onset of vortex-excited oscillations, the magnitudes of the critical velocities are given by equation (5.2), as discussed in Example 8.1, where

$$V_{crit} = V_{r,crit}\ (D/T_n)$$

$$V_{r,crit} = \begin{cases} 1.2 \text{ In line} \\ 3.5 \text{ Cross flow.} \end{cases}$$

The magnitude of the *in line* critical velocity is

$$V_{crit} = 1.2(D/T_n)$$

$$\therefore V_{crit} = 1.2 \times 30/121 \text{ ft/sec} = \underline{0.3\text{ft/sec}}$$
$$= \underline{0.18\text{knots}}$$

for the first bending mode of the cwp ($i = 1$). The magnitude of the *cross flow* critical velocity is

$$V_{crit} = 3.5\ (D/T_n).$$

$$\therefore V_{crit} = 3.5 \times 30/121 = \underline{0.87\text{ ft/sec}}$$
$$= \underline{0.52\text{ knots}}$$

for the first bending mode of the cwp ($i = 1$). These results are listed in Table 8.4.

Note:

It is not the purpose of this brief example to specify the detail design of a prototype OTEC cold water pipe. Nominal dimensions and quantities such as the diameter D, the length L, the structural mass m_s and the cross section rigidity EI are employed to demonstrate the step-by-step calculations that should be followed. Design complexities such as ribs, longitudinal stiffeners, etc. are not considered in this preliminary assessment, but these factors would be important considerations in a complete detail design study.

- *Steady drag amplification due to vortex-excited oscillations.* Equations (5.4), (5.5) and (5.6) for the wake response parameter, the drag coefficient amplification and the cross flow displacement amplitude. Note that the *actual* total drag coefficient is calculated by applying an appropriate drag coefficient for the type of cylinder used in the pipe construction, i.e. smooth or rough at the correct Reynolds number, to the drag amplification C_D/C_{DO}. See Section 5.2, Fig. 5.2, and Example 5.2.

- *Excitation force due to vortex-excited oscillations.* Equations (5.7b) and (5.8) for the maximum excitation force coefficient C_{LE} and the average C_{LE} over the length of a flexible cylinder. The maximum and local displacement amplitudes should be calculated from equations (5.6) and (A16a), respectively. *All* available measurements of C_{LE} to date have been made at *subcritical* Reynolds numbers in air and in water on *smooth* rigid and flexible cylinders. Extrapolation to supercritical Reynolds numbers and rough cylinders should be done with caution.

- *Added mass and damping force coefficients.* It is recommended that an added mass coefficient $C_{am} = 1$ be employed in calculating the vortex-excited response and natural periods of an OTEC cold water pipe. Other unsteady force coefficients can be derived from the hydrodynamic coefficients C_{mh} and C_{dh} given in Section 4. It is important to note that these coefficients contain the added mass component, among others. When total hydrodynamic force coefficients such as C_{dh} and C_{mh} plotted in Figures 4.5 to 4.8 are employed in the equations of oscillatory motion for a flexible beam, care must be taken to insure that such fluid forces as added mass and damping are not duplicated in the formulation. Many standard formulae include these latter forces in the acceleration and damping terms on the left hand side of equation (A1), but they are also included in the force coefficients. Only *structural* mass, damping and stiffness terms should appear on the left-hand side of equation (A1) given in Appendix 4.1. Examples 3.2, 8.2 and 8.3 discuss the calculation of the added mass term in the equation of oscillatory motion.

Example 8.4 Calculation of the peak cross flow displacement amplitude for a *hypothetical* steel OTEC cold water pipe.

PROBLEM STATEMENT:

It is possible to *estimate* the cross flow displacement amplitude of the steel OTEC cold water pipe discussed in Examples 8.2 and 8.3. The assumption of lock-on due to vortex shedding is made and the same general pipe configuration and assumptions of Example 8.3 are considered to apply again to the problem stated below.

RESULTS REQUIRED:

(a) The reduced damping k_s and ζ_s/μ of a hypothetical steel cold water pipe;

(b) The peak cross flow displacement amplitude $\bar{Y}_{MAX}$;

(c) The magnitude V of the incident current velocity at which $\bar{Y}_{MAX}$ is excited.

Step One:

The data required for the calculations are taken from Examples 8.2 and 8.3, references 1 and 24, and Table 8.3:

Effective mass ratio $m_e/\rho D^2 = 1.63$,
Nominal pipe length $L = 3280$ ft,
Nominal pipe diameter $D = 30$ ft,
Natural period $T_n = 121$ sec $(i = 1)$,
Estimated structural damping $\delta = 0.1$ to 0.2; from reference 1,
Strouhal number $St = 0.27$,
Mode shape factor $\gamma_i = 1.527$ $(i = 1)$; from Table 8.3, for a free-pinned beam.

The displacement amplitude $\bar{Y}_{MAX}$ is estimated from equation (5.6),

$$\bar{Y}_{MAX}/D = \frac{1.29\,\gamma_i}{[1 + 0.43(\zeta_s/\mu)]^{3.35}},$$

where $\zeta_s/\mu = 2\,\pi\,St^2 k_s$.

Step Two:

The reduced damping is calculated from the latter equation, so that as the next step

$$k_s = \frac{2m_e\,\delta}{\rho_w D^2}.$$

$$\therefore\ k_s = 2 \times 1.63 \times 0.1 \text{ to } 2 \times 1.63 \times 0.2$$

$$= \underline{0.33 \text{to } 0.66}$$

It is straightforward as the next step to calculate ζ_s/μ, so that

$$\zeta_s/\mu = 2\pi \times (0.17)^2 \times 0.33 \text{ to} 2\pi \times (0.17)^2 \times 0.66$$

$$\zeta_s/\mu = \underline{0.15 \text{ to} 0.30}$$

This range of reduced damping ζ_s/μ falls well toward the left hand portion of Fig. 4.4 which is denoted as being representative of marine structures.

Step Three:

The displacement amplitude $\bar{Y}_{MAX}$ is now estimated from equation (5.6).

$$\therefore\ \bar{Y}_{MAX}/D = (1.29 \times 1.537)/(1 + 0.43 \times 0.15)^{3.35}$$

to

$$(1.29 \times 1.527)/(1 + 0.43 \times 0.30)^{3.35}$$

$$\bar{Y}_{MAX}/D = \underline{1.3 \text{ to } 1.6}$$

When $D = 30$ ft is assumed, $\bar{Y}_{MAX} = \underline{40 \text{ to } 48 \text{ ft}}$ (from equilibrium) at a period of $T_n = 121$ sec. For a free-pinned beam as assumed here, the peak displacement is obtained at the free end for the first two bending modes.

Step Four:

The magnitude V of the flow velocity at which this displacement amplitude is excited can be estimated from the results in Figs. 4.2, 4.3 and 4.13. In those experiments the peak displacement amplitudes were excited in flowing water at

$$V_r = V/f_n D = VT_n/D = 6 \text{ to } 7.5.$$

$$\therefore V = 6(D/T_n) \text{ to } 7.5\ (D/T_n)$$

$$= \underline{1.49 \text{ to } 1.86 \text{ ft/sec}} \text{ or } \underline{0.88 \text{ to } 1.1 \text{ knots}}$$

It should be noted that these results were obtained both in uniform and non-uniform (sheared) incident flows (see Fig. 4.13).

These results are listed in Table 8.4.

9. SUMMARY

9.1 Conclusions. Problems associated with the shedding of vortices often have been overlooked in the past in relation to the design of offshore structures, largely because reliable experimental data and design methods have been unavailable. However, the dynamic analysis of marine structures has become increasingly important and sophisticated in order to predict stress distributions and fatigue life in the ocean environment. These factors are particularly relevant to the OTEC cold water pipe, which must be designed to survive and operate in the ocean environment over a long (20 to 30 years approx.) time period.

This report has summarized the present state of the art concerning the vortex-excited oscillations of marine structures, relative to OTEC cold water pipe applications. Reliable experimental data now are in hand for the dynamic response of and flow-induced forces on model-scale structures at subcritical Reynolds numbers, and based upon these experiments empirical and semi-empirical prediction models have been developed and tested. Many of these existing results and design methods are also directly applicable in the Reynolds number range that characterizes the OTEC cold water pipe.

Prototype and full-scale test data are essential for the effects of vortex shedding and vortex-excited oscillations to be confidently included in the design of long, flexible ocean structures such as the OTEC cold water pipe and other deep water structures such as steel jacketed platforms and marine risers.

9.2 Recommendations. The previous sections of this report have summarized the state of the art for the vortex-excited oscillations of flexible marine structures. Detailed information is available for the resonant response of cylindrical structures oscillating in both the in line and cross flow directions to the relative incident flow at subcritical Reynolds numbers, $Re < 2(10^5)$, as shown in Sections 3 and 4. Limited information on full-scale marine structures is available at Reynolds numbers up to $Re = 10^6$. There is reasonably detailed knowledge of the steady drag amplification that accompanies cross flow oscillations and practical design methods have been developed to predict the steady drag forces that accompany vortex-excited oscillations. Unsteady hydrodynamic force coefficients have been measured at moderate Reynolds numbers, i.e. $Re = 10^3$ to 10^4, and these coefficients have been employed in practical design procedures as described in Sections 4 and 5. However, virtually all reliable measurements have been made at Reynolds numbers below the range of OTEC cold water pipe applications (except for small models and prototypes of the CWP).

On the basis of these results it is recommended that an experimental program be designed and conducted to provide a reliable data base for steady and unsteady hydrodynamic force coefficients in the range of OTEC applications. Both smooth and rough circular cylindrical cross-section models should be employed for completeness. Roughness scaling for the simulation of large Reynolds numbers as discussed by Sarpkaya (39), Hove, Shih and Albano (42), and Szechenyi (83) should be employed to as large an extent as is possible. These hydrodynamic force coefficients can be employed in finite-element computer codes that treat the

OTEC cold water pipe as a flexible beam. One such code, VORTOS, is described in Section 6, but this code has been calibrated only at moderate Reynolds numbers below the range of OTEC applications (62). However, until an OTEC-specific data base is assembled, available coefficients as given in this report and the earlier report of Hove et al (42) may have to be extrapolated with care for use in OTEC cold water pipe design in the diameter range $D = 9.2$m (30 ft) to 30.5m (100 ft). These diameters correspond to a range of nominal Reynolds numbers between $3(10^6)$ and $11(10^6)$ for a one knot relative flow velocity. It has been shown that extrapolations to high Reynolds number can be suitably carried out when they are based on proper considerations of fluid dynamic similitude (35, 42, 83).

In terms of OTEC cold water pipe design it would seem prudent to place the major emphasis near-term on the development and/or adaptation of flexible beam computer codes for analysis of vortex-excited oscillations of the CWP. Evidence obtained from recent experiments conducted by Paidoussis and Helleur (84) strongly indicates that ovalling oscillations of thin-shelled cylinders in a current of air are not caused by the regular vortex shedding. The oscillations are a complex multi-modal response at one or more of the cylindrical shell's natural frequencies, but no lock-on is found between the vortex shedding and the vibration. This finding suggests that the development of a shell-type analysis of the OTEC cold water pipe should be postponed until this question, i.e. the origin of the ovalling oscillations, is answered.

10. REFERENCES

1. M.G. Hallam, N.J. Heaf and L.R. Wootton, *Dynamics of Marine Structures*, Construction Industry Research and Information Association (London) Report UR8, 1978.

2. R.D. Blevins, *Flow-Induced Vibrations*, Van Nostrand Reinhold: New York, 1977.

3. R. King, "A Review of Vortex Shedding Research and Its Application," Ocean Engineering, Vol. 4, 141-171, 1977.

4. T. Sarpkaya, "Vortex-Induced Oscillations, A Selective Review" Trans. of ASME, Journal of Applied Mechanics, Vol. 46, 241-258, 1979.

5. N. Hogben, B.L. Miller, J.W. Searle and G. Ward, "Estimation of fluid loading on offshore structures," Proc. Instn, Civ. Engrs., Vol. 63, 515-562, 1977.

6. *Renewable Ocean Energy Sources, Part I Ocean Thermal Energy Conversion,* Office of Technology Assessment, U.S. Congress, May 1978.

7. "Reports of the Working Groups" in *Proceedings of the Sixth OTEC Conference*, G.L. Dugger (ed.), Appled Physics Laboratory/Johns Hopkins University, 1979.

8. W. Ley, *Engineers's Dreams*, Viking Press: New York, 1960, pp. 189-220.

9. G. Claude, "Power From the Tropical Seas," Mechanical Engineering, Vol. 52, pp. 1039-1044, 1930.

10. P. Archbold, "Development of a Test Program for OTEC-1," paper presented at the 6th OTEC Conference, June 19-22, 1979.

11. R. Scotti, and T. McGuinness, "Design and Analysis of OTEC's Cold Water Pipe," *Proceedings of Oceans IV, Civil Engineering in the Oceans 1979,* ASCE, September 1979.

12. TRW, "Ocean Thermal Energy Conversion Cold Water Pipe Preliminary Design Project — Task 2: Analysis for Concept Selection," prepared for NOAA/DOE, 16 March 1979 (NOAA Contract No. MO-A01-78-00-4141).

13. Science Applications, Inc. "OTEC Modular Experiment Cold Water Pipe Concept Evaluation" Technical Report SAI-063-80R-008-LA, March 1979 (NOAA Contract No. MO-A01-78-00-4142).

14. J.F. George, "System Design Considerations for a 10/40 MW OTEC Pilot Plantship," paper presented at the 6th OTEC Conference, June 19-22, 1979, Washington, D.C.

15. Scott, Robert J., "Conceptual Design and Costs of an OTEC 10/40 MW Spar Platform," paper presented at the 6th OTEC Conference, June 19-22, 1979, Washington, D.C.

16. R.N. Sainsbury and D. King, "The Flow Induced Oscillation of Marine Structures" Proc. Inst. Civil Engrs., Vol. 49, 269-302, 1971.

17. L.R. Wootton, M.H. Warner, R.N. Sainsbury and D.H. Cooper, "Oscillation of Piles in Marine Structures," Construction Industry Research and Information Association Report 41, London, 1972.

18. R. King, "Vortex-Excited Oscillations of a Circular Cylinder in Steady Currents," Offshore Technology Conference Preprint OTC 1948, 1974.

19. R. King, M.J. Prosser and D.J. Johns, "On vortex excitation of model piles in water," J. Sound and Vib., Vol. 29, 169-188, 1973.

20. O.M. Griffin and S.E. Ramberg, "Vortex Shedding from a Cylinder Vibrating In-Line with an Incident Uniform Flow," J. Fluid Mech., Vol. 75, 257-271, 1976.

21. R. King and D.J. Johns, "Wake interaction experiments with two flexible cylinders in flowing water" J. Sound and Vib., Vol. 45, 259-284, 1976.

22. J.D. Hardwick and L.R. Wootton "The Use of Model and Full-Scale Investigations on Marine Structures," Paper 127, Intl. Symp. on Vibration Problems in Industry, Keswick (U.K.), 1973.

23. O.M. Griffin, "Vortex-Excited Cross Flow Vibrations of a Single Cylindrical Tube", Trans. ASME, J. Pressure Vessel Tech., Vol. 102, in press, 1980; see also *Flow-Induced Vibrations,* S.S. Chen and M.D. Bernstein (eds.), ASME: New York, 1-10, 1979.

24. R.B. Dean, R.W. Milligan and L.R. Wootton, "An Experimental Study of Flow-Induced Vibration," E.E.C. Report 4, Atkins Research and Development, Epsom (U.K.), 1977.

25. L.R. Wootton, "The Oscillation of Large Circular Stacks in Wind," Proc. Instn. Civil Engrs., Vol. 43, 573-598, 1969.

26. R.B. Dean and L.R. Wootton, "An Analysis of Vortex Shedding Problems in Offshore Engineering," Report No. 77/14, Atkins Research and Development, Epsom (U.K.), 1977.

27. O.M. Griffin and G.H. Koopmann, "The Vortex-Excited Lift and Reaction Forces on Resonantly Vibrating Cylinders," J. Sound and Vibr., Vol. 54, 435-448, 1977.

28. T. Sarpkaya, "Transverse Oscillation of a Circular Cylinder in Uniform Flow," Proc. ASCE, J. Waterways, Port, Coastal and Ocean Div., Vol. 104, 275-290, 1978.

29. R.A. Skop and O.M. Griffin, "On a Theory for the Vortex-Excited Oscillations of Flexible Cylindrical Structures" J. Sound Vib., vol. 41, 263-274, 1975; see also "The Vortex-Excited Oscillations of Structures," J. Sound and Vib., Vol. 44, 303-305, 1976.

30. W.D. Iwan, "The Vortex-Excited Oscillations of Elastic Structural Elements," Trans. ASME J. Engrg. Indus., Vol. 97, 1378-1382, 1975.

31. R. King, "An Investigation of the Criteria Controlling Sustained Self-Excited Oscillations of Cylinders in Flowing Water" *Proc. Symposium on Turbulence in Liquids,* U. of Missouri, Rolla, 1977.

32. T. Sarpkaya, "Lateral Oscillations of Smooth and Rough Cylinders in Harmonic Flow," *Proc. Symp. Wave-Induced Forces on Cylinders,* Bristol (U.K.), Paper D-5, 1978.

33. P.W. Bearman and I.G. Currie, "Pressure Fluctuation Measurements on an Oscillating Circular Cylinder," J. Fluid Mech., Vol. 91, 661-678, 1979.

34. O.M. Griffin "A universal Strouhal number for the "locking-on" of vortex shedding to the vibrations of bluff bodies," J. Fluid Mech., Vol. 85, 591-606, 1978.

35. O.M. Griffin, "Universal Similarity in the Wakes of Stationary and Vibrating Bluff Bodies," in *Proc. Fifth Int. Conf. on Wind Engrg.,* Vol. 1, Paper V-10, July 1979.

36. S.S. Chen, "Crossflow-Induced Vibrations of Heat Exchanger Tube Banks" Nuc. Engrg. and Design, Vol. 47, 67-86, 1978.

37. J.A. Mercier, "Large Amplitude Oscillations of a Circular Cylinder in a Low-Speed Stream," Ph.D. Thesis, Stevens Institute of Technology, Hoboken NJ, 1973.

38. O.M. Griffin, R.A. Skop and G.H. Koopmann, "The Vortex-Excited Resonant Vibrations of Circular Cylinders" J. Sound and Vib., Vol. 31, 235-249, 1973.

39. T. Sarpkaya, "Effect of Surface Roughness on the Transverse Oscillations of a Circular Cylinder," Naval Postgraduate School Report NRS-69SL79085-IR, August 1979.

40. Y. Nakamura, "Some Research on Aeroelastic Instabilities of Bluff Structural Elements," in *Proc. Fourth Int. Conf. on Wind Effects on Buildings and Structures,* Heathrow (U.K.), 359-368, 1976.

41. B.L. Miller, "The Hydrodynamic Drag of Roughened Circular Cylinders" Paper 9, Roy. Instn. Nav. Arch. Spring Meeting, 1976.

42. D. Hove, W. Shih and E. Albano, "Hydrodynamic Design Loads for the OTEC Cold Water Pipe" Science Applications, Inc. Report SAI-79-559-LA, September 1978.

43. K.C.S. Kwok and W.H. Melbourne, "Cross-Wind Response of Structures Due to Displacement Dependent Lock-in Excitation," in *Proc. Fifth Int. Conf. on Wind Engrg.,* Vol. II, Fort Collins, Co, Paper VI-4, July 1979.

44. P.K. Stansby, "The locking-on of vortex shedding due to the cross-stream vibration of circular cylinders in uniform and shear flows," J. Fluid Mech., Vol. 74, 641-666, 1977.

45. F.J. Fischer, W.T. Jones and R. King, "Current-Induced Oscillations of Cognac Piles During Installation-Prediction and Measurements," in *Proc. Symp. Practical Experiences with Flow-Induced Vibrations* (Preprints), Karlsruhe, Vol. 1, 216-228, September 1979.

46. D.M. Rooney and R.D. Peltzer, "A Wind Tunnel Investigation of Vortex Shedding Patterns Behind the OTEC Cold Water Pipe" Aerospace and Ocean Engineering Department Report, VPI&SU, October 1979.

47. R. King, "Vortex Excited Oscillations of Inclined (Yawed) Cylinders in Flowing Water," BHRA Fluid Engineering Report RR 1214, January 1975.

48. S.E. Ramberg, "The Influence of Yaw Angle Upon the Wakes of Stationary and Vibrating Cylinders," Naval Research Laboratory Memorandum Report 3822, August 1978.

49. G.H. Koopmann, "The vortex wakes of vibrating cylinders at low Reynolds numbers," J. Fluid Mech., Vol. 28, 501-512, 1967.

50. G.H. Toebes, "The Unsteady Flow and Wake Near an Oscillating Cylinder," Trans. ASME J. Basic Engrg., Vol. 91, 831-838, 1969.

51. R.A. Skop and O.M. Griffin, "A Model for the Vortex-Excited Oscillations of Bluff Cylinders," J. Sound Vib., Vol. 27, 225-233, 1973.

52. W.D. Iwan and R.D. Blevins, "A Model for the Vortex-Induced Oscillation of Structures," Trans. ASME, J. Appl. Mech., Vol. 41, 581-586, 1974.

53. S.E. Ramberg and O.M. Griffin, "Velocity Correlation and Vortex Spacing in the Wake of a Vibrating Cable," Trans. ASME, J. Fluids Engrg., Vol. 98, 10-18, 1976.

54. S.E. Ramberg and O.M. Griffin, "The Effects of Vortex Coherence, Spacing and Circulation on the Flow-Induced Forces on Vibrating Cables and Bluff Structures," Naval Research Laboratory Report 7945, January 1976.

55. M. Novak and H. Tanaka, "Pressure Correlations on a Vibrating Cylinder," in *Proc. Fourth Int. Conf. on Wind Effects on Buildings and Structures,* Heathrow (U.K.), September 1975.

56. J.F. Howell and M. Novak, "Vortex Shedding from a Circular Cylinders in Turbulent Flow" in *Proc. Fifth Int. Conf. Wind Engrg.,* Paper V-11, July 1979.

57. R.D. Blevins and T.E. Burton, "Fluid Forces Induced by Vortex Shedding" Trans. ASME J. Fluids Engrg., Vol. 98, 19-24, 1976.

58. O.M. Griffin, R.A. Skop and S.E. Ramberg, "The Vortex Excited Resonant Vibrations of Structures and Cable Systems," Offshore Technology Conference Preprint OTC 2319, 1975.

59. R.A. Skop, O.M. Griffin and S.E. Ramberg, "Strumming Predictions for the Seacon II Emperimental Mooring" Offshore Technology Conference Preprint OTC 2884, 1977.

60. M.J. Mes, "Vortex Shedding Can Cause Pipelines To Break," Pipeline and Gas Journal, August 1976.

61. W.A. Evers and R.B. Dean, "VORTOS — A Program for the Calculation of Vortex-Induced Oscillations in Steady Flow" Atkins Research and Development Report 1978/APR/2, Epsom (U.K.), April 1978.

62. R.B. Dean, Private communication, June 1979.

63. R.A. Skop and J. Mark, "A Fortran IV Program for Computing the Static Deflections of Structural Cable Arrays," Naval Research Laboratory Report 7640, August 1973.

64. R.A. Skop and G.J. O'Hara, "The Static Equilibrium Configuration of Cable Arrays by Use of the Method of Imaginary Reactions," Naval Research Laboratory Report 6819, February 1969.

65. F. Rosenthal and R.A. Skop, "Guyed Towers Under Arbitrary Loads," Proc. ASCE, J. Structural Division, to appear, May 1980.

66. S.S. Sergev and W.D. Iwan, "The Natural Frequencies and Mode Shapes of Cables with Attached Masses," Civil Engineering Laboratory, Technical Memorandum M-44-79-3, in press, 1979.

67. T.R. Kretschmer, G.A. Edgeton, S.A. Black and N.D. Albertsen, "Seafloor Constuction Experiment, Seacon II: An Instrumented Tri-Moor for Evaluating Undersea Cable Structure Technology," Civil Engineering Laboratory, Naval Construction Battalion Center, Technical Report R 848, December 1976.

68. A.B. Griffin, TRW, Private communication, August 1979.

69. R.D. Young, J.R. Fowler, E.A. Fisher and R.R. Luke, "Dynamic Analysis as an Aid to the Design of Marine Risers," Trans. ASME, J. Pressure Vessel Tech., Vol. 100, 200-205, 1978.

70. R.M. Sexton and L.K. Agbezuge, "Random Wave and Vessel Motion Effects on Drilling Riser Dynamics," Offshore Technology Conference Preprint OTC 2650, 1976.

71. R.N. Gardner and M.A. Kotch, "Dynamic Analysis of Risers and Caissons by the Element Method," Offshore Technology Conference Preprint OTC 2651, 1976.

72. R. Grant and D. Patterson, "Riser Fairing for Reduced Drag and Vortex Suppression," Offshore Technology Conference Preprint OTC 2921, 1977.

73. R. King, M.J. Prosser and R.L.P. Verley, "The Suppression of Structural Vibrations Induced by Currents and Waves," *B.O.S.S. Conference Proceedings.* (Trondheim), Vol. I, 263-283 (1976).

74. _____, "STARSTRAKE for the Suppression of Vortex Shedding from Circular Structures in Tides and Currents" Fathom Oceanology Ltd. Test Report 6.841 T, October 1978.

75. B.E. Hafen and D.J. Meggitt, "Cable Strumming Suppression" Civil Engineering Laboratory, Naval Construction Battalion Center, Technical Note N-1499, September 1977.

76. J.E. Kline, J.J. Nelligan and J.S. Diggs, " A Survey of Recent Investigations into the Nature of Cable Strumming, its Mechanism and Suppression" MAR Inc. Technical Report 210, July 1978.

77. J.K. Vandiver and T.P. Pham, "Performance Evaluation of Various Strum Suppression Devices," MIT Ocean Engineering Department Report 77-2, March 1977.

78. A.B. Griffin et al, "Ocean Thermal Energy Conversion Cold Water Pipe Preliminary Design Project, Baseline Design Phase; Final Briefing," TRW Defense and Space Systems Group, 30 August 1979.

79. D. Hove, D. Hervey et al, "OTEC Cold Water Pipe System Design Study; Final Briefing," Science Applications Inc. and Brown & Root Development Inc., 30 August 1979.

80. R.E.D. Bishop and D.C. Johnson, *The Mechanics of Vibration,* Chapter 7, Cambridge University Press: Cambridge, 1960.

81. R.W. Clough and J. Penzien, *Dynamics of Structures,* Chapters 18-20, McGraw-Hill: New York, 1975.

82. _____ "Wind and Water Current Induced Oscillations in Tubulars" Petroleum Engineer International, Vol. 51, No. 12, 46, 1979.

83. E. Szechenyi, "Supercritical Reynolds Number Simulation for Two-Dimensional Flow over Circular Cylinders," J. Fluid Mech., Vol. 70, 529-542, 1975.

84. M.P. Paidoussis and C. Helleur, "On Ovalling Oscillations of Cylindrical Shells in Cross-Flow" J. Sound Vib., Vol. 63, 527-542, 1979.

11. APPENDICES

Appendix 4.1. THE PREDICTION OF CROSS FLOW-INDUCED FORCES AND DISPLACEMENTS

4.1.1 Equations of Motion. The equation for the resonant cross flow vibration of an elastically-mounted, rigid cylindrical structure, *with the vortex and vibration frequencies locked on*, can be written in general as

$$\ddot{y} + 2\,\zeta_s\,\dot{y} + y = \mu\left(\frac{\omega_s}{\omega_n}\right)^2 (\tilde{C}_L - \tilde{C}_R), \tag{A1}$$

where $(\dot{\cdot}) = \frac{d}{d\tau}$. Here $y = \bar{y}/D$, $\tau = \omega_n t$, the mass ratio $\mu = \frac{\rho D^2}{8\pi^2 St^2 m}$ and ζ_s is the *structural* damping ratio. The fluid force coefficients are

$$\text{Lift: } \tilde{C}_L = \frac{\bar{F}_L}{1/2\rho V^2 D} = C_L \sin(\alpha\tau + \phi),\ \alpha = \frac{\omega}{\omega_n}, \tag{A2a}$$

$$\text{Reaction: } \tilde{C}_R = \frac{\bar{F}_R}{1/2\rho V^2 D} = C_R \sin(\alpha\tau + \phi_1),\ \alpha = \frac{\omega}{\omega_n}, \tag{A2b}$$

as suggested by Griffin and Koopmann (27) and Griffin (23), where ϕ and ϕ_1 are the phase angles between the lift and the displacement and between the reaction and the acceleration, respectively. The two forces represented by $\tilde{C}_L$ and $\tilde{C}_R$ are orthogonal, as will be shown later.

If the cross flow tube displacement y is written as

$$y = Y \sin \alpha\tau, \quad \alpha = \frac{\omega}{\omega_n} \tag{A3}$$

with $Y = \bar{Y}/D$, then the equation of motion separates into

$$\sin \alpha\tau: \; -\alpha^2 Y + Y - \mu\left(\frac{\omega_s}{\omega_n}\right)^2 [C_L \cos\phi - C_R \cos\phi_1] = 0 \tag{A3a}$$

$$\cos \alpha\tau: \; 2\zeta_s Y - \mu\left(\frac{\omega_s}{\omega_n}\right)^2 [C_L \sin\phi - C_R \sin\phi_1] = 0 \tag{A3b}$$

when the coefficients of $\sin \alpha t$ and $\cos \alpha t$ are grouped appropriately. The various force components are identified as follows:

STRUCTURAL				FLUID		
INERTIA		STIFFNESS		INERTIA	ADDED MASS	
$-\alpha^2 Y$	$+$	Y	$= \mu\left(\frac{\omega_s}{\omega_n}\right)^2$	$[C_L \cos\phi - C_R \cos\phi_1]$		(A4a)
STRUCTURAL				FLUID		
DAMPING				EXCITATION	DAMPING	
$+ 2\zeta_s Y$			$= \mu\left(\frac{\omega_s}{\omega_n}\right)^2$	$[C_L \sin\phi - C_R \sin\phi_1]$.		(A4b)

A decomposition of the system such as this allows the fluid and structural forces to be separated completely. The various fluid forces then can be measured individually or deduced from the total measured force.

Using a different approach Sarpkaya (4, 28) has expressed the measured total fluid force on a resonantly vibrating cylinder as the sum of two components

$$C_{\text{TOTAL}} = \frac{\bar{F}}{\frac{1}{2}\rho V^2 D} = C_{mh} \sin \alpha\tau - C_{dh} \cos \alpha t \ , \tag{A5}$$

where C_{mh} is an "inertia" force and C_{dh} is a "drag" force. These components are related to Sarpkaya's "generalized force coefficients" C_{dl} and C_{ml} (28) by

$$C_{dh} = \frac{8}{3\pi} C_{dl} \left[2 \pi \frac{\bar{Y}}{D}\right]^2 V_r^{-2} \tag{A6a}$$

and

$$C_{mh} = \pi^2 C_{ml} \left[2 \pi \frac{\bar{Y}}{D}\right] V_r^{-2} \tag{A6b}$$

where V_r is the "reduced velocity" $V_r = \frac{2\pi V}{\omega_n D}$ or $\frac{V}{f_n D}$.

In this case the equation of motion for the cylinder becomes

$$\ddot{y} + 2\zeta_s \dot{y} + y = \mu \left(\frac{\omega_s}{\omega_n}\right)^2 (C_{mh} \sin \alpha\tau - C_{dh} \cos \alpha\tau) \ . \tag{A7}$$

The force component C_{dh} is negative when energy is transferred to the cylinder, as is the case for resonant, vortex-excited oscillations. If a steady-state response is assumed, then

$$y = Y \sin (\alpha\tau - \epsilon) \ ,$$

where ϵ is an undefined phase angle. This form of the equation of motion separates into

$$\sin \alpha\tau : -\alpha^2 Y \cos \epsilon + 2 \zeta_s Y \sin \epsilon + Y \cos \epsilon - \mu \left(\frac{\omega_s}{\omega_n}\right)^2 C_{mh} = 0 \tag{A8a}$$

and

$$\cos \alpha\tau : \alpha^2 Y \sin \epsilon + 2 \zeta_s Y \cos \epsilon - Y \sin \epsilon + \mu \left(\frac{\omega_s}{\omega_n}\right)^2 C_{dh} = 0 \tag{A8b}$$

when the coefficients of $\sin \alpha\tau$ and $\cos \alpha\tau$ are again grouped appropriately.

Upon rearranging, these equations reduce to

STRUCTURAL INERTIA		STRUCTURAL STIFFNESS		FLUID FORCE TERMS	(A9a)
$-\alpha^2 Y$	$+$	Y	$= \mu \left(\frac{\omega_s}{\omega_n}\right)^2$	$[C_{dh} \sin \epsilon - C_{mh} \cos \epsilon]$	

STRUCTURAL DAMPING		FLUID FORCE TERMS	(A9b)
$2 \alpha \zeta_s Y$	$= \mu \left(\frac{\omega_s}{\omega_n}\right)^2$	$[-C_{dh} \cos \epsilon + C_{mh} \sin \epsilon]$.	

which are of the same form as those derived above. The two approaches are in fact identical when

$C_L \sin \phi = - C_{dh} \cos \epsilon$,	EXCITATION *	(A10a)
$C_L \cos \phi = C_{dh} \sin \epsilon$,	FLUID INERTIA	(A10b)
$C_R \sin \phi_1 = -C_{mh} \sin \epsilon$,	FLUID REACTION (DAMPING)	(A10C)
$C_R \cos \phi_1 = C_{mh} \cos \epsilon$,	ADDED MASS	(A10d)

These relations can be used to compare recent measurements of the various force components. A similar decomposition of the fluid forces has been suggested recently by Chen (36) in a recent study of heat exchanger tube vibrations. Blevins (2) also has proposed the use of a force decomposition such as that given by equations (A4b) and (A9b).

* These equations are discussed further in a Section 4.1.2 of the appendix.

From the above system of equations it follows that $\tan \phi_1 = \tan \epsilon$ and

$$\tan \phi = -\frac{1}{\tan \epsilon} = = \frac{1}{\tan \phi_1} . \tag{A11}$$

(Recall that ϵ and ϕ are measured from y, whereas ϕ_1 is measured from $\dot{y}$.) It also follows from these equations that

$$C_L^2 = C_{dh}^2 \text{ , or } |C_L| = |C_{dh}| ,$$

and that

$$C_R^2 = C_{mh}^2 \text{ , or } |C_R| = |C_{mh}| .$$

An expression that relates the displacement amplitude Y and the total fluid force can be obtained by squaring and adding equations (A3a) and (A3b) to yield

$$[(1-\alpha^2)^2 + (2\zeta_s\alpha)^2]\ Y^2 = \mu^2 \left(\frac{\omega_s}{\omega_n}\right)^4 [C_L^2 + C_R^2] \tag{A12}$$

upon applying the result $\tan \phi = -\dfrac{1}{\tan \phi_1}$. The phase angles ϕ and ϕ_1 can be retrieved from equations (A3a) and (A3b), and after some manipulations the results are

$$\phi = \text{arc tan} \left(\frac{C_R + W\ C_L}{C_L - W\ C_R}\right) , \tag{A13a}$$

and

$$\phi_1 = \text{arc tan} \left(\frac{W\ C_R - C_L}{C_R + W\ C_L}\right) . \tag{A13b}$$

The parameter W is related to the structural parameters of the resonantly vibrating system by

$$W = \tan \gamma = \frac{2\alpha\zeta_s}{1-\alpha^2} . \tag{A13c}$$

Similar results are obtained from the notation adopted by Sarpkaya (28). The equations (A9) reduce to

$$2\,\alpha\,\zeta_s\ Y = \mu \left(\frac{\omega_s}{\omega_n}\right)^2 \ C_T \sin(\epsilon - \beta') \tag{A14a}$$

$$(1-\alpha^2)\ Y = \mu\left(\frac{\omega_s}{\omega_n}\right)^2 \ C_T \cos(\epsilon - \beta') \tag{A14b}$$

where

$$\beta' = \arctan\left(\frac{C_{dh}}{C_{mh}}\right) \qquad C_T = (C_{mh}^2 + C_{dh}^2)^{1/2}\,.$$

If $W = \tan\gamma$ as before, then

$$\epsilon = \gamma + \beta'$$

or, in an analogous form,

$$\epsilon = \arctan\left(\frac{C_{mh}\ W + C_{dh}}{C_{mh} - W\ C_{dh}}\right) \tag{A15}$$

These solutions are based upon the assumption that the fluid forces are independent of the resonant motion of the cylinder. In reality, there is a complex nonlinear dependence between the fluid forces and the displacement, c.f., Fig. 4.9. Also, the maximum displacement is dependent upon the mass ratio and structural damping of the cylinder and its mountings. When the force coefficients are assumed to be known, as from experiments, these analytical models can be used to predict the cylinder displacement and vice versa.

4.1.2 Work and Energy Considerations It is useful to consider the work and the energy dissipation over each cycle of the cylinder's oscillation. The work done and energy dissipated by the various forces in equations (A1) and (A7) are found by evaluating the integral

$$\sum\int_0^T \bar{F}\ d\bar{y} = \sum\int_0^T \bar{F}\ \frac{d\bar{y}}{dt}\ dt = 0\,.$$

Employing the nomenclature introduced earlier, and evaluating this integral for the structural and fluid dynamic forces in equation (A1), one obtains

$$2\zeta_s\int_0^{\omega_n T} (\dot{y})^2\ d\tau = \mu\left(\frac{\omega_s}{\omega_n}\right)^2\left\{\int_0^{\omega_n T} C_L \sin(\alpha\tau + \phi)\ \dot{y}\ d\tau - \int_0^{\omega_n T} C_R \sin(\alpha\tau + \phi_1)\ \dot{y}\ d\tau\right\}. \tag{A16}$$

The structural inertia and stiffness terms are conservative and do no net work over a cycle of the oscillation. The structural velocity is

$$\dot{y} = \alpha \; Y \cos(\alpha\tau) \; ,$$

so that equation (A16) reduces to

$$2\,\zeta_s \int_0^{\omega_n T} (\dot{y})^2 \, d\tau = \mu \left(\frac{\omega_s}{\omega_n}\right)^2 \{\pi \; C_L \; Y \sin\phi - \pi \;\; C_R \; Y \sin\phi_1\} \; . \tag{A17}$$

When equation (A7) is evaluated in the same manner, one obtains

$$2\,\zeta_s \int_0^{\omega_n T} (\dot{y})^2 \, d\tau = \mu \left(\frac{\omega_s}{\omega_n}\right) \{\pi \; C_{mh} \; Y \sin\epsilon - \pi \;\; C_{dh} \; Y \cos\epsilon\} \; . \tag{A18}$$

A straightforward comparison of equation (A17) with equation (A18) shows that

$$C_L \sin\phi = -\, C_{dh} \cos\epsilon \qquad \text{EXCITATION} \tag{A10a}$$

$$C_R \sin\phi_1 = -\, C_{mh} \sin\epsilon \qquad \text{FLUID REACTION (DAMPING)} \tag{A10c}$$

as had been obtained previously. The "generalized force coefficient" C_{mh} from Sarpkaya's formulation (28) has a component $-C_{mh} \sin\epsilon$ which acts to oppose the velocity $\dot{y}$ of the structure (since ϵ typically is negative for vortex-excited, resonant oscillations) and acts effectively as a fluid reaction force. Likewise, the force coefficient C_{dh}, which is negative during vortex-excited oscillations as shown in Figs. 4.6 and 4.8, is in effect an exciting force which transfers energy to the vibrating cylinder through the component $-\, C_{dh} \cos\epsilon$. This latter force is in phase with the velocity term $\dot{y}$ and drives the resonant vibration. The reaction or damping effect of the fluid can be measured in terms of an effective fluid damping factor ζ_F as shown in references 23 and 27.

A necessary prerequisite for resonant, self-excited oscillations is a positive values of the excitation term in equation (A18), or

$$-\pi \; C_{dh} \; Y \cos\epsilon > 0.$$

Since C_{dh} is negative this implies that $\cos\epsilon > 0$, and leads to the condition

$$C_{mh} - W\,C_{dh} > 0 \tag{A19a}$$

for self-excited oscillations since

$$\cos\epsilon = \frac{C_{mh} - W\,C_{dh}}{\sqrt{(C_{mh} - W\,C_{dh}) + (C_{dh} + W\,C_{mh})^2}}\,.$$

In the notation adopted by Griffin and Koopmann, energy is transferred to a vibrating cylinder when

$$\pi\,C_L\,Y\sin\phi > 0\,.$$

Since C_L is positive, the appropriate condition for self-excited oscillations in $\sin\phi > 0$. This leads to the condition

$$C_R + W\,C_L > 0 \tag{A19b}$$

since

$$\sin\phi = \frac{C_R + W\,C_L}{\sqrt{(C_R + W\,C_L)^2 + (C_L - W\,C_R)^2}}\,.$$

This is analogous to the condition relating to C_{mh} and C_{dh}. A somewhat similar and related development of the relationships between the hydrodynamic forces and the resonant vibrations during lock-on is given by Sarpkaya (4).

4.1.3 Flexible cylinders. It is relatively simple matter to extend the analysis to the case of flexible cylinder with a normal mode shape $\psi_i(z)$, following the "wake-oscillator" formulations of Skop and Griffin (29), Iwan (30) and Blevins (2). If a pure mode response is assumed, then the displacement of the flexible cylinder is

$$Y_i = Y\,\psi_i(z)\,\sin\alpha\tau \tag{A20}$$

at each spanwise point $z = \bar{z}/L$, and the maximum displacement is scaled by the factor

$$Y_{EFF,MAX} = Y\,I_i^{1/2}\;/\;|\psi_i(z)|_{MAX} = Y/\gamma_i \tag{A21}$$

where

$$I_i = \frac{\int_0^1 \psi_i^4(z)\, dz}{\int_0^1 \psi_i^2(z)\, dz} \text{ and } \gamma_i = \frac{|\psi_i(z)|_{MAX}}{I_i^{1/2}} \tag{A22}$$

for a cylinder of length L. For the special case of a circular cylinder $I_i = |\psi_i(z)|_{MAX} = 1$, and other values of I_i and ψ_i for a variety of flexible cylindrical cross-sections are tabulated in Table A1. The parameter γ_i can be calculated directly from the entries in Table A1.

The model just discussed also can be extended to the case of a flexible cylinder by means of a normal mode approach. The cross flow displacement of the cylinder is assumed to take the form

$$y(z,t) = \sum_{i=1}^{\infty} Y_i(t)\, \psi_i(z) \tag{A23}$$

which is a standard expansion of the normal modes (2). When equation (A23) is substituted into equation (A1), the result is a generalized form for the equation of motion given by

$$\sum_{i=1}^{\infty} (m(z)\, Y_{i,tt} + 2m(z)\omega_{ni}\, \zeta_{si}\, Y_{i,t} + m(z)\omega_{ni}^2\, Y_i)\psi_i = \frac{\rho\, D^2\, \omega_s^2}{8\pi^2 St^2}\, (\tilde{C}_L - \tilde{C}_R) \tag{A1a}$$

where, in general $\tilde{C}_L$ and $\tilde{C}_R$ are assumed to be functions of both z and t, and the mass per unit length m is a function of z. If this equation is multiplied through by $\psi_i(z)$ and integrated over the length $L\,(z = \bar{z}/L)$ of the cylinder, then the balance of forces for the ith mode is

$$(Y_{i,tt} + 2\, \omega_{ni}\, \zeta_{si}\, Y_{i,t} + \omega_{ni}^2\, Y_i)\left(\int_0^1 \psi_i^2(z)\, m(z)\, dz\right) = \frac{\rho D^2 \omega_s^2}{8\pi^2 St^2}\left[\int_0^1 \tilde{C}_L \psi_i(z)\, dz - \int_0^1 \tilde{C}_R \psi_i(z)\, dz\right] \tag{A24}$$

when the normal modes of the structure satisfy the orthogonality condition

$$\int_0^1 m(z)\psi_i(z)\, \psi_j(z)\, dz = \left| \begin{matrix} O & i \neq j \\ m & i = j \end{matrix} \right. . \tag{A25}$$

Table A1. Normal Modes $\psi_i(z)$ and Corresponding Values of $I_i^{-1/2}$ for Various Structural Forms

I. Pivoted Rigid Rod

Normal modes: $\psi_1 = \bar{z}/L$, $\psi_{i\neq 1} = 0$

$I_i^{-1/2}$: $(5/3)^{1/2} = 1.2910$

II. Taut String

Normal modes: $\psi_i = \sin i\pi\bar{z}/L$

$I_i^{-1/2}$: $(4/3)^{1/2} = 1.1547$

III. Pinned-Pinned Beam

Normal modes: $\psi_i = \sin i\pi\bar{z}/L$

$I_i^{-1/2}$: $(4/3)^{1/2} = 1.1547$

IV. Cantilevered Beam

Normal modes; $\psi_i = \cosh \lambda_i\bar{z}/L - \cos \lambda_i\bar{z}/L - \alpha_i(\sinh \lambda_i\bar{z}/L - \sin \lambda_i\bar{z}/L)$

i	λ_i	α_i	$I_i^{-1/2}$
1	1.87510410	0.73409550	0.6525
2	4.19409113	1.01846644	0.7494
3	7.85475743	0.99922450	0.7686

V. Clamped-Clamped Beam

Normal modes: $\psi_i = \cosh \lambda_i\bar{z}/L - \cos \lambda_i\bar{z}/L - \alpha_i(\sinh \lambda_i\bar{z}/L - \sin \lambda_i\bar{z}/L)$

i	λ_i	α_i	$I_i^{-1/2}$
1	4.75300408	0.98250222	0.7348
2	7.8532046	1.00077731	0.7694
3	10.9956078	0.99996645	0.7817

VI. Clamped-Pinned Beam

Normal modes: $\psi_i = \cosh \lambda_i\bar{z}/L - \cos \lambda_i\bar{z}/L - \alpha_i(\sinh \lambda_i\bar{z}/L - \sin \lambda_i\bar{z}/L)$

i	λ_i	α_i	$I_i^{-1/2}$
1	3.92660230	1.00077730	0.7694
2	7.06858275	1.00000144	0.7891
3	10.21027613	1.00000000	0.7972

VII. Free-Pinned Beam

Normal modes: $\psi_i = \cosh \lambda_i(\bar{z}/L) + \cos \lambda_i(\bar{z}/L) - \alpha_i[\sinh \lambda_i(\bar{z}/L) + \sin \lambda_i(\bar{z}/L)]$

i	λ_i	α_i	$I_i^{-1/2}$
1	3.92660	1.000773	0.7628
2	7.06858	1.000000	0.7890
3	10.2102	1.000000	0.7972

In terms of the variables given in the first paragraph of Section 4.1.1, Equation (A24) reduces to

$$\omega_{ni}^2(\ddot{Y}_i + 2\zeta_{si}\,\dot{Y}_i + Y_i) = \frac{\rho D^2\omega_s^2}{8\pi^2 St^2}\left\{\frac{\int_0^1 \bar{C}_L\psi_i(z)\,dz}{\int_0^1 m(z)\psi_i^2(z)\,dz} - \frac{\int_0^1 \bar{C}_R\psi_i(z)\,dz}{\int_0^1 m(z)\psi_i^2(z)\,dz}\right\}, \tag{A26}$$

where Y_i is the generalized displacement and the integrals on the right-hand side are generalized force coefficients. When "equivalent" force coefficients and the "equivalent" mass are introduced by

$$\bar{C}_{LE} = \frac{\int_0^1 \bar{C}_L\psi_i(z)\,dz}{\int_0^1 \psi_i(z)\,dz}, \tag{A27a}$$

$$\bar{C}_{RE} = \frac{\int_0^1 \bar{C}_R\psi_i(z)\,dz}{\int_0^1 \psi_i(z)\,dz}, \tag{A27b}$$

and

$$m_E = \frac{\int_0^1 m(z)\psi_i^2(z)\,dz}{\int_0^1 \psi_i^2(z)\,dz} \tag{A27c}$$

the equation of motion reduces to

$$\ddot{Y} + 2\zeta_s\dot{Y} + Y = \mu\left(\frac{\omega_s}{\omega_n}\right)^2(\bar{C}_{LE} - \bar{C}_{RE})\frac{\int_0^1 \psi(z)\,dz}{\int_0^1 \psi^2(z)\,dz}. \tag{A28}$$

The subscript i is dropped since a single mode response is understood in this equation. In the case of the flexible cylindrical structure, a work and energy balance similar to equation (A16) leads to the result

$$2\zeta_s\int_0^{\omega_n T}(\dot{Y})^2 dt = \pi\mu\left(\frac{\omega_s}{\omega_n}\right)^2(C_{LE}Y\sin\phi - C_{RE}Y\sin\phi_1)\,\frac{\int_0^1 \psi(z)\,dz}{\int_0^1 \psi^2(z)\,dz}$$

where C_{LE} and C_{RE} are "equivalent" force coefficients similar in form to those given by equations (A27a) and (A27b).

An approach such as this can be adapted readily to finite-element matrix methods of structural analysis (81), as shown by Evers and Dean (61) and by Hove, Shih and Albano (42), respectively, for an empirical formulation and a "wake-oscillator" formulation of the vortex-excited oscillation problem.

Appendix A.1 NOMENCLATURE AND LIST OF SYMBOLS (other symbols not listed here are defined in Appendix 4.1).

a,b,c	Coefficients defined in Table 5.2
a_1, b_1, c_1, d_1	Coefficients defined in Table 5.3.
C_d'	Unsteady drag coefficient on a cylinder vibrating in the in line direction.
C_{dh}	Unsteady force coefficient on a cylinder vibrating in the cross flow direction; see equation (A5).
C_{mh}	Unsteady force coefficient on a cylinder vibrating in the cross flow direction; see equation (A5).
C_D, C_{DO}	Steady drag coefficient on a vibrating (stationary) cylinder.
C_L	Lift coefficient; see equation (A2a).
C_{LE}	Excitation force coefficient; see equation (A10a).
C_R	Reaction force coefficient; see equation (A2b).
C_{RE}	Fluid reaction (damping) force coefficient; see equation (A10c).
D	Cylinder diameter (m or ft).
EI	Cross section rigidity; see equation (8.1).
f_n	Natural frequency (Hz).
f_s	Strouhal frequency (Ha).
I_i	Modal scaling factor; see equation (4.36).
k_s	Reduced damping; see equation (3.1).
L	Cylinder length (m or ft).
m	Cylinder mass per unit length (kg/m or lb_m/ft).
m_e	Effective mass per unit length (kg/m or lb_m/ft); see equation (5.1) and example 8.3.
Re	Reynolds number, VD/ν.

St	Strouhal number, f_s D/V.
T	Temperature (°C or °F).
T_i	Natural period of vibration in the i th normal mode (sec).
u	Wake velocity fluctuation (m/s or ft/sec); see equation (4.4).
V	Incident flow velocity (m/s or ft/sec or knots).
V_r	Reduced velocity, $V/f_n D$; see equation (3.2).
V_r, $crit$	Critical reduced velocity; see equation (5.2) and examples 8.1 and 8.2.
ω_r	Response parameter, $(1 + 2\bar{Y}/D)\ (V_r\ St)^{-1}$; see equation (5.4).
W	Phase angle function; see equation (A13c).
$\bar{X}$	In line displacement amplitude (m or ft).
$\bar{y}$	Cross flow displacement (m or ft).
$\bar{Y}$	Cross flow displacement amplitude (m or ft).
Y	Normalized displacement amplitude, $\bar{Y}/D$.
$Y_{EFF,MAX}$	Normalized displacement amplitude; see equation (4.3a).
$\bar{z}$	Coordinate measurement along the cylinder or CWP (m or ft).
β	Yaw angle (deg or rad).
β'	Phase angle (deg or rad); see Table 4.2 and example 4.2.
$\bar{\beta}$	Shear flow parameter; see equation (4.4)
δ	Log decrement of structural damping.
ϵ	Phase angle (deg or rad); see equation (A15).
γ_i	Normalizing factor; see equation (5.3).
ϕ	Phase angle (deg or rad); see equation (A13a).
ϕ_1	Phase angle (deg or rad); see equation (A13b).
γ_i	Flexible beam parameter; see equation (8.1) and Table 8.3.

μ	Mass ratio, see equation (A1).
ν	Kinematic fluid viscosity (m^2/sec or ft^2/sec).
ρ	Fluid density (kg/m^3 or lb_m/ft^3).
ρ_{AB}	Correlation coefficient; see equation (4.44).
$\psi_i(z)$	Mode shape for i th flexible beam mode; see Table A1.
ζ_s	Structural damping ratio; see equation (A1).

Appendix A.2 LIST OF FIGURES

Figure 2.1 A schematic of Georges Claude's 800 KW_e open-cycle OTEC plant on-board the 10,000 ton cargo ship Tunisie.

Figure 2.2 A diagram of OTEC-I.

Figure 2.3. Typical rigid-wall OTEC cold water pipe concept.

Figure 2.4. Typical compliant-wall OTEC cold water pipe concept.

Figure 2.5. Overall layout of a bottom-mounted OTEC cold water pipe.

Figure 3.1. Vortex-excited displacement of a flexible cantilever (from equilibrium) in the in line direction.

Figure 3.2. Composite stability diagram for the first three normal modes of a flexible cantilevered circular cylinder.

Figure 3.3. Displacement amplitude and frequency ranges over which the in line vibrations of a cylinder control the vortex shedding (lock-on boundaries).

Figure 3.4. Fluctuating drag coefficient C'_d (Force/$\frac{1}{2}\rho V^2 DL$) plotted against in line displacement amplitude.

Figure 3.5. Fluctuating drag coefficient C'_d (Force/$1/2\ \rho V^2 DL$) plotted against the in line displacement amplitude.

Figure 3.6. A comparison of the full scale and 1/27-scale model results for vortex-excited in line oscillations.

Figure 3.7. A comparison of full scale and 1/24-scale model results for vortex-excited in line oscillations.

Figure 4.1. Cross flow-induced displacement amplitude $\bar{Y}/D$ and frequency f of circular cylinders in water.

Figure 4.2. Inverse reduced velocity V_r^{-1} for maximum displacement amplitudes.

Figure 4.3. Observed cross flow displacement amplitude $\bar{Y}/D$ for full-scale marine piles.

Figure 4.4. Maximum vortex-excited cross flow displacement amplitude $2Y_{EFF,MAX}$ of circular cylinders.

Figure 4.5. The inertia coefficient C_{mh} at the locked-on vibration frequency, for $\bar{Y}/D = 0.5$.

Figure 4.6. The "drag" coefficient C_{dh} at the locked-on vibration frequency, for $\bar{Y}/D = 0.5$.

Figure 4.7. The inertia coefficient C_{mh} at the locked-on vibration frequency, for $\bar{Y}/D = 0.75$.

Figure 4.8. The "drag" coefficient C_{dh} at the locked-on vibration frequency, for $\bar{Y}/D = 0.75$.

Figure 4.9. The excitation component C_{LE} of the lift force.

Figure 4.10. The fluid reaction force coefficient C_{RE}.

Figure 4.11. The steady drag coefficient C_D due to vortex-excited cross flow oscillations.

Figure 4.12. Total hydrodynamic force coefficient $C_{T,MAX}$, (Force/$\frac{1}{2}\rho V^2 DL$), measured on vibrating smooth and rough circular cylinders.

Figure 4.13. Measured cross flow displacement amplitude $\bar{Y}/D$ plotted against the reduced velocity V_r, for a cantilevered flexible cylinder in uniform and shear flows.

Figure 4.14. The cross flow displacement amplitude $\bar{Y}/D$ for flexible, yawed cylinders.

Figure 4.15. Cross flow lock-on boundaries (in terms of the cross flow displacement amplitude $2\bar{Y}/D$) plotted against the ratio of vibration and Strouhal frequencies.

Figure 4.16. Spanwise correlation coefficients ρ_{AB} for the velocity in the wake of a vibrating cable.

Figure 4.17. Distribution of displacement amplitude $\bar{Y}/D$, magnitude of the spanwise correlation coefficient ρ_{AB}, and the spectral content of the vortex shedding in the wake of a cable.

Figure 4.18. Spanwise correlation coefficient R_p between the fluctuating pressures measured on a vibrating pivoted rigid cylinder.

Figure 5.1. Flow diagram of the steps required for the calculation of the response of a structure due to vortex shedding.

Figure 5.2. Flow diagram of the steps required for the calculation of the steady drag amplification due to vortex-excited oscillations.

Figure 6.1. A comparison of the measured cross flow oscillations. of a flexible cylinder with the predicted response from VORTOS.

Figure 6.2. A schematic drawing of the SEACON II cable structure.

Figure 6.3. A comparison of the measured and predicted motions of a point on the SEACON II delta.

Figure 6.4. A comparison of TRW HULPIPE and NOAA/DOE model predicted bending stresses.

Figure 7.1. Photographs of the three common types of vortex suppression devices.

Figure 7.2. A photograph of a fairing (section) constructed for a 24 inch diameter riser.

Figure 7.3. A comparison of the response of flexible cylinders with and without vortex spoilers.

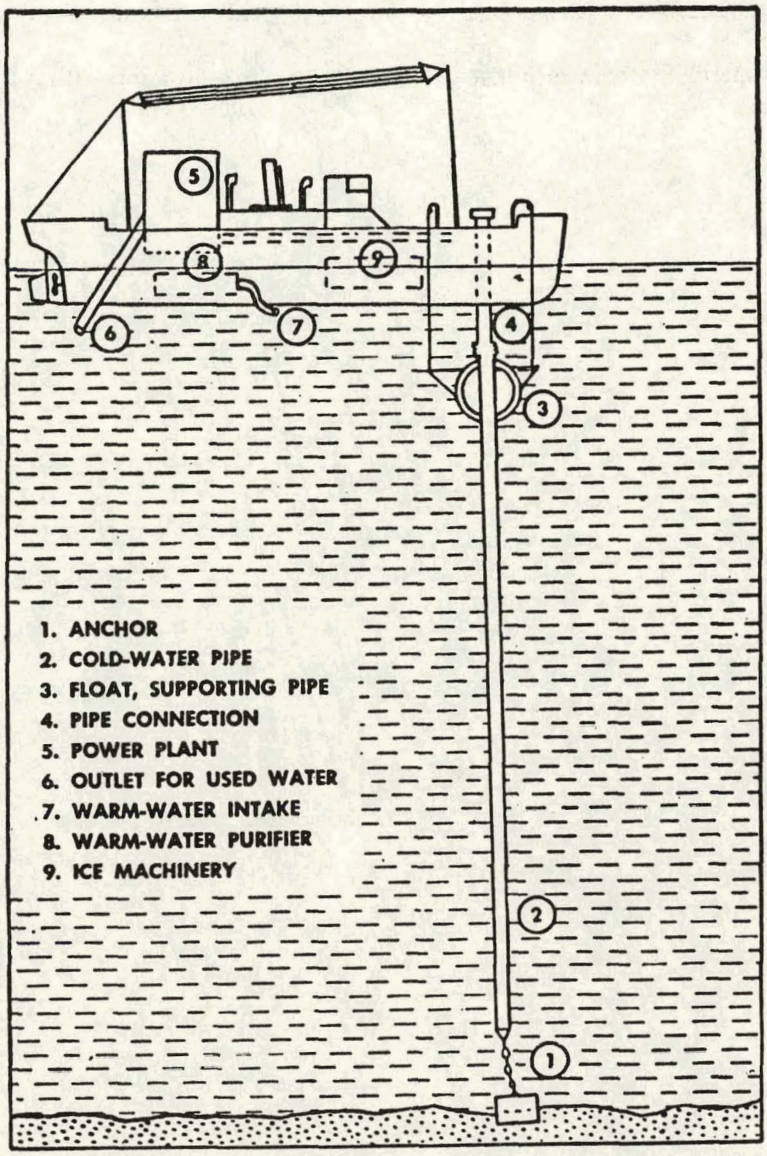

Figure 2.1 A schematic of Georges Claude's 800 KW_e open cycle OTEC plant on-board the 10,000 ton cargo ship Tunisie (From *Engineers' Dreams* by Willy Ley. © 1954 by Willy Ley and reprinted by permission of Olga Ley).

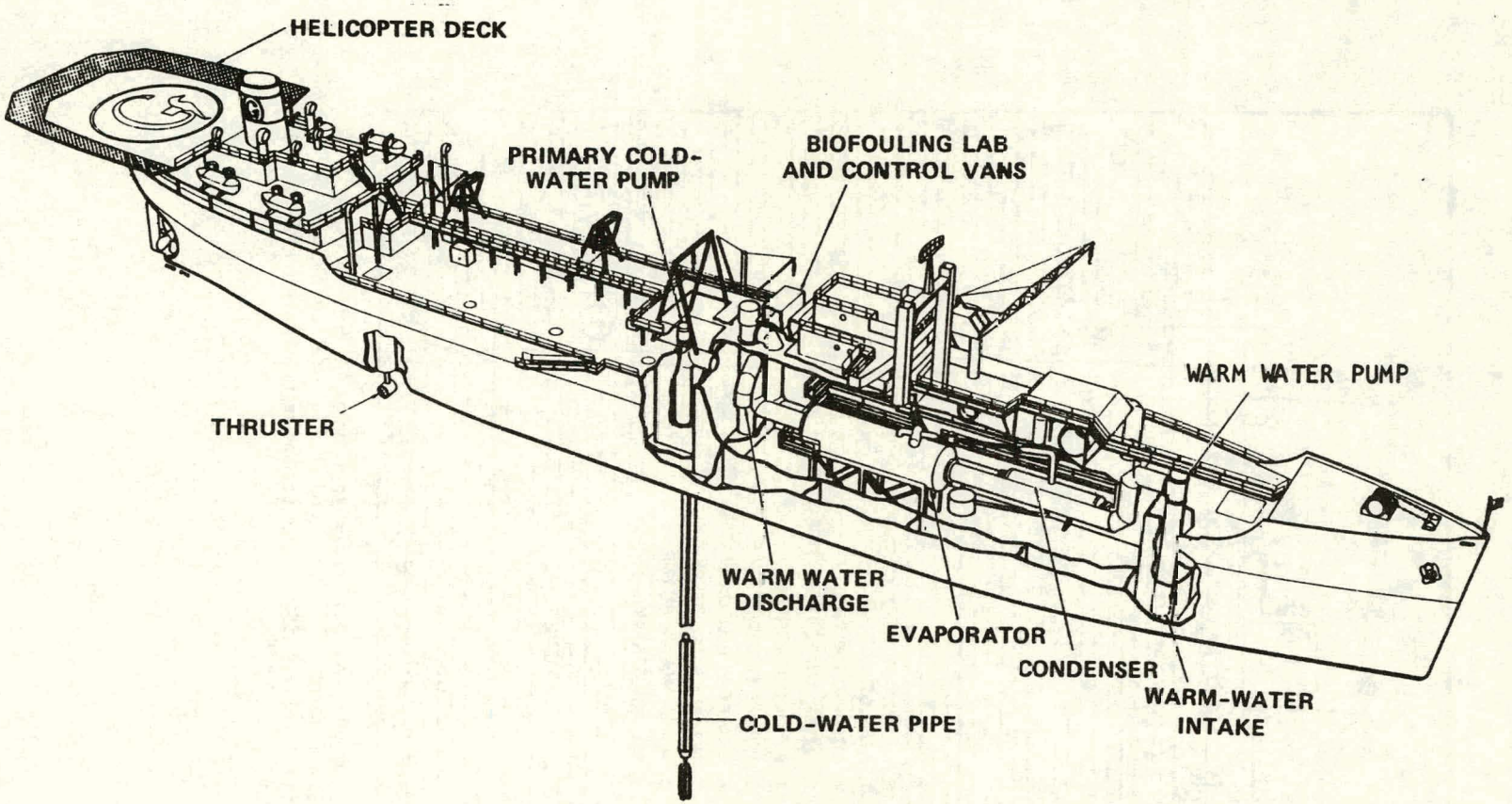

Isometric Cutaway of Chepachet Outfitted as OTEC-1 Test Platform

Figure 2.2 A line drawing of the Navy tanker which is being converted to an OTEC test platform, called OTEC-I.

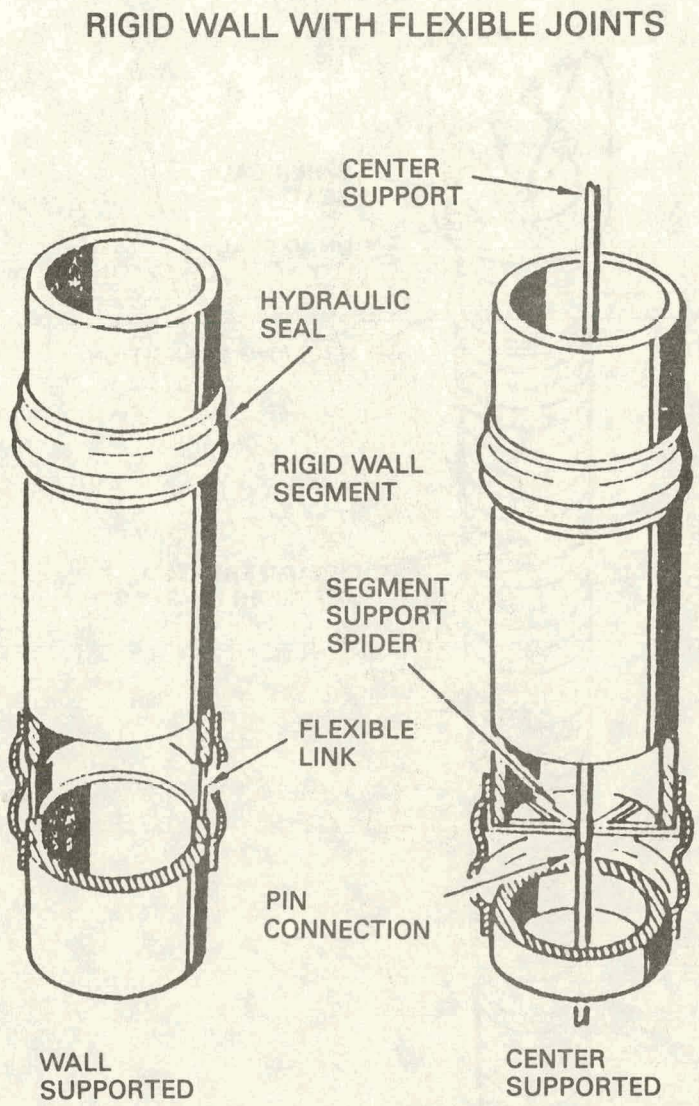

Figure 2.3. Typical rigid-wall OTEC cold water pipe concept (no articulated joints) for a10/40 MW_e plant.

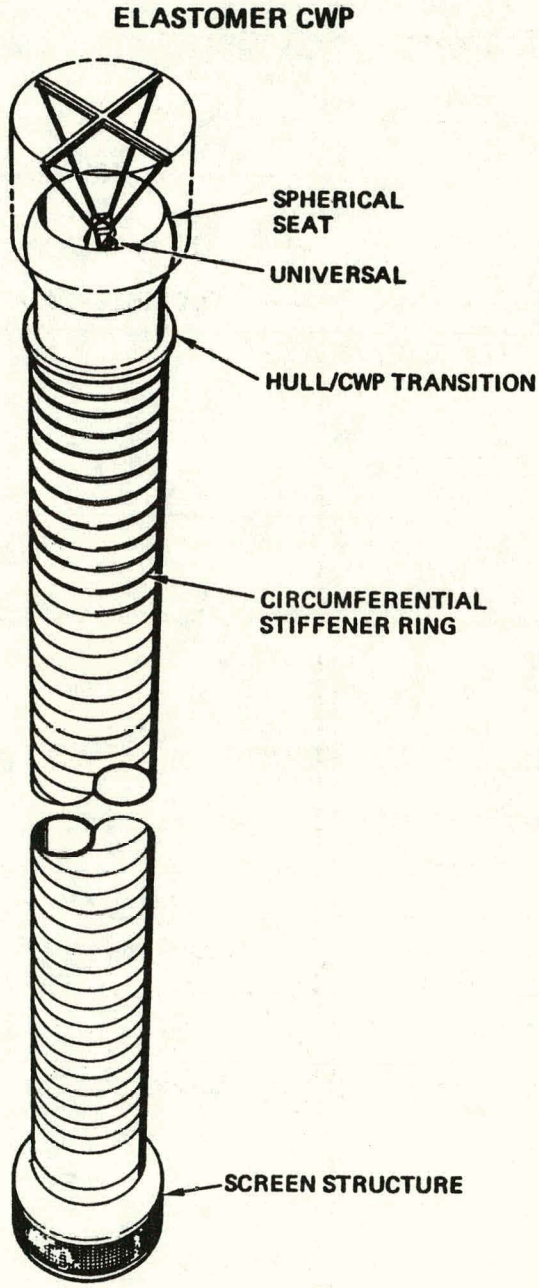

Figure 2.4. Typical compliant-wall OTEC cold water pipe concept (steel cable — reinforced elastomeric construction) for a 10/40 MW_e plant.

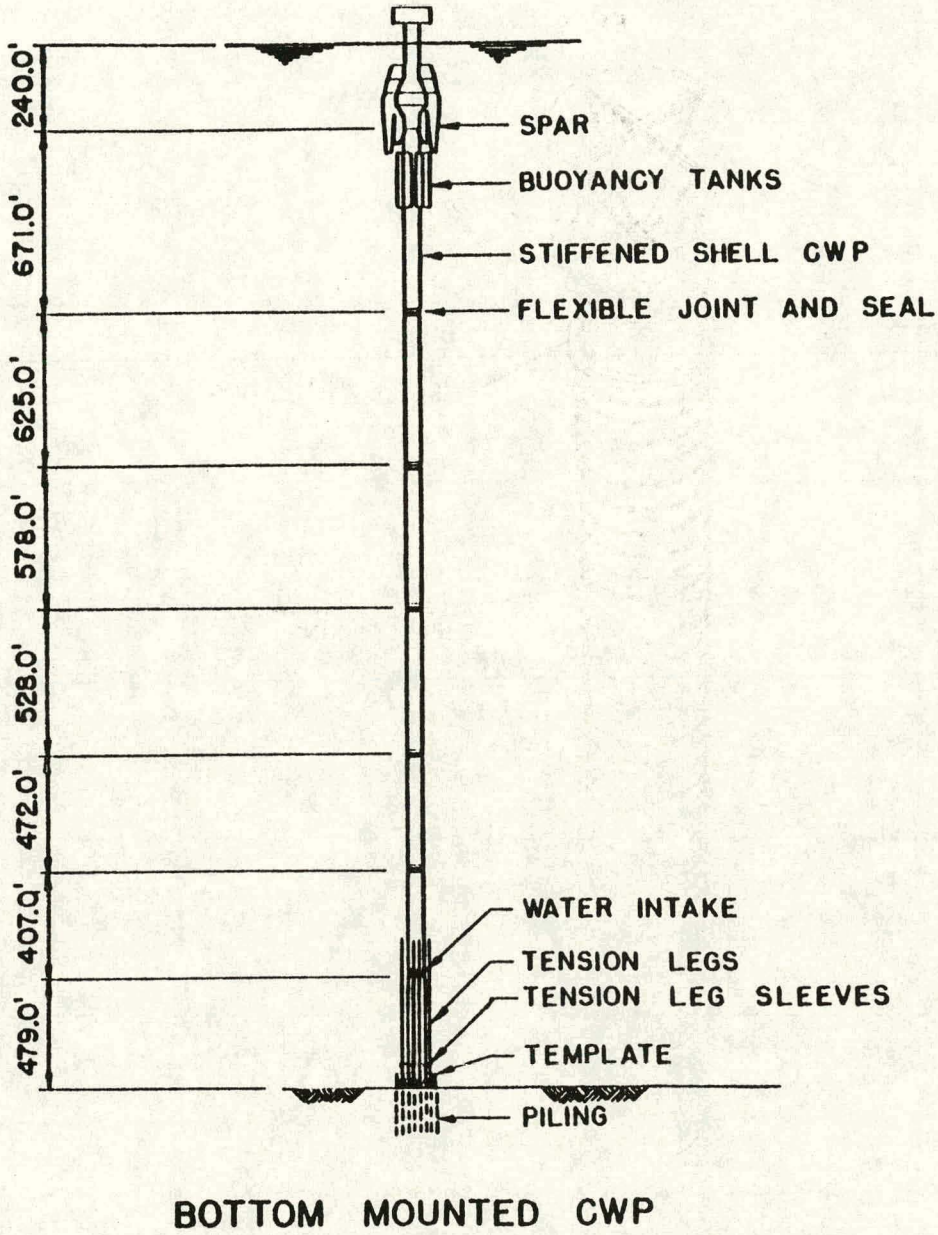

Figure 2.5. Overall layout of a bottom-mounted OTEC cold water pipe and 10/40 MW_e plant.

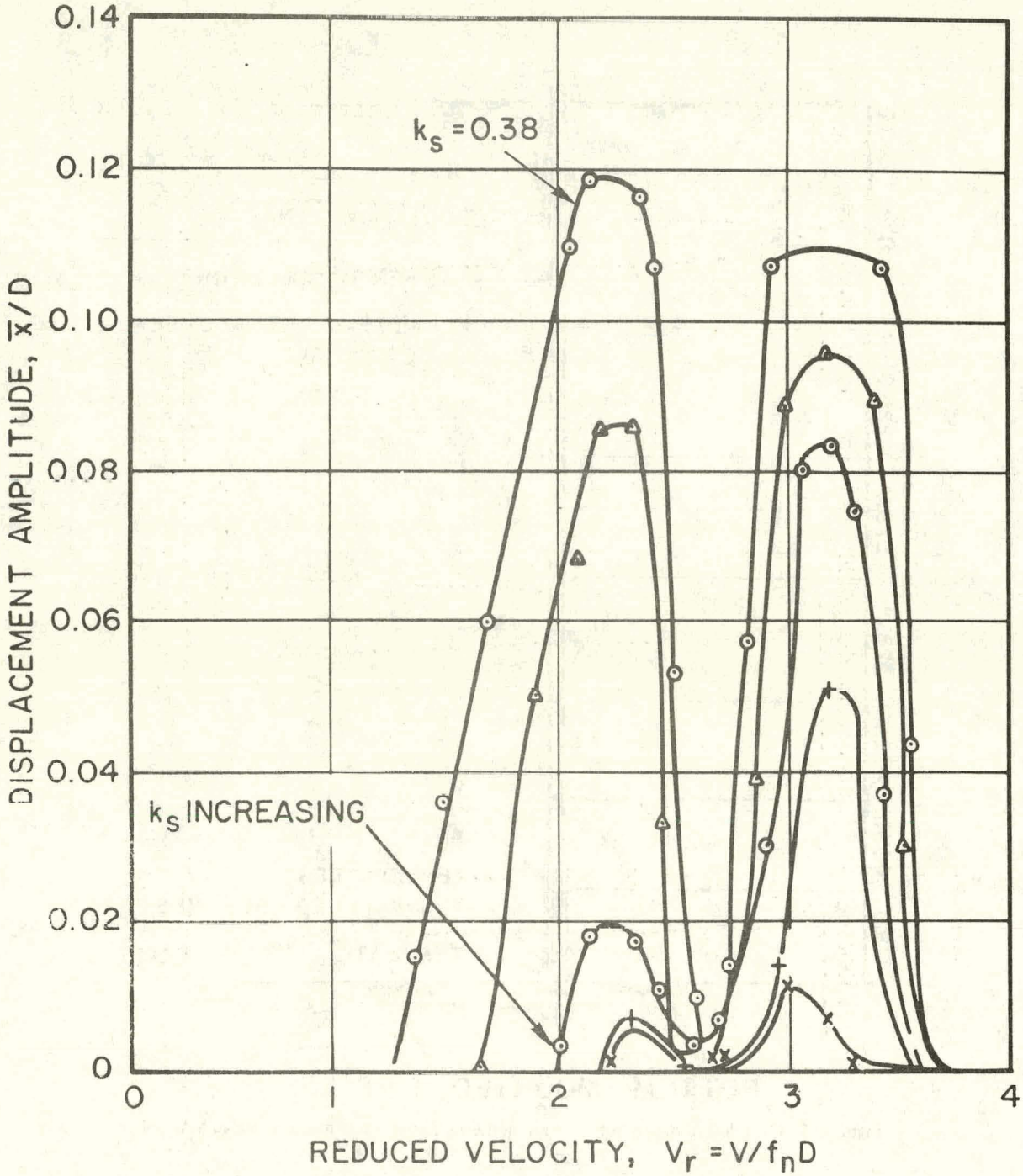

Figure 3.1 Vortex-excited displacement of a flexible cantilever (from equilibrium) in the in line direction plotted against the reduced velocity $V_r = V/f_nD$. The reduced damping of the structure is denoted by k_s, the diameter of the cylinder is denoted by D and the cylinder's natural frequency by f_n; from King (18).

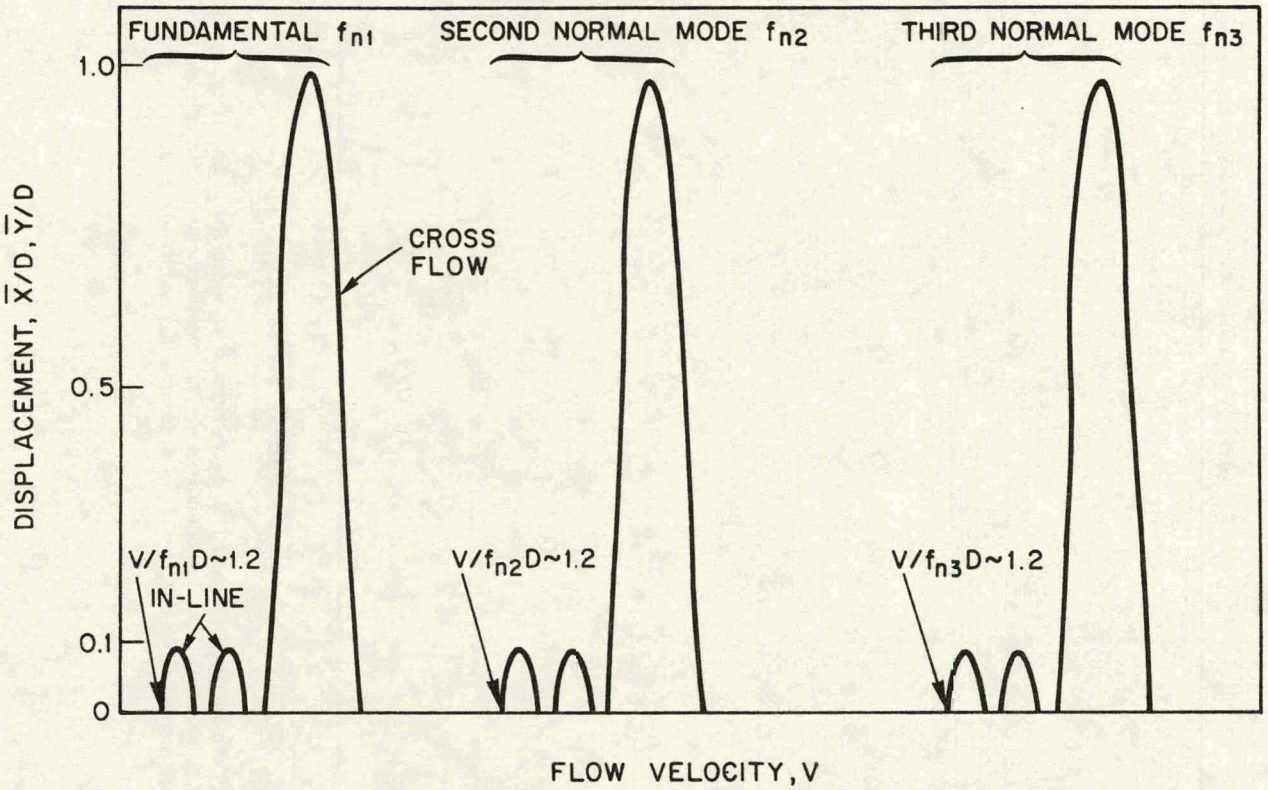

Figure 3.2. Composite stability diagram for the first three normal modes of a flexible cantilevered circular cylinder as a function of the incident water velocity. Both in line (small displacement) and cross flow (large displacement) instabilities are shown; from King (19).

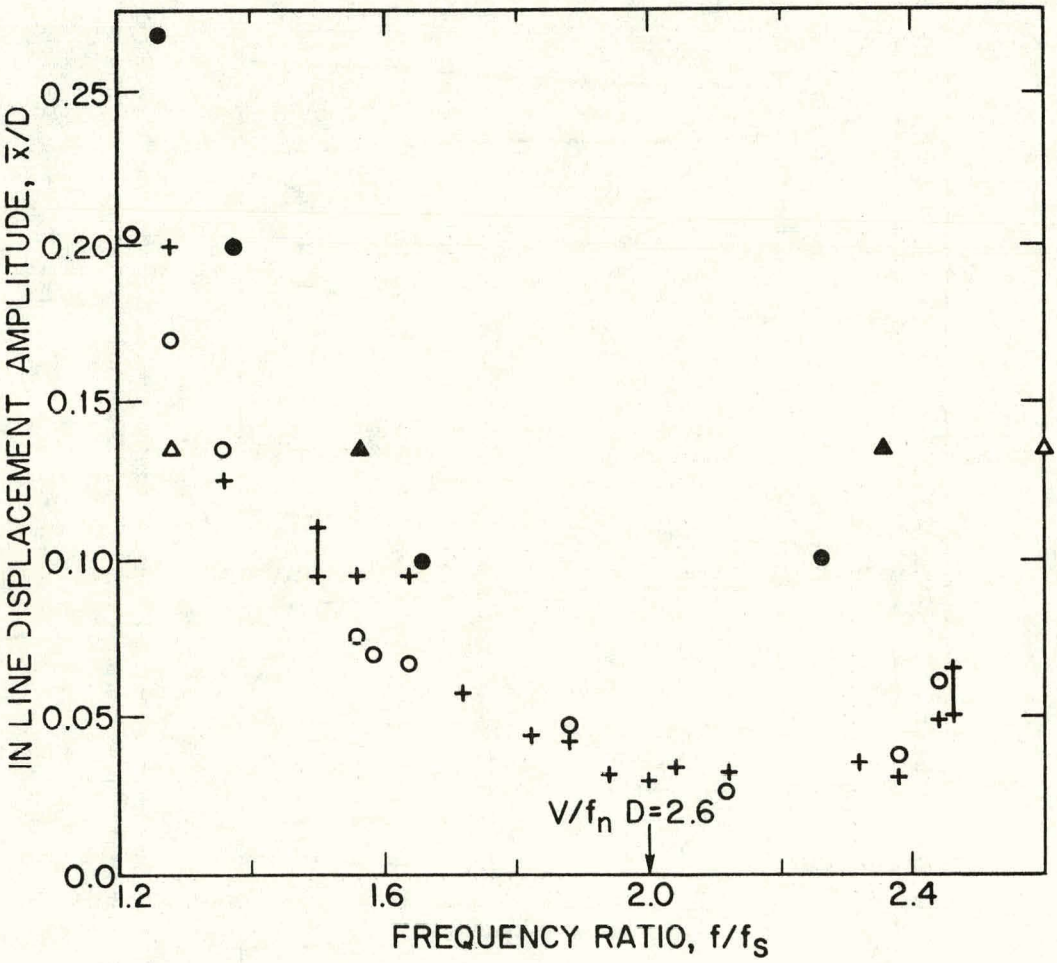

Figure 3.3. Displacement amplitude and frequency ranges over which the in line vibrations of a cylinder control the vortex shedding (lock-on boundaries). The measurements at frequencies near twice the Strouhal frequency correspond to $V/f_n D = 2$ to 4.4; from Griffin and Ramberg (20).

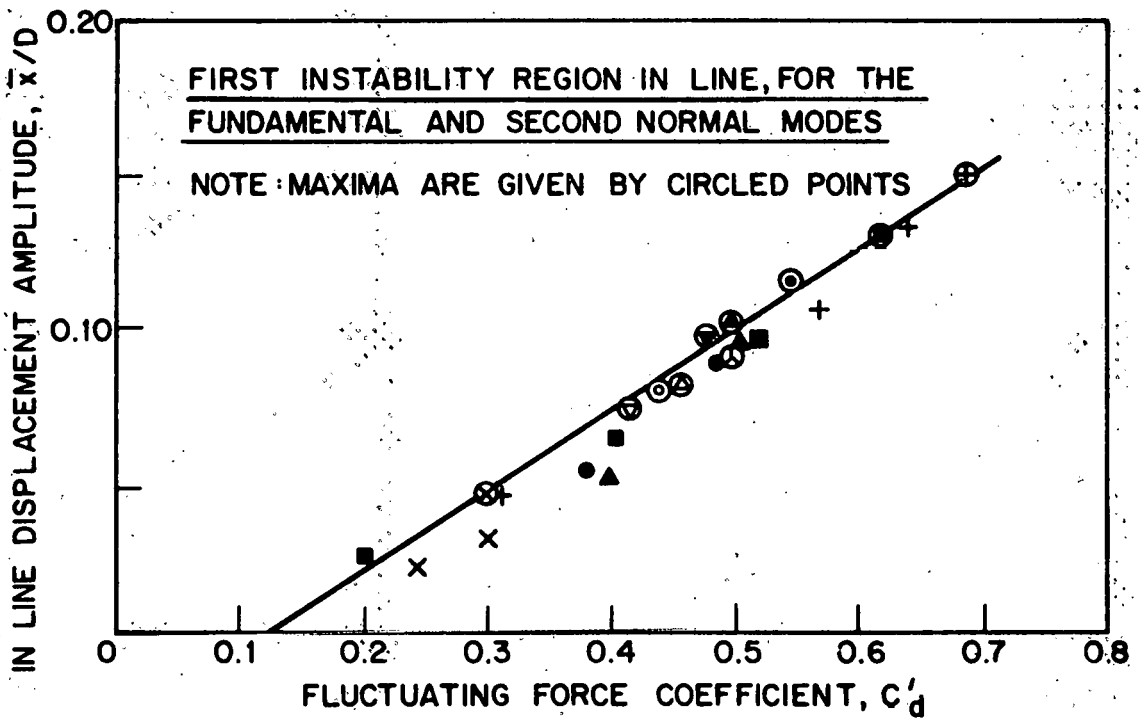

Figure 3.4. Fluctuating drag coefficient C'_d (Force/$\frac{1}{2}\rho V^2 DL$) plotted against in line displacement amplitude $\bar{x}/D$ (from equilibrium), for the fundamental and second normal modes of a flexible, cantilevered circular cylinder. The circles denote the maxima of C'_d for a given run; from King (19).

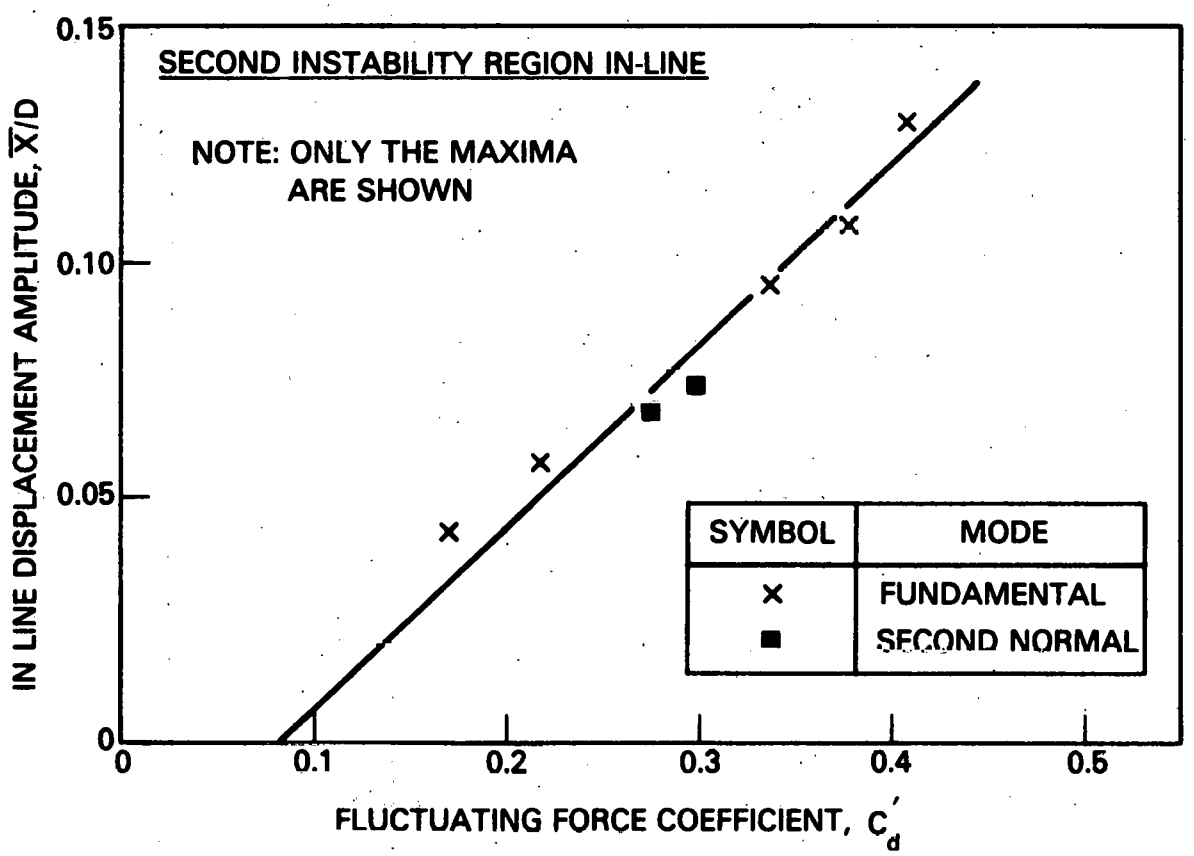

Figure 3.5. Fluctuating drag coefficient C_d' (Force/$1/2\,\rho V^2 DL$) plotted against the in line displacement amplitude, for the fundamental and second normal modes of a flexible, cantilevered circular cylinder. Only the maxima for a given run are shown on the figure; from King (19).

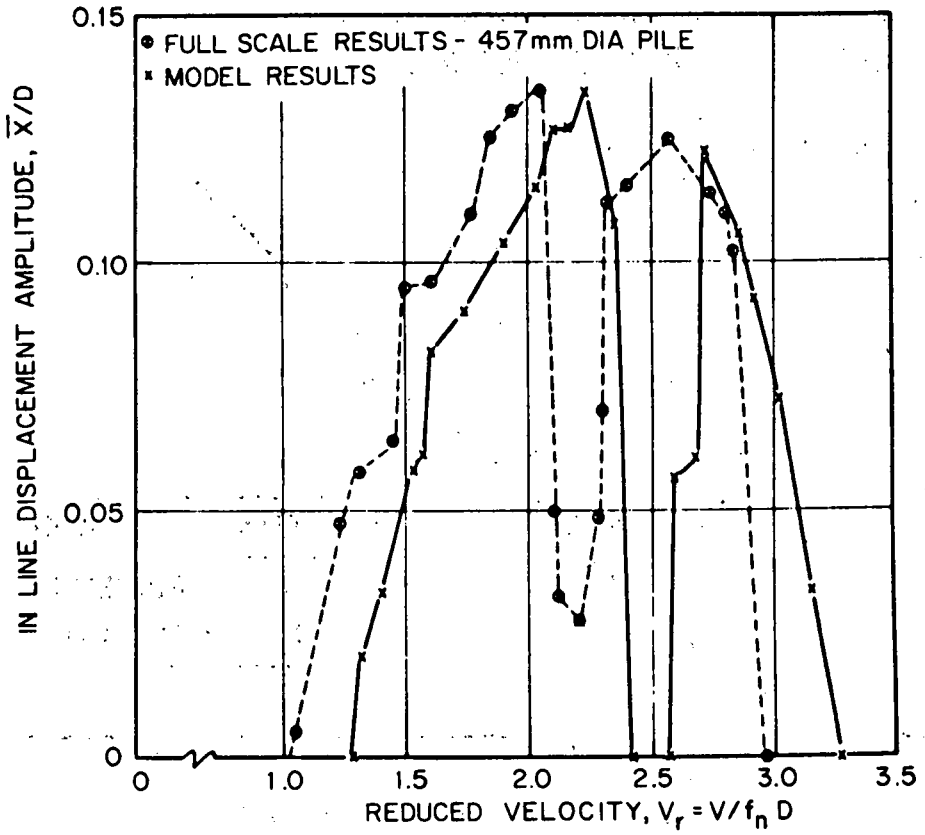

Figure 3.6. A comparison of the full-scale and 1/27-scale model results for vortex-excited in line oscillations of a flexible, cantilevered circular cylinder. The full-scale Reynolds number was about $6(10^5)$ and $k_s = 0.3$ for both cases; from King (18).

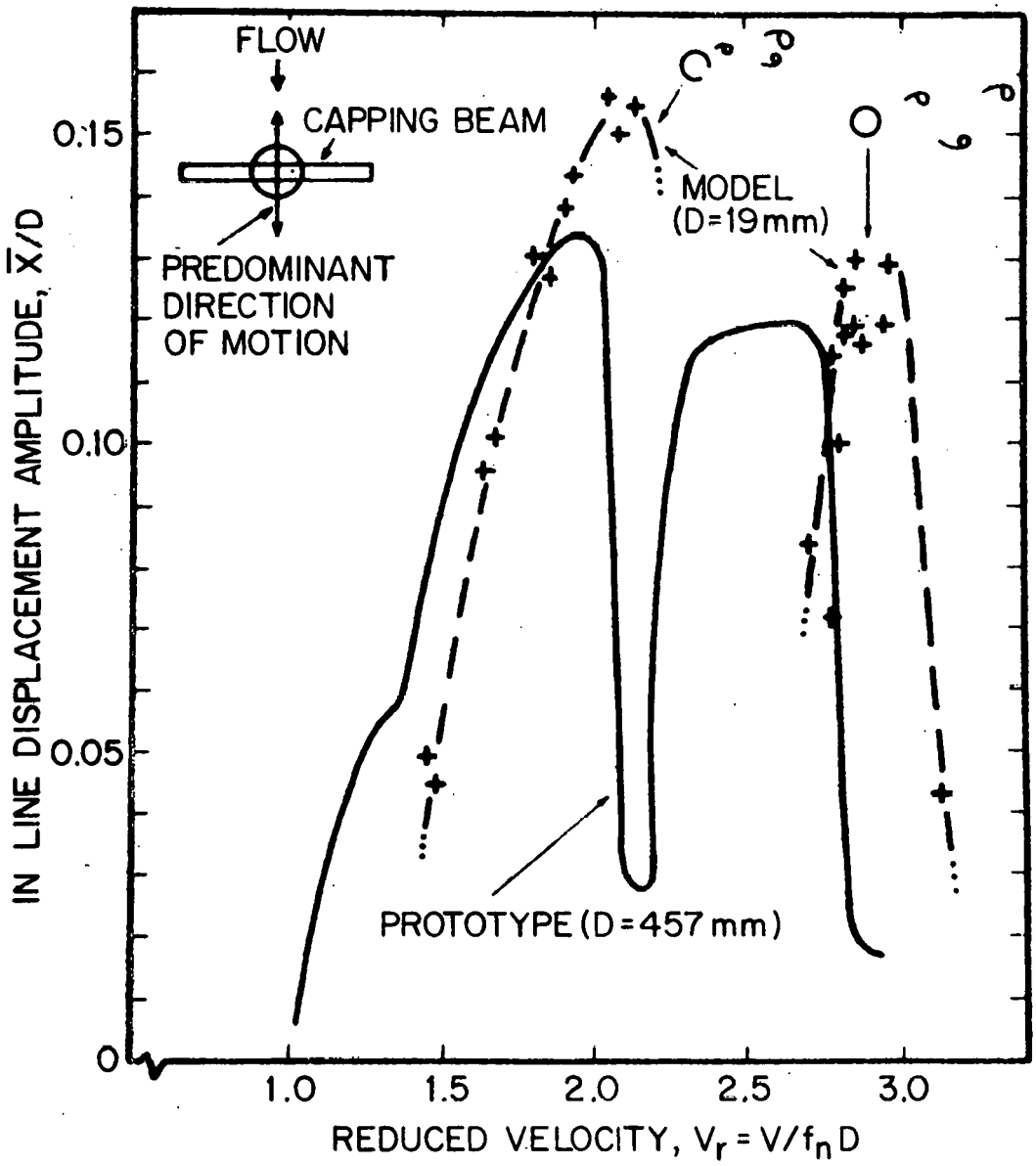

Figure 3.7. A comparison of full-scale and 1/24-scale model results for vortex-excited in line oscillations of a flexible cantilevered circular cylinder. The full scale Reynolds number was about 10^6; from Hardwick and Wootton (22).

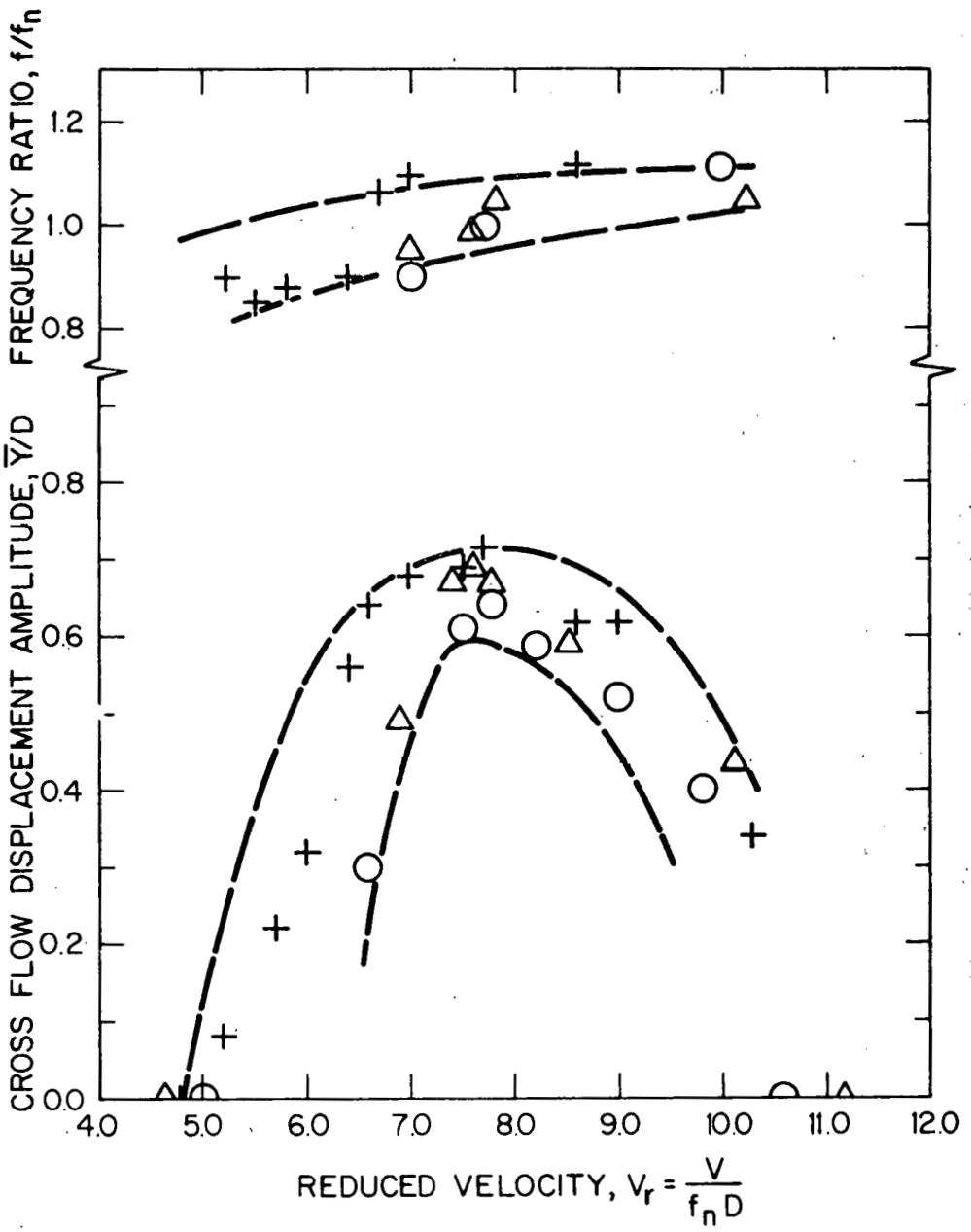

Figure 4.1. Cross flow-induced displacement amplitude $\bar{Y}/D$ and frequency f (scaled by the natural frequency f_n) of three circular cylinders in water, plotted against the reduced velocity V_r; data taken by Glass (1970), from Griffin (23).

Legend for Data Points

	L/D	f_n (Hz)	$2m/\rho D^2$
0	8.5	2.4	7.6
+	11.8	1.8	7.6
Δ	15.4	1.3	7.6

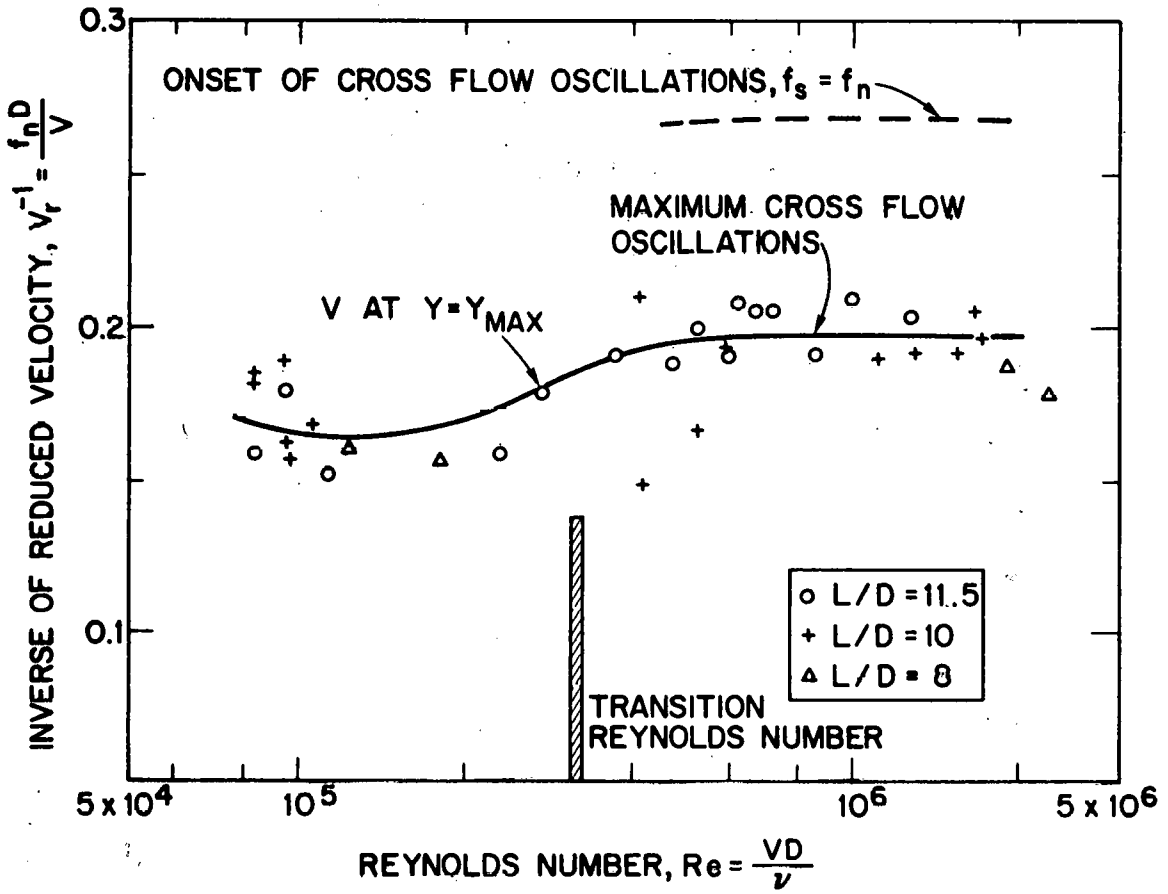

Figure 4.2. Inverse reduced velocity V_r^{-1} for maximum displacement amplitudes plotted against the Reynolds number for roughened cylinders. The inverse of V_r is the Strouhal number based on f_n. Maximum peak displacement ———; onset of vortex-excited oscillations — — —; from Wootton (25).

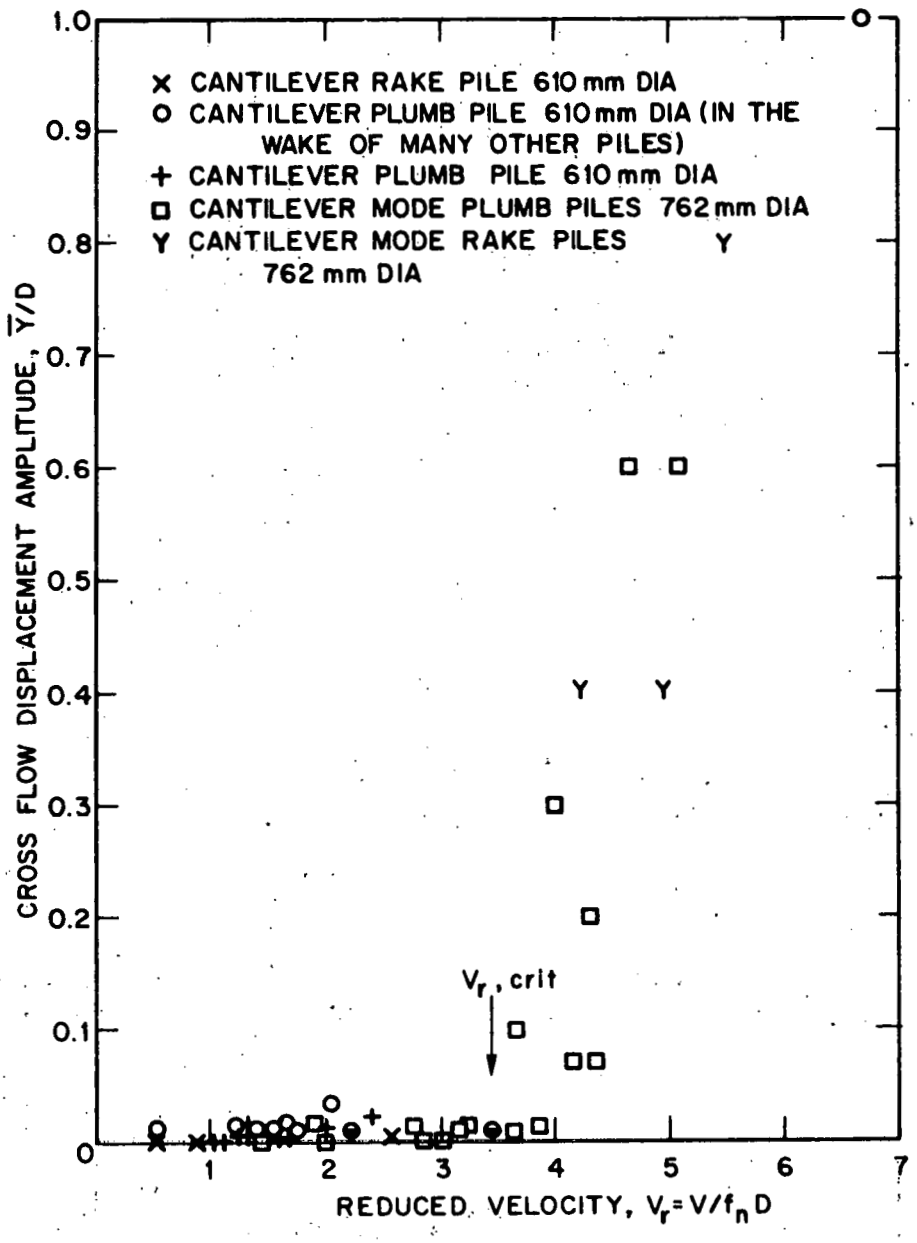

Figure 4.3. Observed cross flow displacement amplitude $\bar{Y}/D$ (from equilibrium) plotted against reduced velocity V_r for full-scale marine piles; from Sainsbury and King (16).

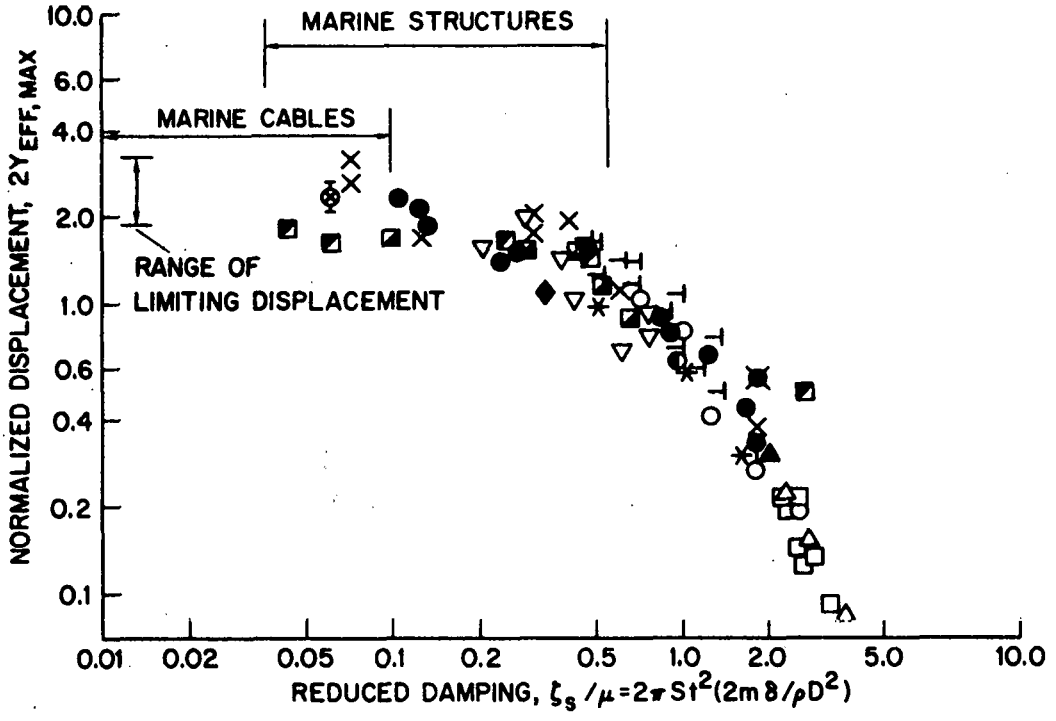

Figure 4.4. Maximum vortex-excited cross flow displacement amplitude $2Y_{EFF,MAX}$ of circular cylinders, scaled as in equation (4a), plotted against the reduced damping $\zeta_s/\mu = 2\pi St^2\ (2m\delta/\rho D^2)$. The legend for the data points is given in Table 4.1; from Griffin (23).

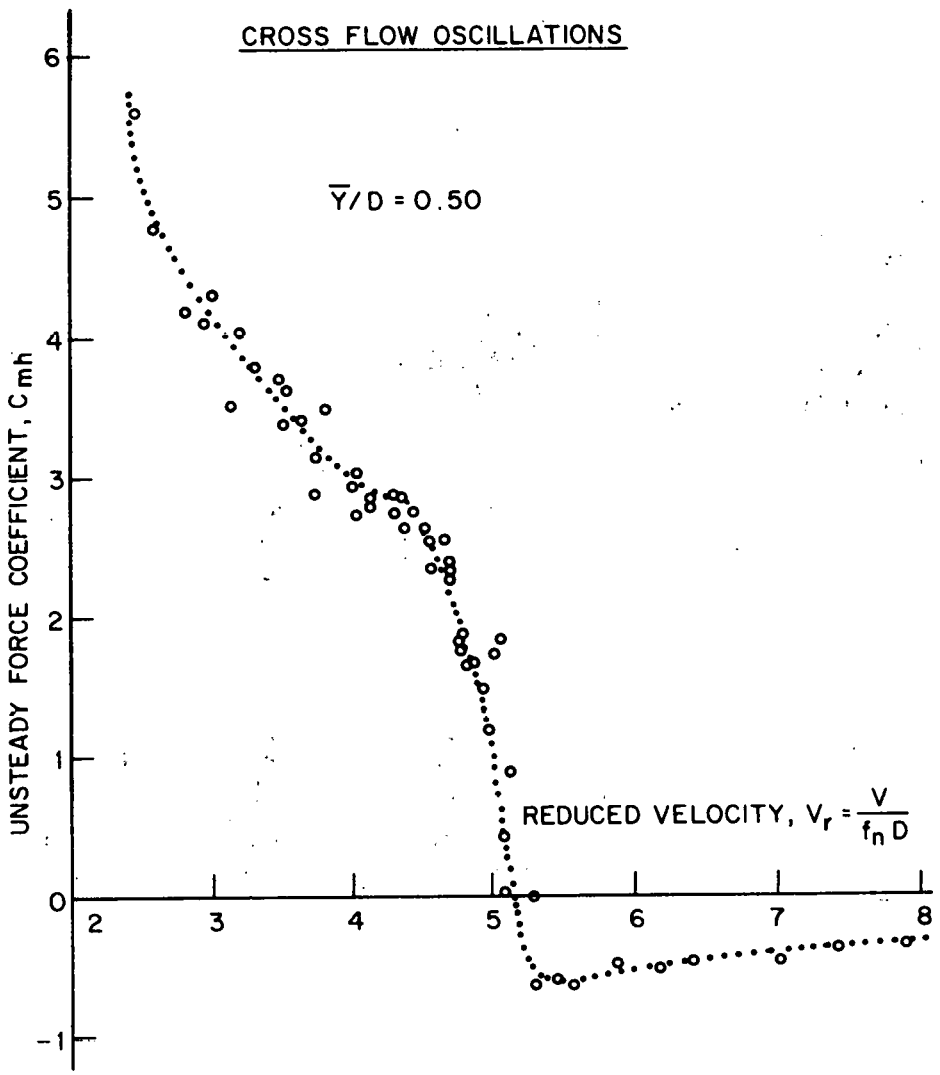

Figure 4.5. The inertia coefficient C_{mh} at the vibration frequency plotted against the reduced velocity V_r for $\bar{y}/D = 0.5$. The data are from Sarpkaya (28) and were measured in water with uniform, steady fluid motion past a cylinder oscillating normal to the flow. The coefficient C_{mh} was derived from the total unsteady transverse force. Lock-on occurs near $V_r = 5$.

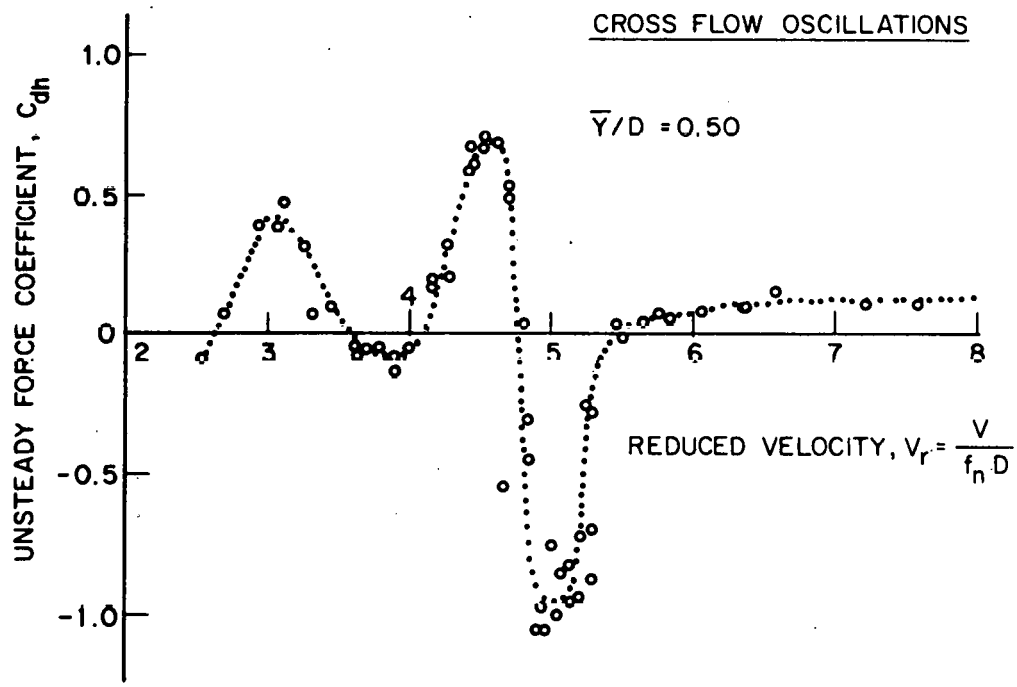

Figure 4.6. The "drag" coefficient C_{dh} at the vibration frequency plotted against the reduced velocity V_r for $\bar{y}/D = 0.5$. The data are from Sarpkaya (28) and were measured in water with uniform, steady fluid motion past a cylinder oscillating normal to the flow. The coefficient C_{dh} was derived from the total unsteady transverse force. Lock-on occurs near $V_r = 5$.

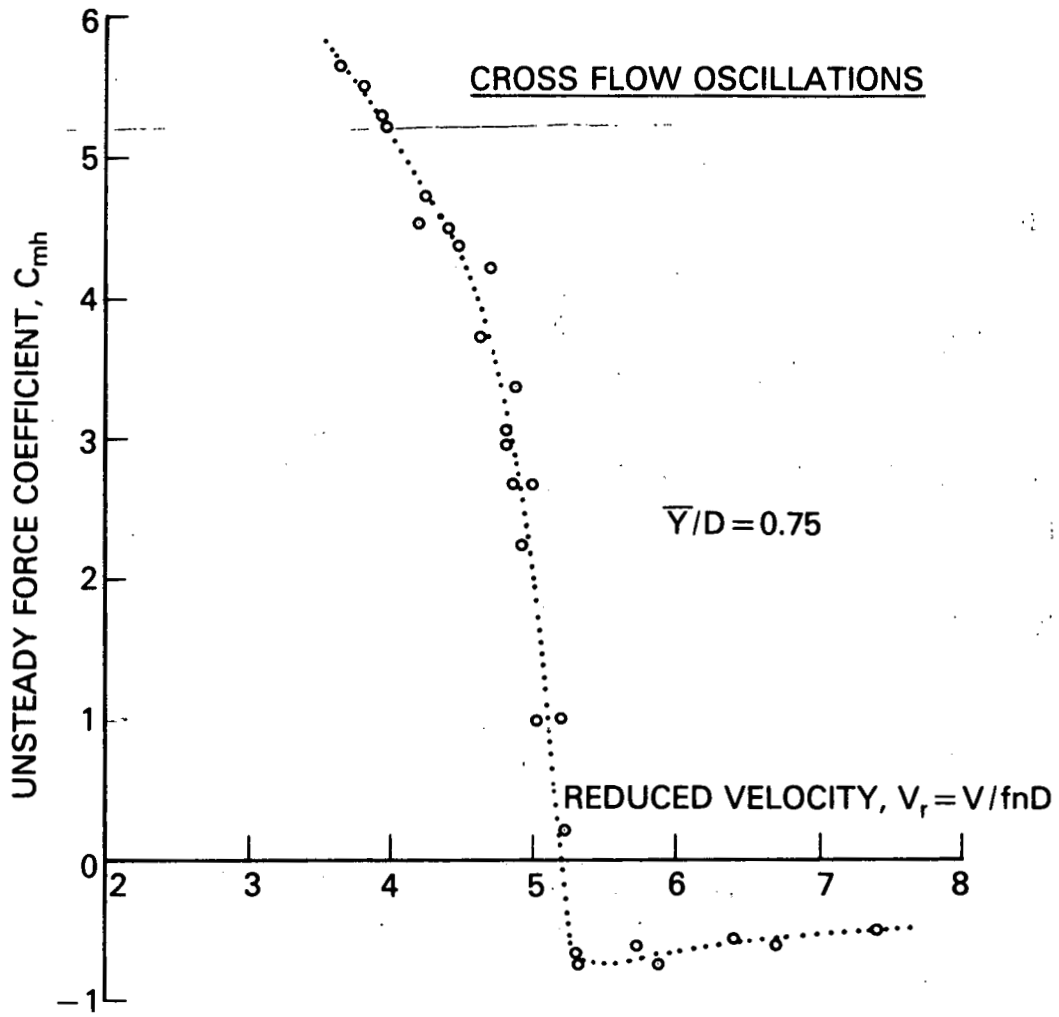

Figure 4.7. The inertia coefficient C_{mh} at the vibration frequency plotted against the reduced velocity V_r for $\bar{y}/D = 0.75$. The data are from Sarpkaya (28) and were measured in water with uniform, steady fluid motion past a cylinder oscillating normal to the flow. The coefficient C_{mh} was derived from the total unsteady transverse force. Lock-on occurs near $V_r = 5$.

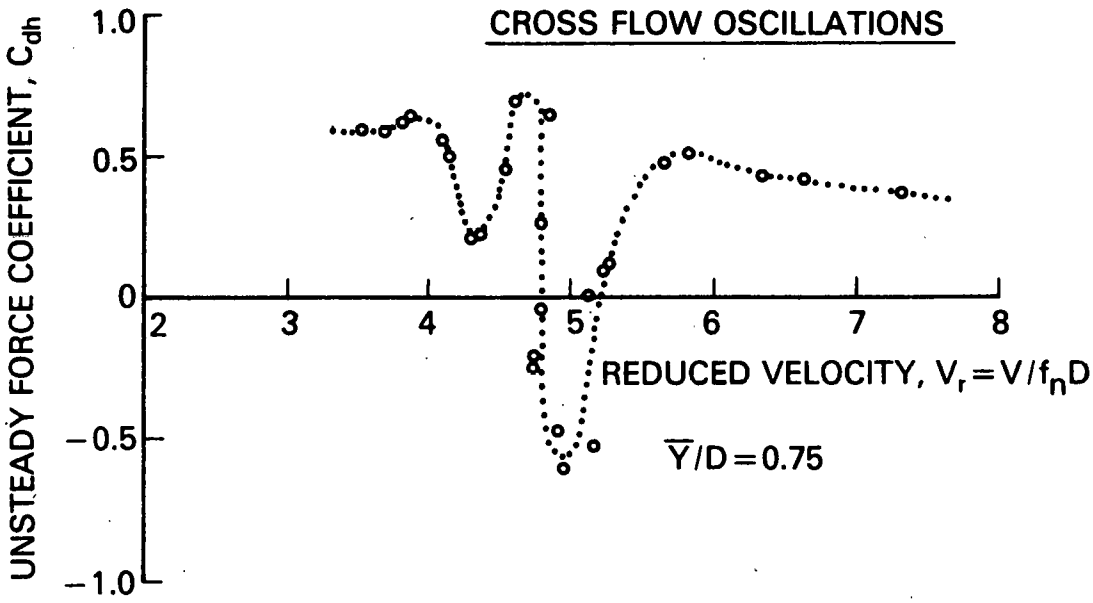

Figure 4.8. The "drag" coefficient C_{dh} at the vibration frequency plotted against the reduced velocity V_r for $\bar{y}/D = 0.75$. The data are from Sarpkaya (28) and were measured in water with uniform, steady fluid motion past a cylinder oscillating normal to the flow. The coefficient C_{dh} was derived from the total unsteady transverse force. Lock-on occurs near $V_r = 5$.

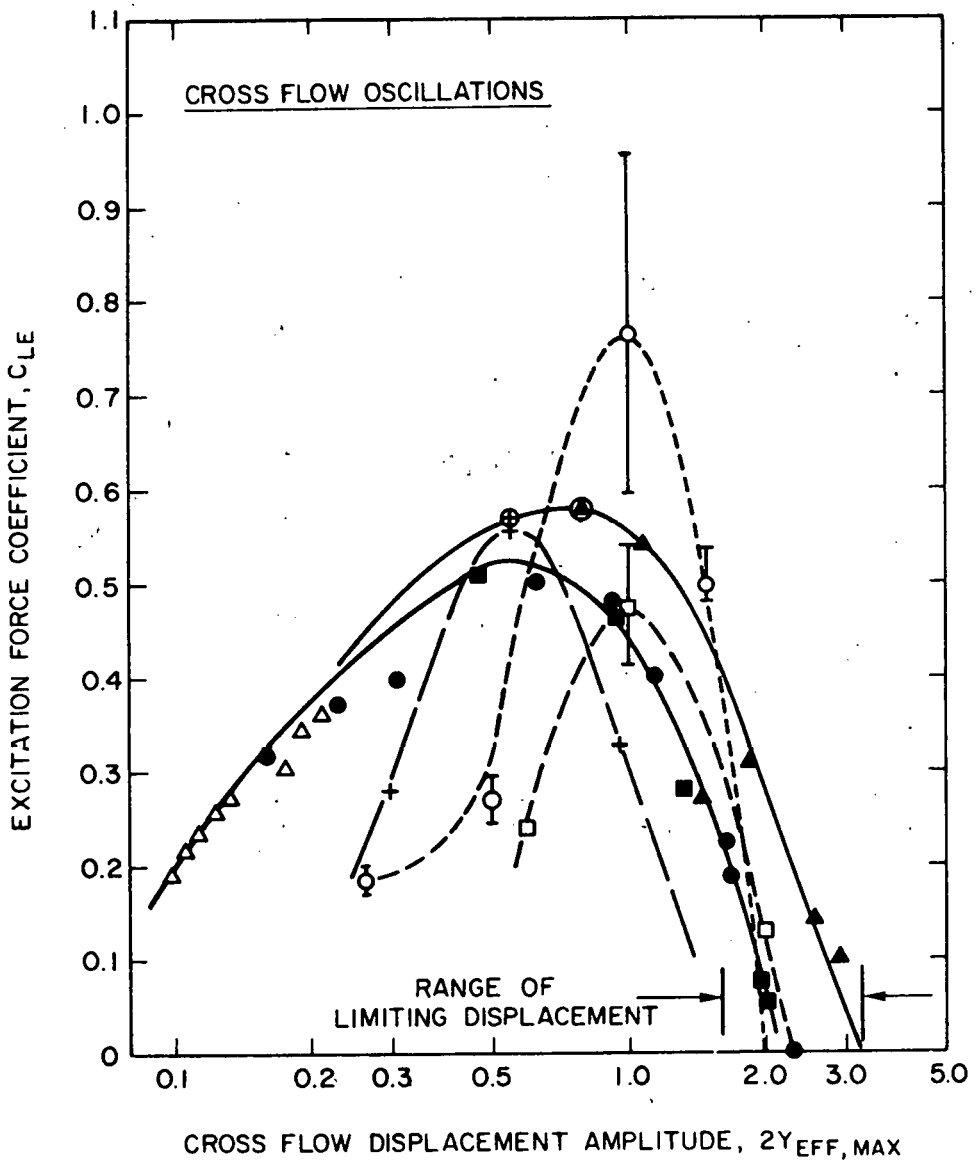

Figure 4.9. The excitation component C_{LE} of the lift force, equation (A10a), plotted against the vortex-excited cross flow displacement $2Y_{EFF,MAX}$ (peak-to-peak), as in equation (4a). The legend for the data points is given in Table 4.2; from Griffin (23).

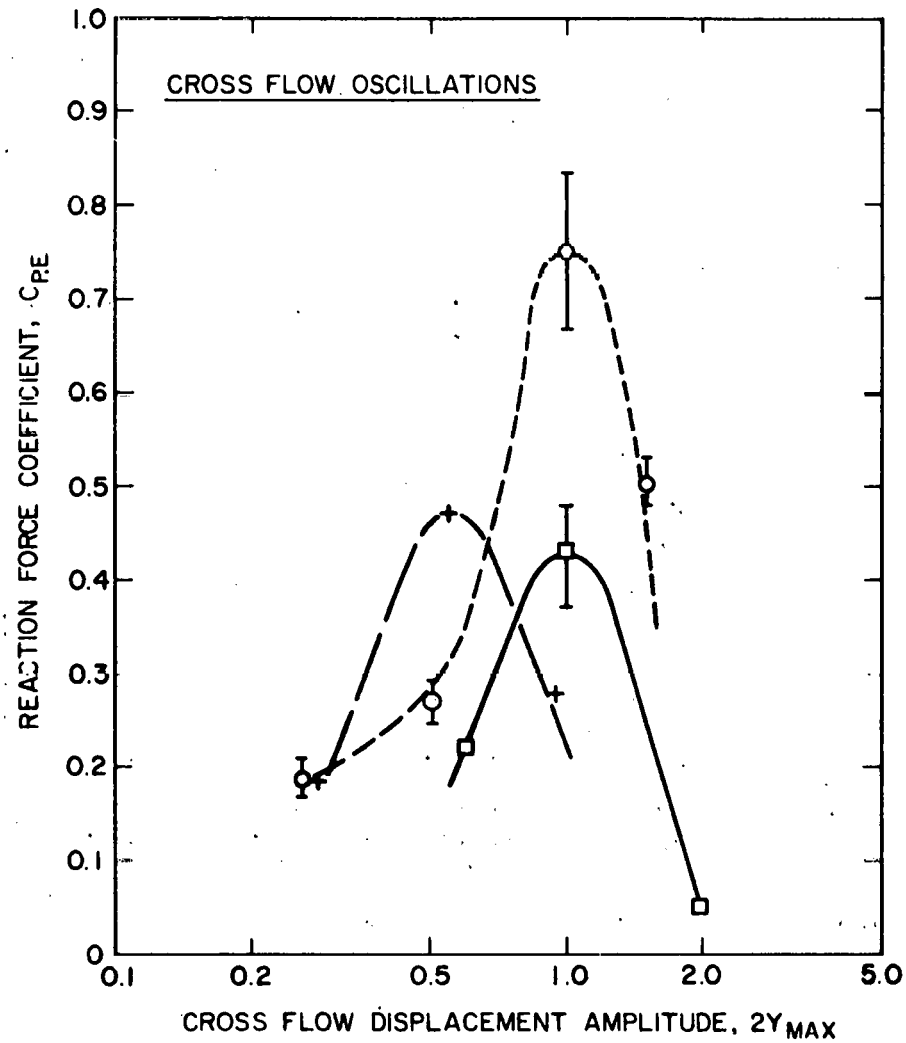

Figure 4.10. The fluid reaction coefficient C_{RE}, equation (A10c), plotted against the maximum cross flow displacement $2Y_{MAX}$ for a circular cylinder vibrating in uniform flow. Legend for data points: ———, Griffin and Koopmann (27); — —, Mercier (37); – – – Sarpkaya (28).

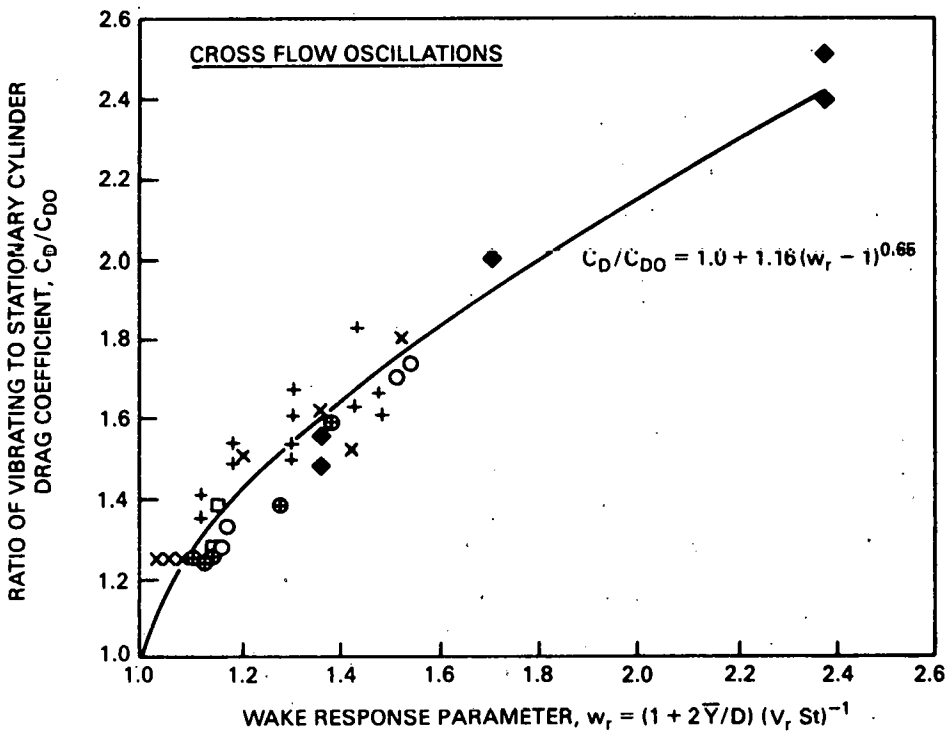

Figure 4.11. The ratio of the steady drag coefficient C_D due to vortex-excited cross flow oscillations and the steady drag coefficient C_{DO} on a stationary circular cylinder plotted against the wake response parameter w_r. Here $2Y/D$ is the peak-to-peak displacement amplitude (D is the diameter of the cylinder), V_r is the reduced velocity and St is the Strouhal number. A detailed legend for the data points is given in reference 59.

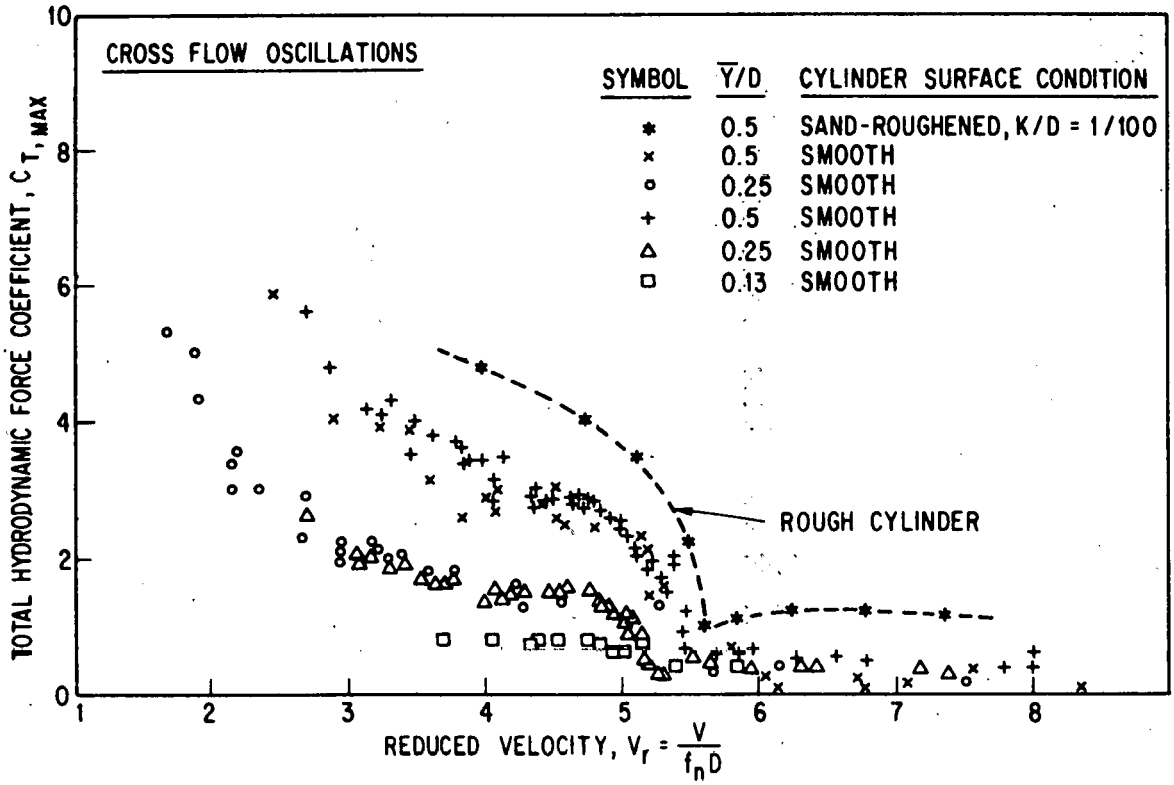

Figure 4.12. Total unsteady transverse force coefficient at the locked-on vibration frequency (Force/$\frac{1}{2}\rho V^2 DL$), $C_{T,MAX}$, measured on smooth and rough circular cylinders vibrating in the cross flow direction, plotted against the reduced velocity V_r; from Sarpkaya (39). The measurements were made under the same conditions as in Figures 4.5 through 4.8, and lock-on occurs near $V_r = 5$.

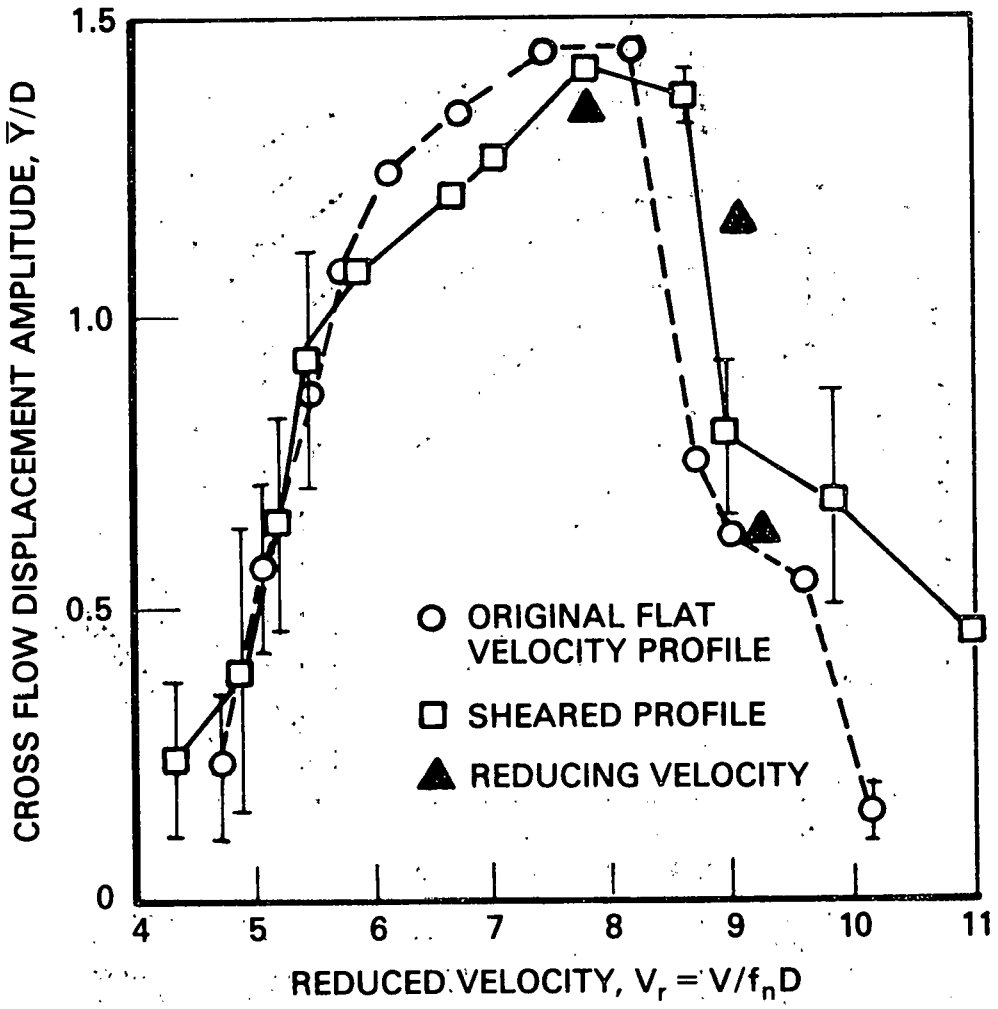

Figure 4.13. Measured peak cross flow displacement amplitude $\overline{Y}/D$ plotted as a function of the reduced velocity V_r. A slender, fully submerged and cantilevered circular cylinder was employed as the model (L/D = 52, D = 12.7 mm (0.5 in)) for experiments conducted in uniform ($\bar{\beta} = 0$) and shear ($\bar{\beta} = 0.01$ to 0.015) flows of water. The cylinder was a 1:168 scale model of a full-scale marine pile with the same specific gravity (SG = 1.5); from experiments reported by Fischer, Jones and King (45). In the case of the shear flow V is the maximum value in the nonuniform incident velocity profile. The figure was provided by the Shell Development Company.

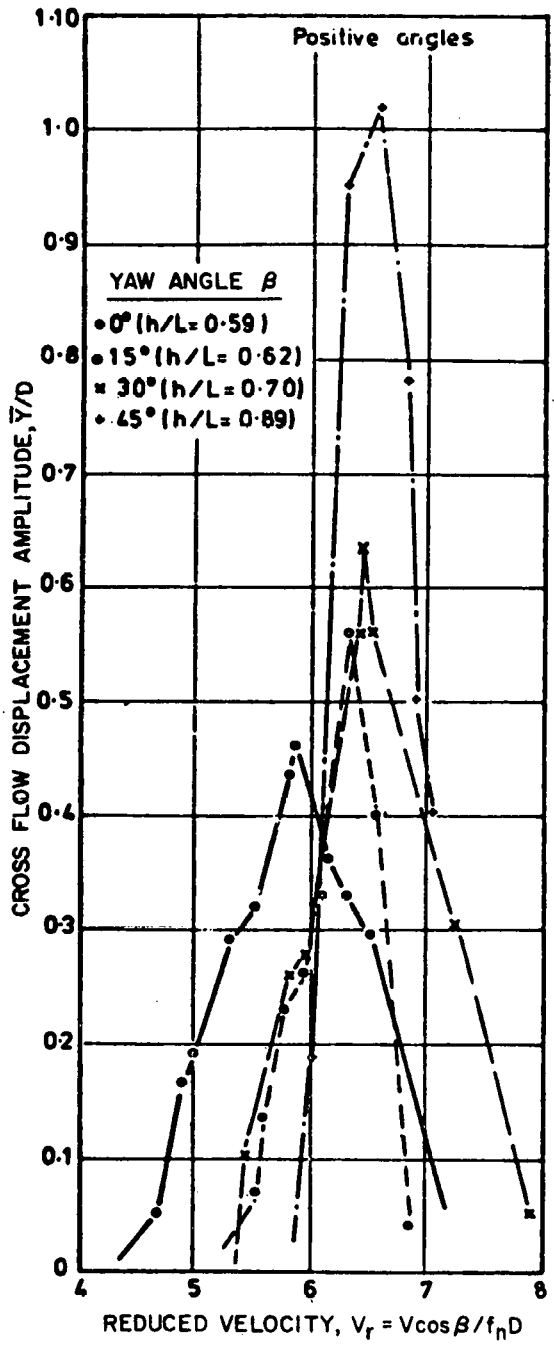

Figure 4.14. The cross flow induced displacement amplitude $\bar{Y}/D$ for flexible, yawed cylinders in uniform flow plotted against the reduced velocity V_r; from King (47). The reduced velocity is based upon the component of the incident flow normal to the cylinder, $V\cos\beta$, where β is the yaw angle. The Reynolds number of the experiments was $Re \approx 10^4$.

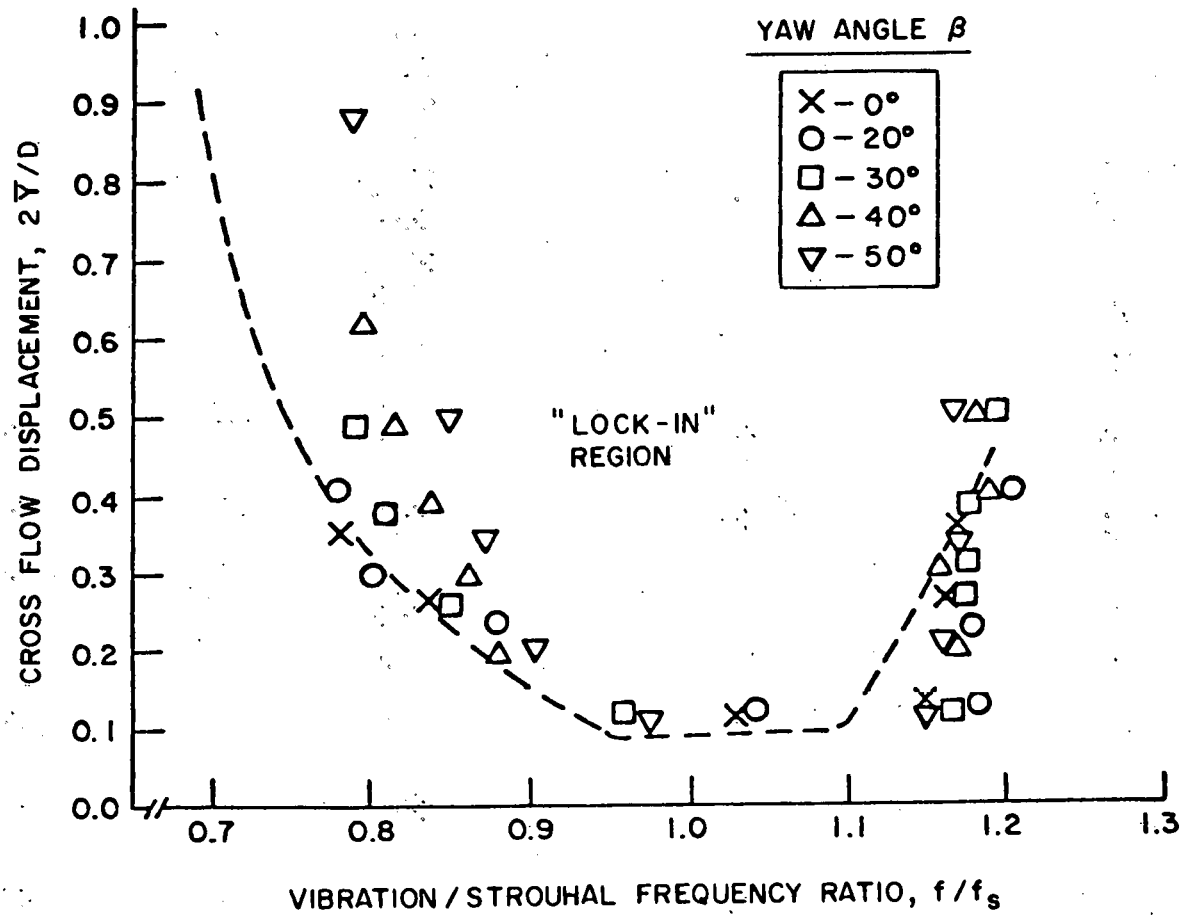

Figure 4.15. Lock-on boundaries (in terms of the cross flow displacement amplitude $2\bar{Y}/D$) plotted against the ratio of vibration and Strouhal frequencies; from Ramberg (48). The Strouhal frequency f_s was estimated from the cosine law relation $f_s = 0.21\ V \cos\beta/D$. *Lock-on* occurs *inside* the area bounded by the data points and dashed lines, and the latter correspond to the case of flow normal to the vibrating cylinder.

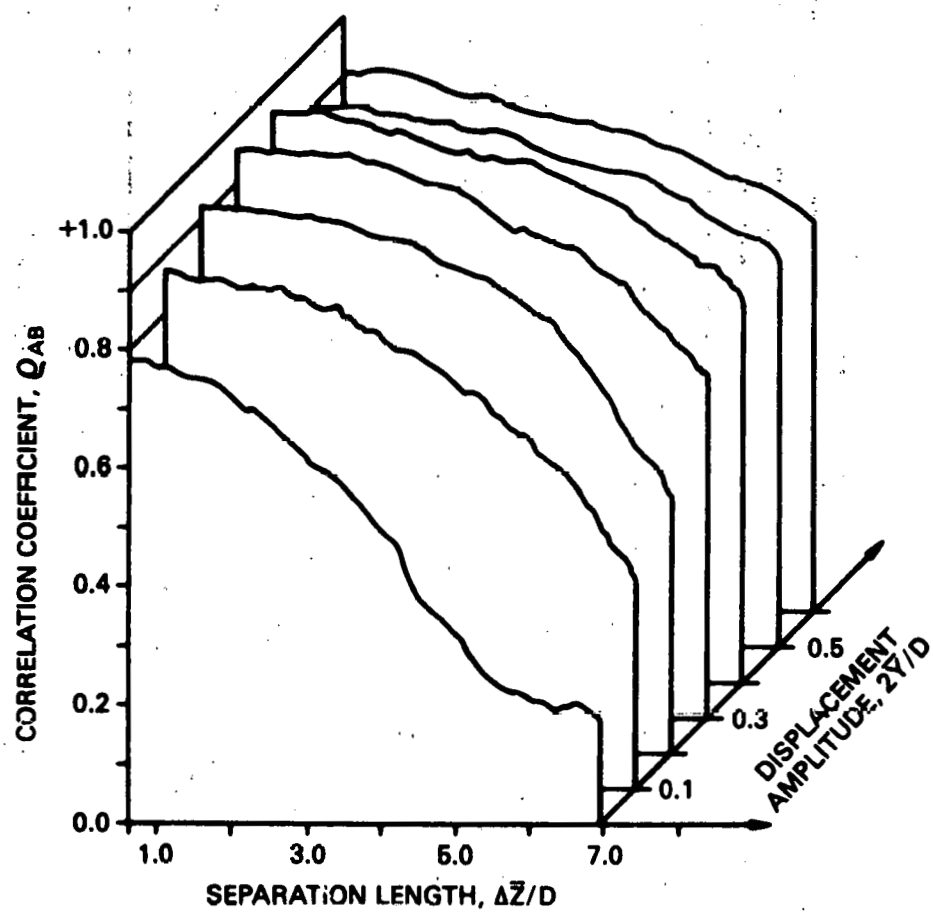

Figure 4.16 Spanwise correlation coefficients ρ_{AB} for the velocity signals measured in the wake of a vibrating cable at a Reynolds number of 1300 from reference 53. The spanwise separation between the two measuring probes is given by $\Delta z/D$ and the vibration displacement amplitude by $\bar{Y}_{MAX}/D$. Vibration frequency equal to 90 percent of the Stroubal frequency f_s.

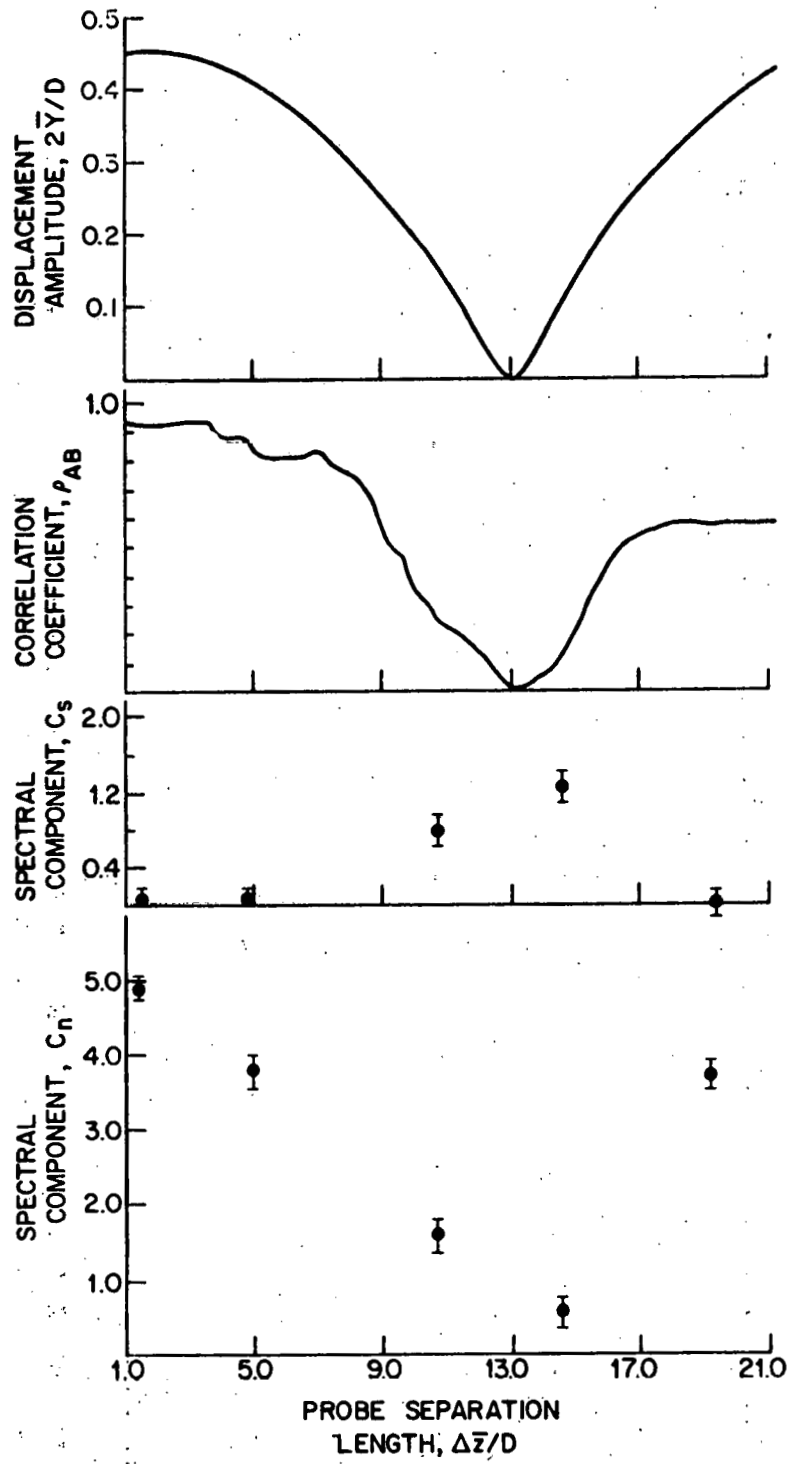

Figure 4.17 Distribution of displacement amplitude $\bar{Y}/D$, magnitude of the spanwise correlation coefficient ρ_{AB}, and the spectral content of the vortex shedding at the vibration frequency $f(C_n)$ and at the Stroubal frequency $f_s(C_s)$; from reference 54. The spanwise separation between the measuring probes is given by $\Delta\bar{z}/D$ and the vibration displacement amplitude by $\bar{Y}/D$. Vibration frequency equal to 86 percent of the Stroubal frequency f_s, Reynolds number = 610.

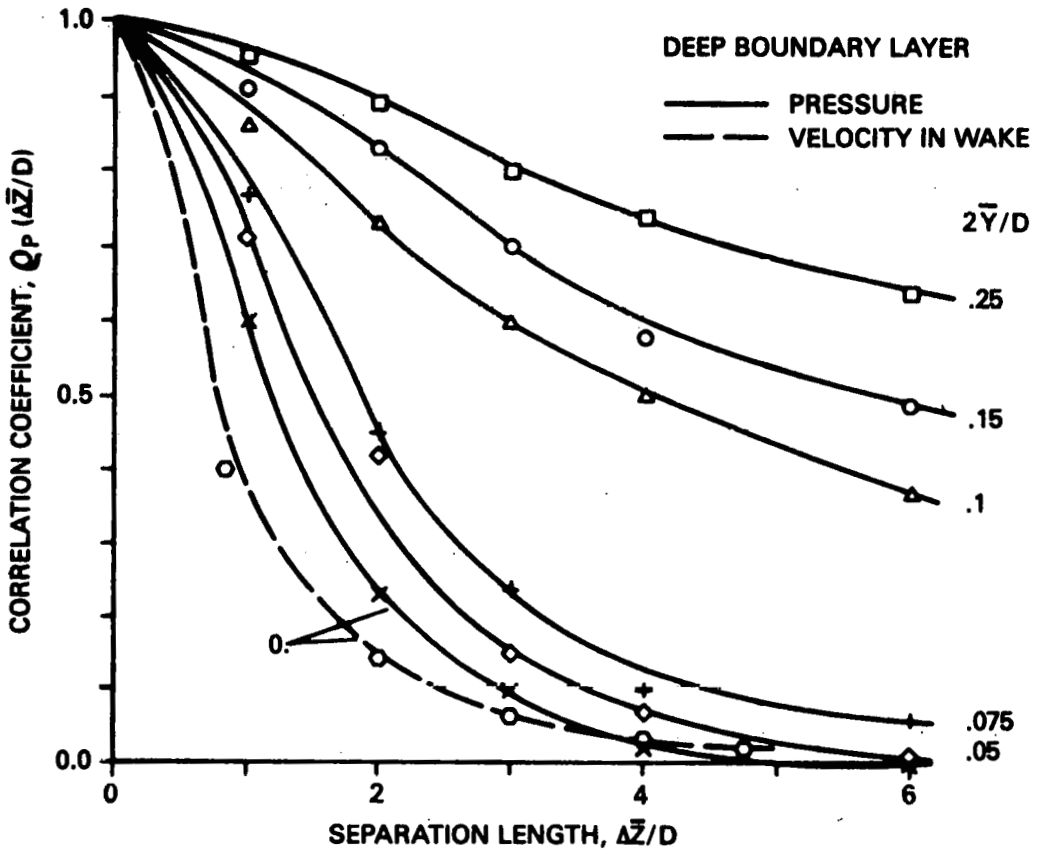

Figure 4.18 Spanwise correlation coefficient R_p between the fluctuating pressures measured on a vibrating pivoted rigid cylinder in a deep boundary layer flow; from reference 56. The peak-to-peak tip displacement amplitude of the cylinder is given by $2\bar{Y}/D$ and the spanwise separation between the pressure taps is given by $\Delta\bar{z}/D$. Reynolds number = 75,000.

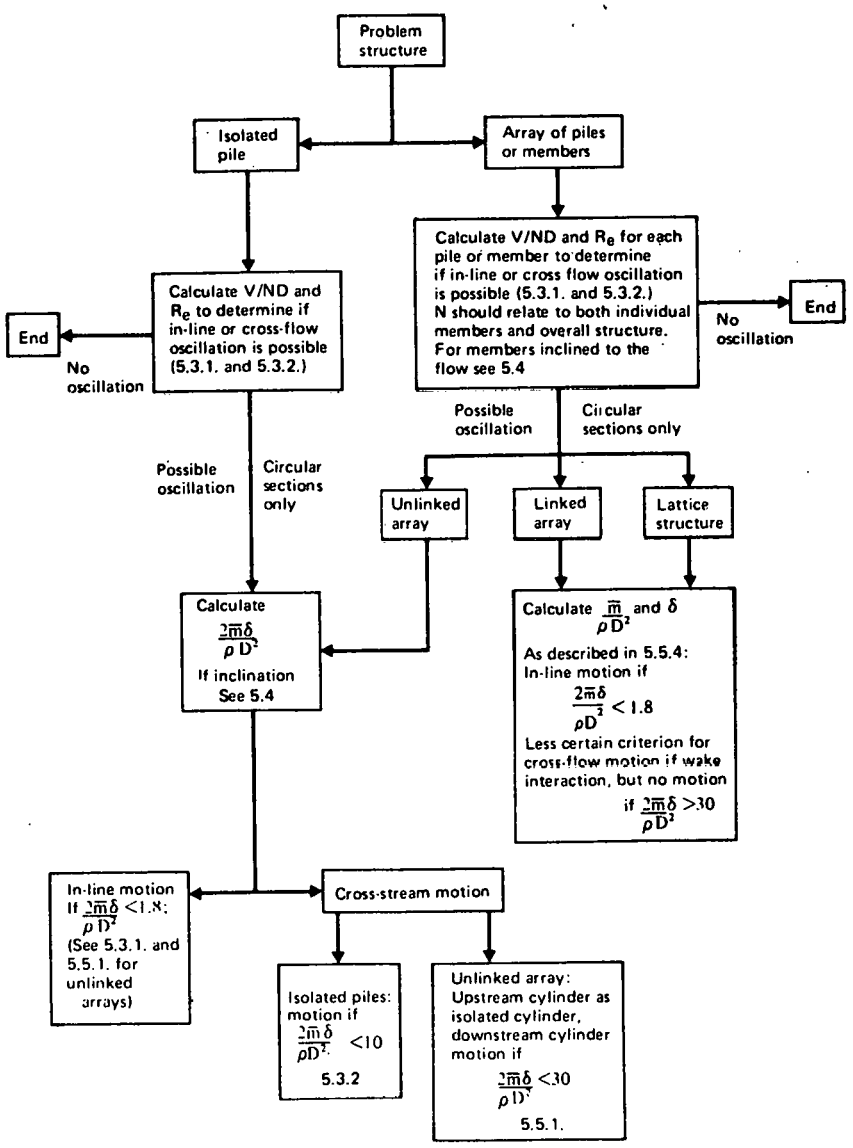

Layout for the calculation of the response due to vortex shedding

Figure 5.1. Flow diagram of the steps required for the calculation of the response of a structure due to vortex shedding; adapted from Hallam, Heaf and Wootton (1). Numbers in the boxes refer to relevant sections of reference 1.

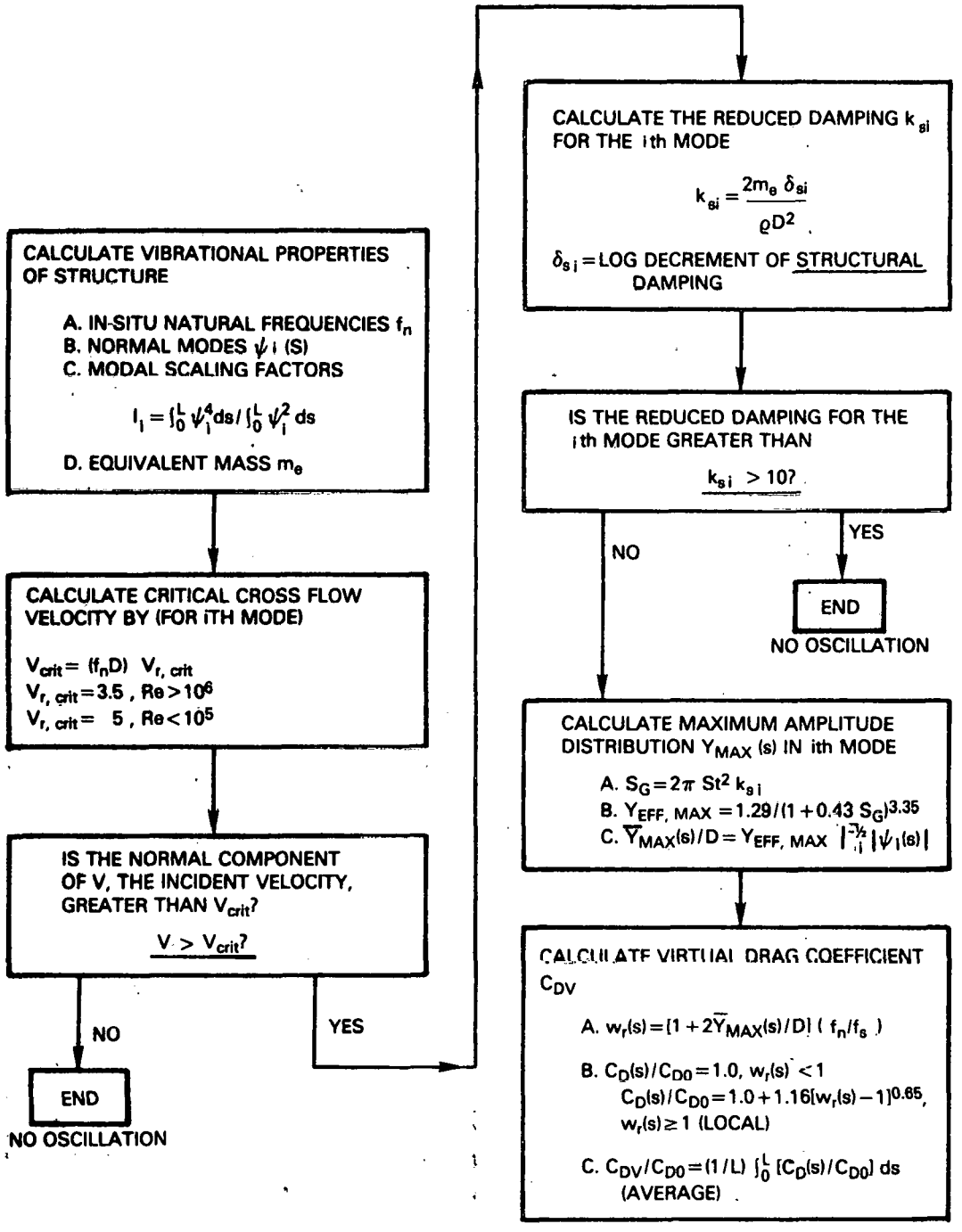

Figure 5.2. Flow diagram of the steps required for the calculation of the steady drag amplification due to resonant vortex-excited oscillations; adapted from Skop, Griffin and Ramberg (59).

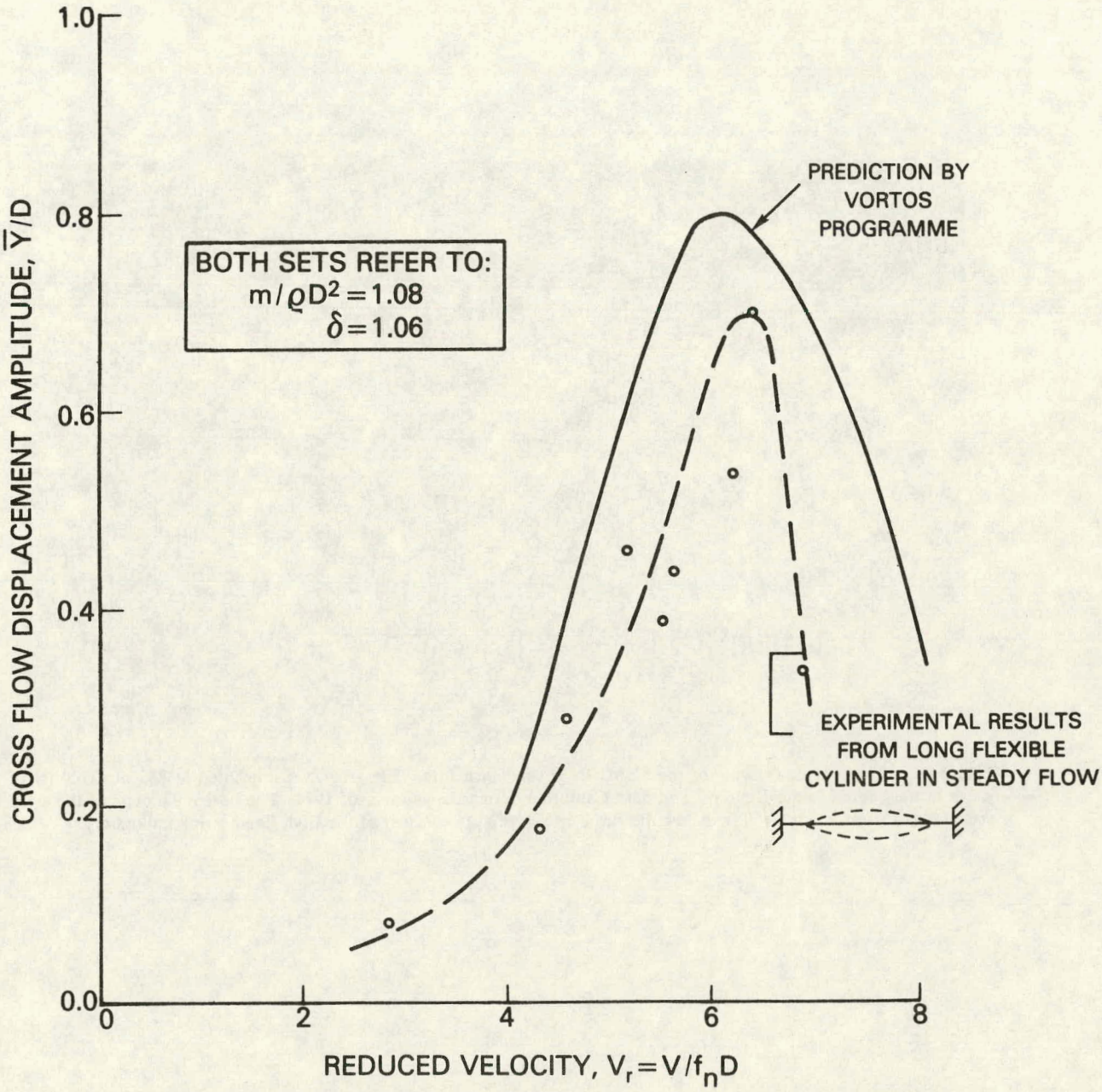

Figure 6.1. A comparison of the measured cross flow oscillations (from equilibrium) of a flexible cylinder with the predicted response from the VORTOS code; from Dean and Wootton (15).

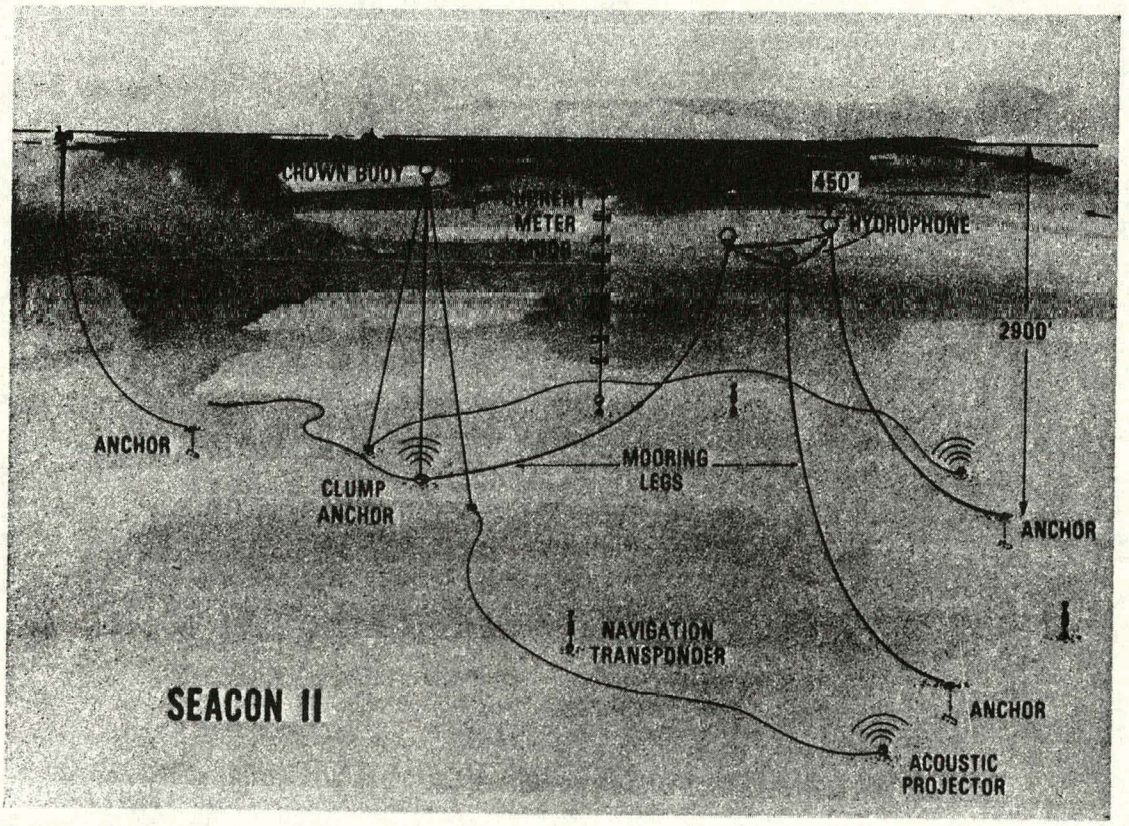

Figure 6.2. A schematic drawing of the SEACON II cable structure. The array was implanted in 885 m (2900 ft) of water in the Santa Monica Basin off Southern California during the summer of 1974. The horizontal delta of the array was approximately 137 m (450 ft) below the surface (67). Figure courtesy of the Civil Engineering Laboratory.

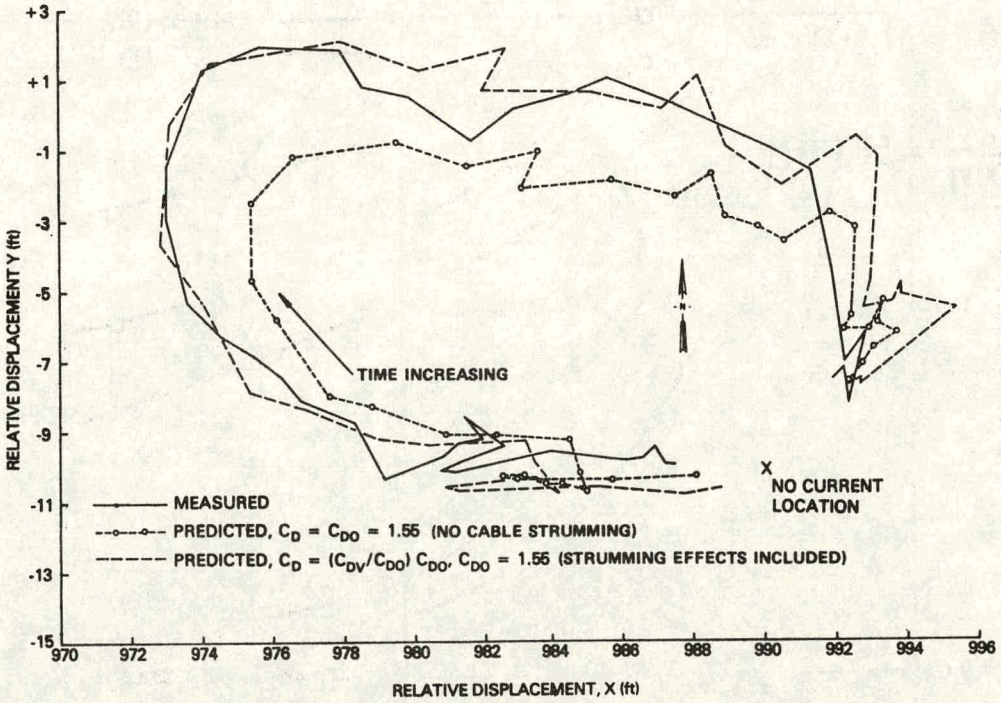

Figure 6.3. A comparison of the measured and predicted motions of a point near the intersections of cables 1 and 3 on the SEACON II delta (59). The time period covered is a semidiurnal tidal cycle from 2120, 12/11/75 to 0920, 12/12/75. The drag coefficient C_{DO} was measured in water on a short segment of the SEACON delta cable, $D = 18.5$ mm (0.75 in).

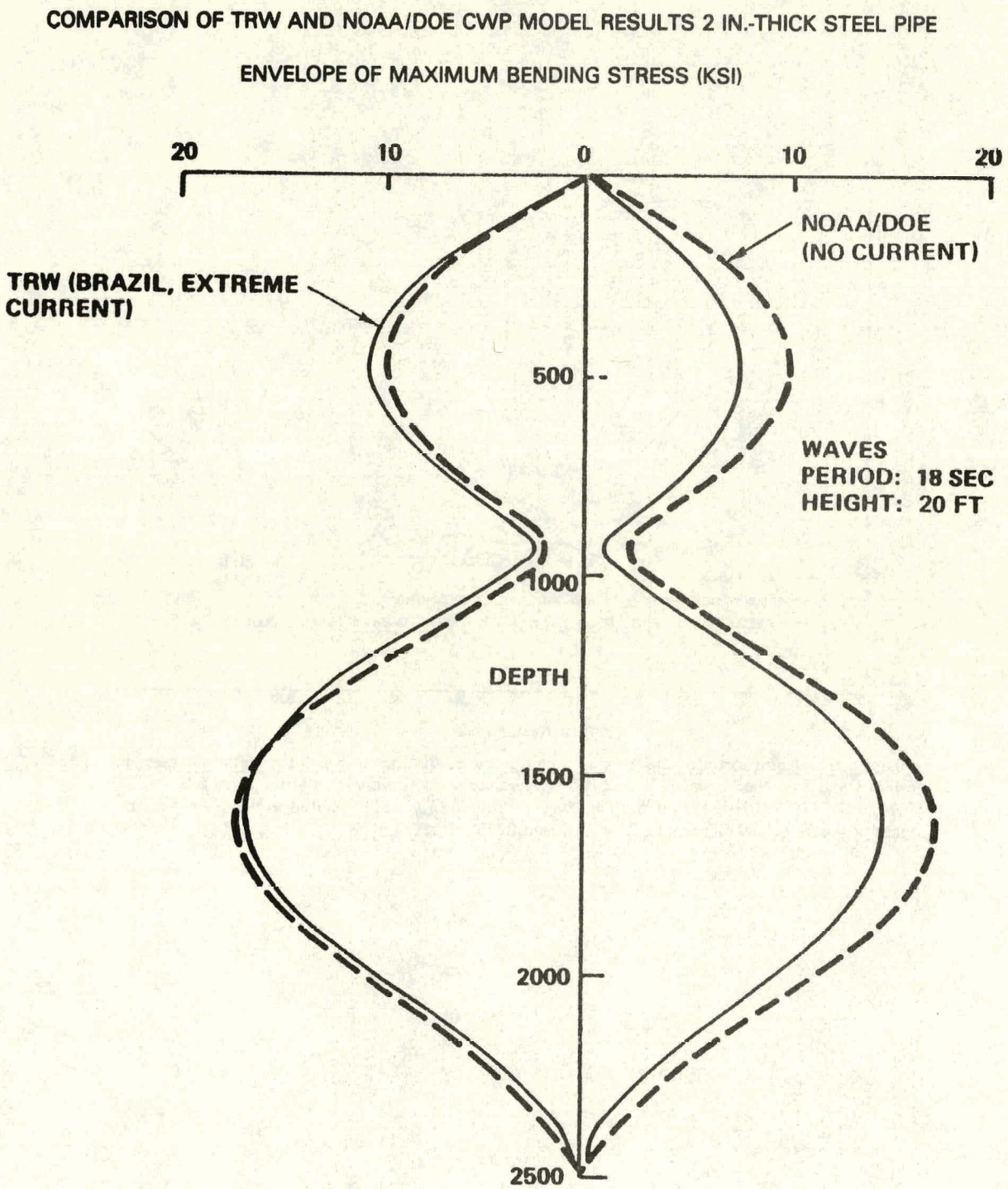

Figure 6.4. Comparison of TRW HULPIPE and NOAA/DOE predicted bending stresses on a 2 inch thick steel CWP configuration; from reference 12.

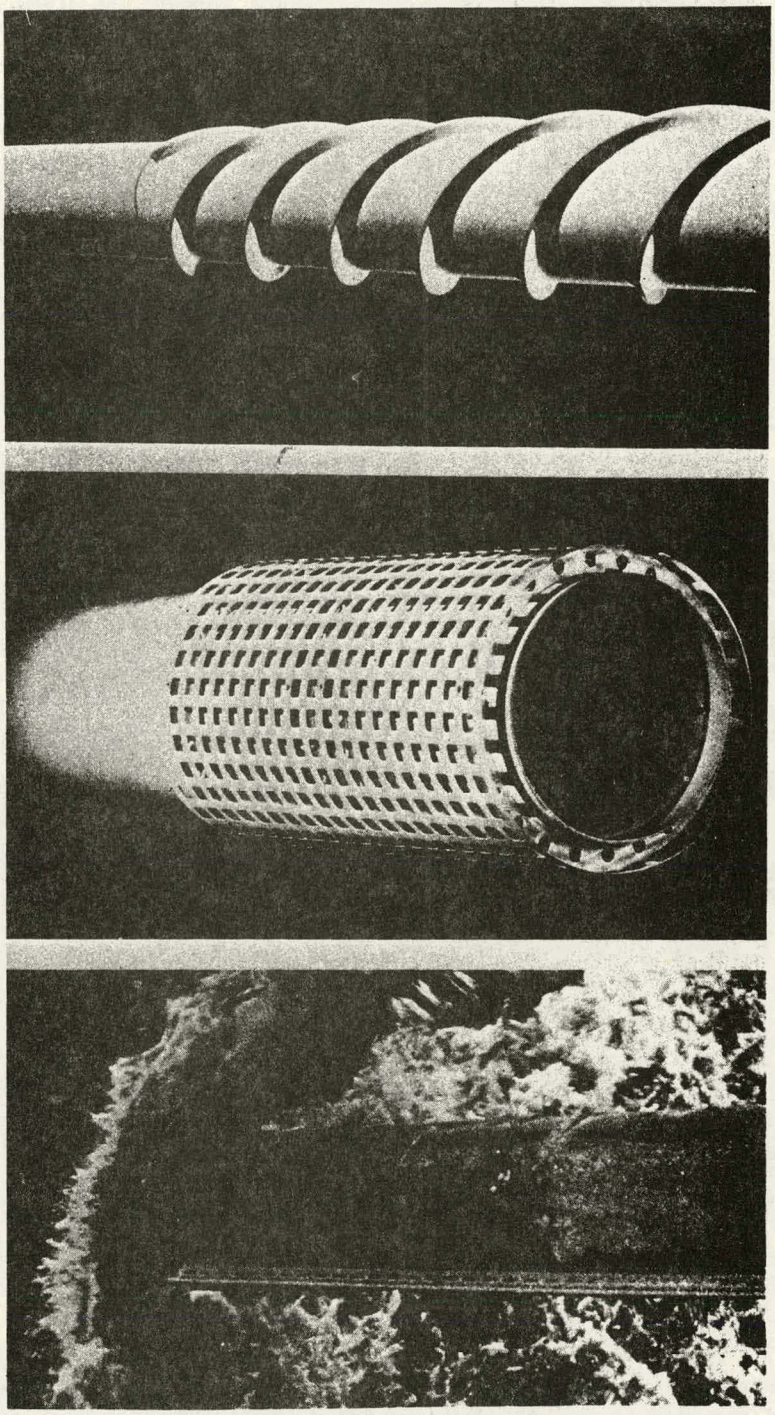

(a) Strake

(b) Porous shroud

(c) Radial fin

Figure 7.1. Photographs of the three common types of vortex suppression devices; from Hallam, Heaf and Wootton (1).

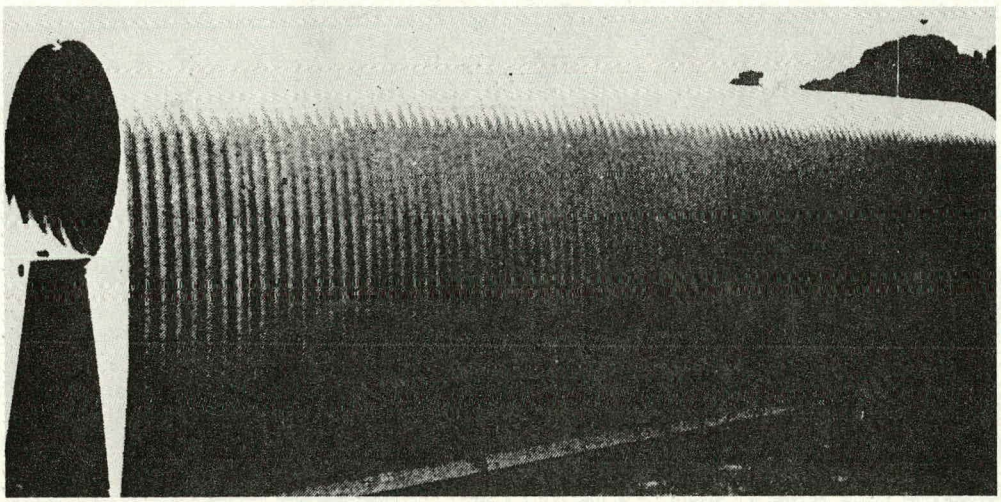

Figure 7.2. A photograph of the fairing (section) constructed for a 610 mm (24 in) diameter riser designed to operate in water depths of 500 feet and 8 knot currents; from Grant and Patterson (72).

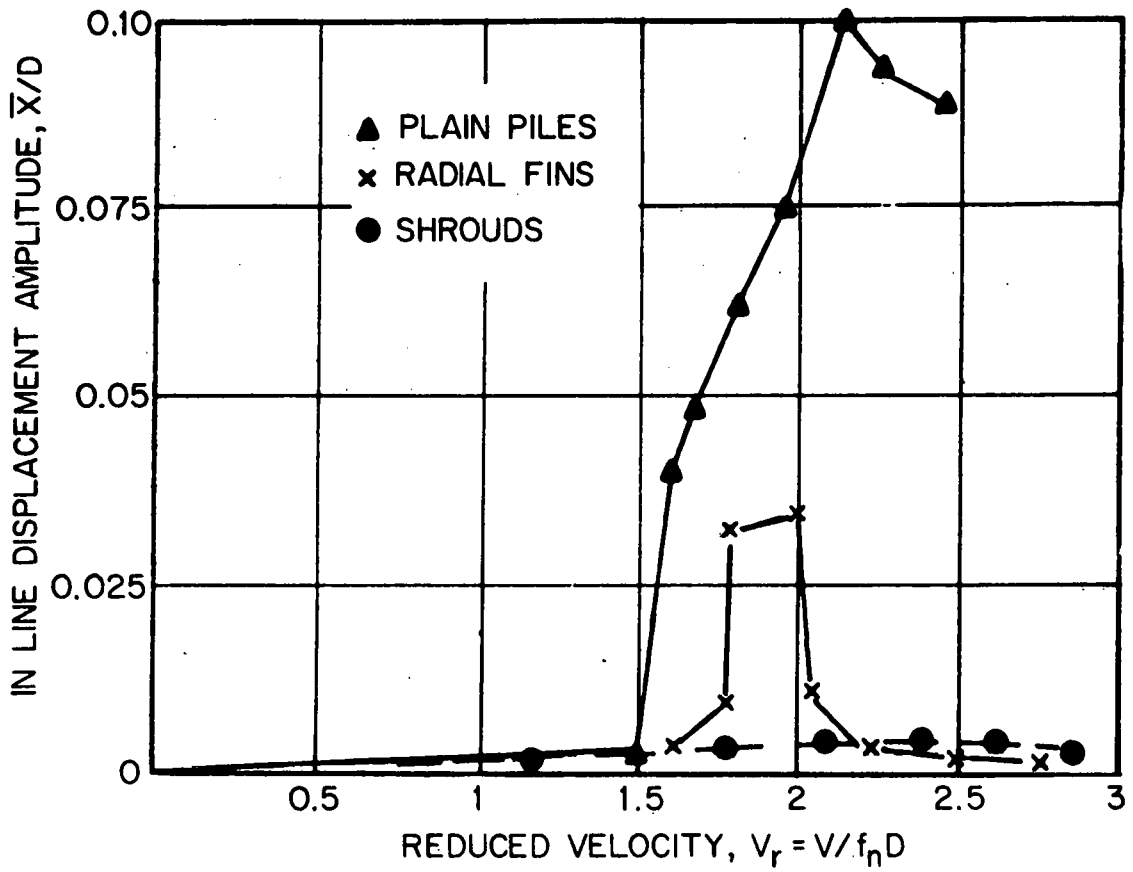

Figure 7.3. A comparison of the in line displacement amplitude response of a tripod of raked (yawed) flexible cylinders with and without vortex spoilers. The Reynolds number of the experiments was about 10^4; from King, Prosser and Verley (73).

☆U.S. GOVERNMENT PRINTING OFFICE: 1980-640-258/364